THEORETICAL AND EXPERIMENTAL STUDIES OF MODIFIED HUMIDIFICATION DEHUMIDIFICATION CYCLES

BY

SAMIH MUBAROK ELMUTASIM ELSHIEKH

A Thesis Presented to the
DEANSHIP OF GRADUATE STUDIES

KING FAHD UNIVERSITY OF PETROLEUM & MINERALS

DHAHRAN, SAUDI ARABIA

In Partial Fulfillment of the
Requirements for the Degree of

MASTER OF SCIENCE

In

MECHANICAL ENGINEERING

APRIL 2017

KING FAHD UNIVERSITY OF PETROLEUM & MINERALS

DHAHRAN- 31261, SAUDI ARABIA

DEANSHIP OF GRADUATE STUDIES

This thesis, written by **SAMIH MUBARAK ELMUTASIM ELSHIEKH** under the direction his thesis advisor and approved by his thesis committee, has been presented and accepted by the Dean of Graduate Studies, in partial fulfillment of the requirements for the degree of **MASTER OF SCIENCE IN MECHANICAL ENGINEERING.**

Dr. Syed M. Zubair
(Advisor)

Dr. Zuhair Mattoug Gasem
Department Chairman

Dr. Mohamed A. Antar
(Member)

Dr. Salam A. Zummo
Dean of Graduate Studies

Dr. Palanichamy Gandhidasan
(Member)

15/6/12

Date

To Afaf, my beloved aunt who passed away during my first semester here, and to my father, mother, siblings, family, friends and loved ones.

ACKNOWLEDGMENTS

All praise and thanks are due to Almighty Allah, Most Gracious and Most Merciful, for grant me health, knowledge, and patience to complete this work.

Thereafter, acknowledgment is due to KFUPM and Mechanical Engineering Department for supporting my research through its remarkable facilities and for granting me the opportunity to pursue my master degree. I acknowledge, the valuable time, support, guidance, and encouragement dedicated to me by my thesis advisor, Dr. Syed M. Zubair. I am highly grateful to my thesis committee member Dr. Mohammed A. Antar for his valuable guidance, suggestions, and motivation. His support and co-operation towards this research during experiments was of great value. I am also grateful to my Committee member, Dr. Palanichamy Gandhidasan for his constructive guidance and support.

I am short of words when it comes to the people who gave me life and raise me to become the person I am now. I would like to thank my parents (Mubarak Elmutasim & Siham Ibrahim) for everything they have done for me. I would like also to thank my siblings, extended family, and friends for their continuous encouragement and support.

I am deeply indebted and grateful to Mr. Mohammad S. A. Karam (Heat Engines Lab Engineer) for his help and support during experiments and also thanks are due to my colleagues Suhaib Mustafa, Mohamed Ali Mahmoud and Muhammad Ahmad for their help and support. Finally, I would like to thank the Sudanese community here at KFUPM for making my stay here as pleasant as possible.

TABLE OF CONTENTS

LIST OF TABLES

LIST OF FIGURES

LIST OF ABBREVIATIONS

Nomenclature

Acronyms

GOR	gained output ratio
HDH	humidification-dehumidification
HX	heat exchanger
MX	mixing chamber
$OAOW$	open-air open-water
$CWOA$	closed-water open-air
$CAOW$	closed-air open-water
RO	reverse osmosis
PT	Pelton turbine
PX	pressure exchanger
CRF	capital recovery factor

Symbols

$\dot{m}$	mass flow rate (kg/s)
MR	water-to-air mass flow rate ratio (–)
$\dot{Q}$	heat transfer rate (kW)
$\dot{X}$	the rate of exergy (kW)

χ	the fraction of saline water mass flow rate (kg/s)
y	the fraction of brine mass flow rate (kg/s)
h	specific enthalpy (kJ/kg)
h^*	specific enthalpy (kJ/kg dry air)
h_{fg}	specific enthalpy of vaporization (kJ/kg)
RR	recovery ratio (%)
$\dot{W}$	work rate (kW)
$\dot{V}$	volume flow rate (m^3/s)
SEC	specific energy consumption (kWh/m^3)
i	Interest rate (-)
Z	capital cost ($)
$\dot{Z}$	investment cost rate ($/s)
C	Cost ($/m^3$)
$\dot{C}$	stream cost rate ($/s)
P	Pressure (kPa)
m	the slope of humidifier and dehumidifier line (°C.kg dry air/kJ)
C	the intersection of humidifier and dehumidifier line (°C)
c_p	specific heat capacity at constant pressure (kJ/kg. K)
tan	the correspondent point at humidifier line to the tangent point at air curve

$\tan'$	the tangent point at air curve
X	salinity (ppm)
T	temperature (°C)
ε	effectiveness (–)
Ψ	enthalpy pinch (kJ/kg dry air)
ω	absolute humidity (kg water vapor per kg dry air)
φ	relative humidity (–)

Superscript

n	amortization period

Subscripts

0, 1, ...	state points
a	Air
w	saline water
cw	cooling water
deh	Dehumidifier
hum	humidifier
RO	reverse osmosis
PX	pressure exchanger
PT	Pelton turbine
P	pump

$\text{int}\,ake$	entering stream
HX	heat exchanger
in	entering
fw	fresh water
mix	mixer
ext	extraction point
b	Brine
II	second law
is	isentropic
OM	operation and maintenance
D	destroyed
$fluid$	working fluid
$output$	product stream

ABSTRACT

Full Name : [Samih Mubarak Elmutasim Elshiekh]

Thesis Title : [Theoretical and Experimental Studies of Modified Humidification Dehumidification Cycles]

Major Field : [Mechanical Engineering]

Date of Degree : [April,2017]

Humidification dehumidification (HDH) systems are robust and known to withstand a wide range of saline water without the need of complex maintenance. In this study, an experimental investigation of a modified closed-water open-air (CWOA) is conducted to evaluate the performance of this system. An analytical model is then validated against the experimental results and this model is used to evaluate the performance of both open-air open-water and modified CWOA cycles. An exergo-economic analysis is also presented for both systems as well as an alternative option to modification namely coupling the HDH system with an RO module is also explored. Another system is also studied; that is, the closed-air open-water (CAOW) HDH system. The CAOW HDH arrangement is modified by incorporating heat recovery options. The heat recovery process is executed through two approaches, (i) a mixing chamber and, (ii) by a heat exchanger. Thermal balancing through air extraction is also evaluated for the basic as well as the modified cycles. Zero, single and double extractions models are evaluated for the conventional CAOW water heated cycle and both the modified cycles. An operating scheme is also developed to decide when to use the modified cycle or the basic cycle with or without extraction.

ملخص الرسالة

الاسم الكامل: سامح مبارك المعتصم الشيخ

عنوان الرسالة: دراسات نظرية و تجريبية للدورات التبخيرية و التكثيفية المعدلة

التخصص: هندسة ميكانيكية

تاريخ الدرجة العلمية: أبريل 2017

الأنظمة التبخيرية التكثيفية متينة و معروفة بتحملها لمدى واسع من ملوحة المياه من دون الحوجة لصيانة معقدة. في هذه الدراسة، تم أجراء تحقيق تجربي لتقييم أداء نظام تبخيري تكثيفي معدل ذو دورة مياه مغلقة و هواء مفتوحة. الأنموذج النظري تم التحقق من فعاليته بالمقارنة مع النتائج المتحصل عليها من التجربة و تم استخدام هذا الأنموذج لتقييم كلا الدورتين الرئيسية و المعدلة. تحليل اكسيرجو-اقتصادي أيضا تم تقديمه لكلتا الدورتين مع استكشاف خيار بديل تحديدا عملية ربط المنظومة التبخيرية التكثيفية مع وحدة تنقية المياه بالتناضح العكسي. نظام تبخيري تكثيفي آخر ذو دورة هواء مغلقة و مياه مفتوحة تمت دراسته. الترتيبات للنظام التبخيري التكثيفي مغلق الهواء مفتوح الماء تم تعديله بإدخال خيار عملية استرجاع حراري. عملية الاسترجاع الحراري تم تنفيذها باستخدام طريقتين هما (أ) غرفة خلاط و (ب) مبادل حرار. التوازن الحراري عن طريق استخلاص الهواء تمت دراسته للمنظومة الأساسية و المعدلة. الأنموذج صفري و أحادي و ثنائي الاستخلاص تم تقييمهم عن طريق تطبيقهم على النظام التبخيري التكثيفي الأساسي مغلق الهواء مفتوح الماء الذي يتم تسخين تيار المياه فيه و الأنظمة المعدلة كذلك. تم تطوير مخطط تشغيلي لتقرير متى يتم استخدام النظام المعدل أو النظام الأساسي مع استخلاص أو من دون استخلاص.

CHAPTER 1

INTRODUCTION

There is about 40% of the world population that is suffering from the water shortage problems. It is expected to reach 60% by 2025 [1]. A large portion of the world population lives within 70 km of sea shores [2], which qualifies for industrial desalination as a promising solution to this crisis. Industrial desalination is classified into thermal, mechanical and electrical techniques. One of the promising thermal techniques is the humidification-dehumidification (HDH) desalination system. The HDH desalination system is suitable for small-scale freshwater production. Thus, it is more suitable for villages and small communities due to its simplicity. These systems are considered to have some advantages over other desalination technologies such as their capacity to operate over a wide range of untreated water quality with minimum maintenance requirements [3]. The basic drawbacks of HDH systems remain that the total heat input is relatively high compared to other conventional thermal desalination technologies; however, renewable energy as a source of heat input can be utilized in these systems.

1.1 Classification of HDH Systems

The classification of HDH systems may be according to whether air or water is heated and to the nature of the air or water stream loop i.e. either open or closed loop, as explained by Narayan et al. [4].

1.1.1 Water Heated Closed-Water Open-Air System

Figure 1.1 illustrates a water heated, closed-water open-air cycle. In this configuration, the water loop starts from the dehumidifier, where the saline water is preheated before it enters a water heater. After that, it continues to a humidifier where the evaporation process takes place and then the rest of the brine water is collected and circulated back to the dehumidifier inlet. At the dehumidifier inlet, a make-up for the evaporated water is needed to guarantee that the water cycle is closed. The air that enters the humidifier picks up the water vapor and leaves as hot and humid. It then passes through the dehumidifier where its moisture content is extracted in cooling and dehumidification process. The desalinated water is then collected as a product and the air is thrown away. The major problem of this configuration occurs when the humidifier doesn't cool the water enough, which leads to a high-water temperature that enters the dehumidifier. When the saline water enters the dehumidifier with a high temperature it will affect the cooling and dehumidification process and consequently results in less fresh water product. This issue can be resolved by employing an effective humidifier.

1.1.2 Water Heated Closed-Air Open-Water System

The configuration for this system is shown in Figure 1.2. As the previous system, the saline water follows the same path, but here the water after collected as brine water is thrown away. The air loop is closed, unlike the closed-water open air system. The air enters the humidifier and gets hot and humid and then dehumidified in the dehumidifier, where water vapor is condensed and collected as fresh water and the air is brought back to the humidifier. The problem with this configuration is that the thrown water has high

amount energy and from an environmental point of view it is a high salinity water which is being rejected to the environment.

1.1.3 Air Heated Closed-Air Open-Water System

Figure 1.3 exhibits the configuration of this system. Air is heated in an air heater and then passes through the humidifier where it is cooled and humidified. After the humidifier, it enters the dehumidifier where it further cooled and the moisture content is removed as fresh water. Air is then brought back to the heater to close the loop. The saline water enters the dehumidifier where it warms up before it is sprayed in the humidifier. In the humidifier water is heated and part of it is evaporated in a heat and mass transfer process. The remaining water brine is then collected and rejected to the environment.

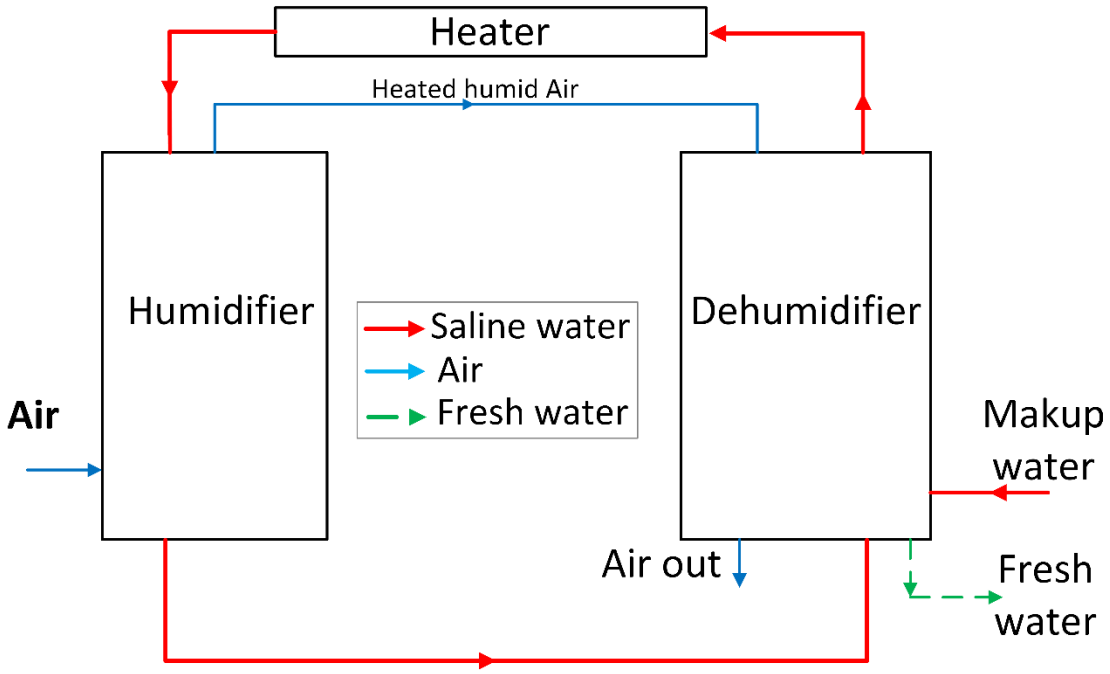

Figure 1.1 Water heated closed-water open-air HDH system [4].

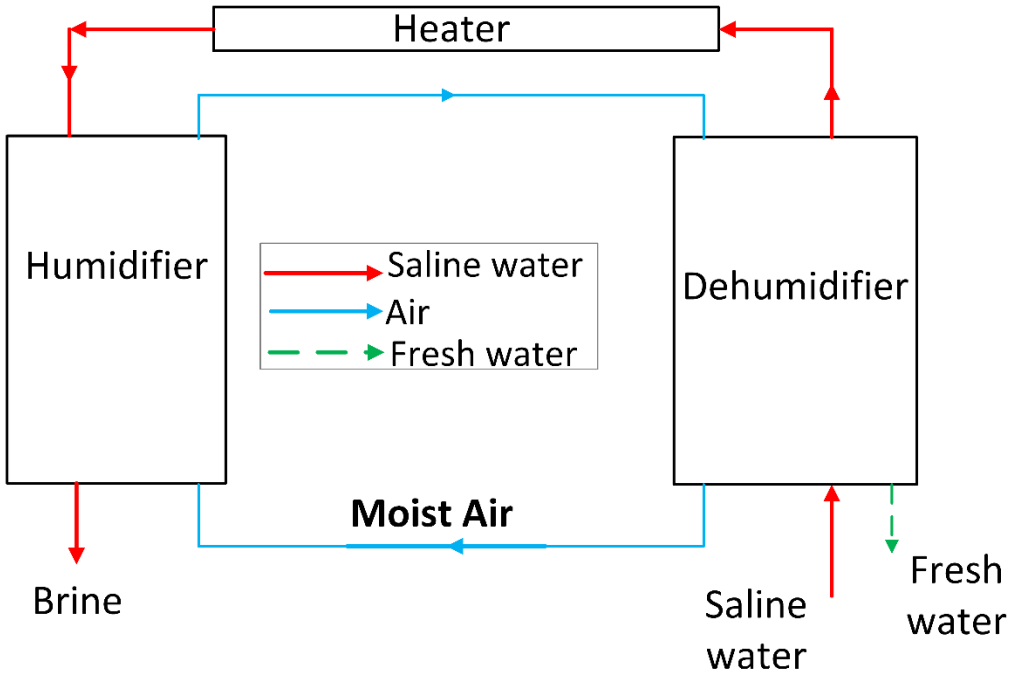

Figure 1.2 Water heated closed-air open-water HDH system [4].

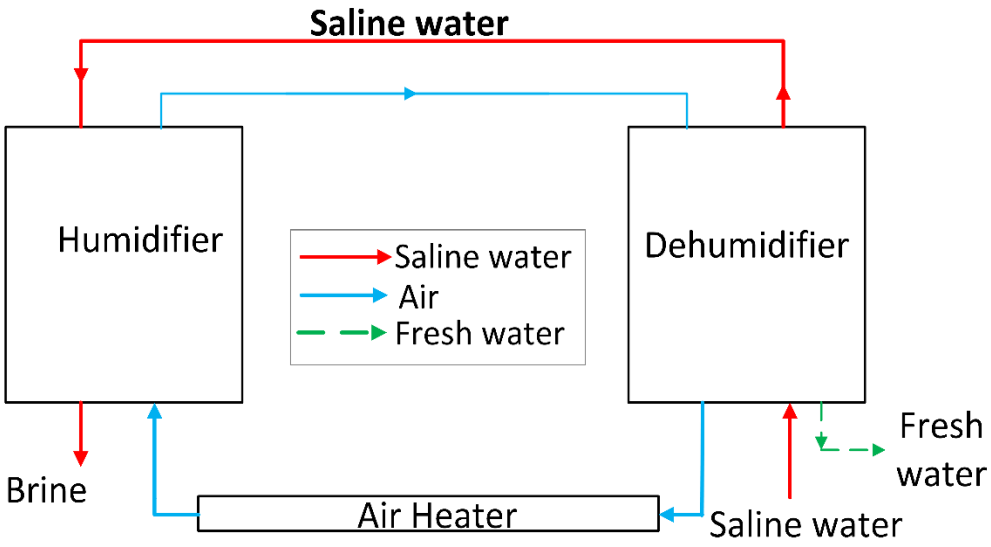

Figure 1.3 Air heated closed-air open-water HDH system [4].

1.1.4 Air Heated Open-Air Open-Water System

In this system both air and water loops are open. The cycle arrangement is shown in Figure 1.4. Air enters the humidifier where it undergoes heating and humidification process before it is further heated by an air heater. The humid air leaves the heater at high temperature and then loses it to heat the saline water in the dehumidifier. Air is then cooled down and dehumidified and the fresh water is collected at the exit of the dehumidifier. As air is thrown away, saline water enters the dehumidifier and then sprayed in the humidifier where the evaporation process takes place. The brine water is then collected at the end of the humidification process and thrown away.

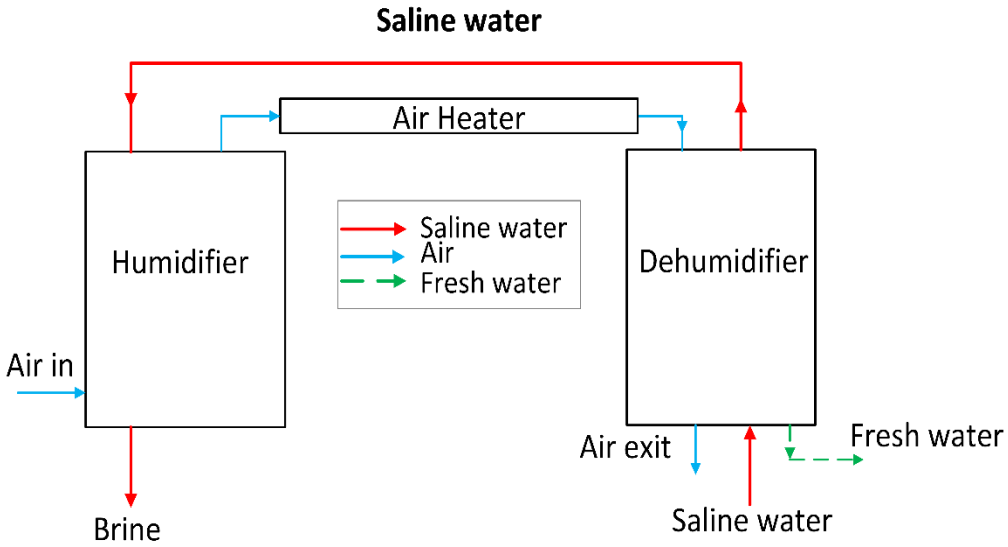

Figure 1.4 Air heated open-air open-water HDH system [4].

1.2 Research Objectives

The objectives of this study are dedicated to investigating different HDH cycles experimentally and analytically. Experimental investigation of a modified closed-water

open-air (CWOA) is conducted to evaluate the performance of this system. An analytical model then validated against the experimental results and used to evaluate the performance both open-air open-water and modified (CWOA) cycles. An exergo-economic analysis is also presented for both systems and an alternative option to modification namely coupling the HDH system with an RO module is also explored. Another system is also studied which the closed-air open-water (CAOW) HDH system. The CAOW HDH arrangement is modified by incorporating heat recovery options. The heat recovery process is executed through two approaches, (i) a mixing chamber and, (ii) by a heat exchanger. Thermal balancing through air extraction is also evaluated for the basic as well as the modified cycles. Zero, single and double extractions models are evaluated for the conventional CAOW water heated cycle and both the modified cycles. An operating scheme is also developed to decide when to use the modified cycle or the basic cycle with or without extraction. The specific objectives of this study are summarized as follows:

1. Literature review to examine the state of HDH systems.
2. Prepare an analytical model for the experimental set-up to conduct a thermodynamic study of the modified closed water open air cycle.
3. Experimental investigation of modified CWOA and validate the analytical model.
4. Conduct an exergo-economic analysis of the basic and modified cycles and explore options of coupling the HDH water heated basic OAOW with an RO module.

5. Use the enthalpy pinch model in the literature to balance water heated CAOW HDH cycle.
6. Validate this model against the literature and then use it to examine zero, single and double extractions for both conventional and modified cycles.

CHAPTER 2

LITERATURE REVIEW

2.1 Humidification Dehumidification Systems Status

The energy demand for producing the convenient amount of potable water is very high [5,6]. The conventional desalination systems depend on fossil fuels as their main energy source. The environmental impact of these sources accompanied with their unsustainable nature urge the need to come up with more sustainable techniques [7].The conventional systems are still better in terms of efficiency and economic feasibility than sustainable desalination technologies. However, the desalination systems that use renewable energy have a good chance to outperform the conventional plants in the long term [8]. In recent studies, HDH systems that are powered by solar energy are considered to be the optimal solution for decentralized areas with small capacities. It requires low maintenance costs and it is considered to be environmentally friendly [9–11]. Many studies reviewed the optimization and economic feasibility of HDH systems powered by renewable energy [10,12,13]. They found that through optimization and for certain operating and geographical constraints the total production cost can be cut by 7-28%. Furthermore, the use of solar energy with HDH systems to desalinate the brackish water in rural territories proved to be a cost-effective process.

In contrast, some of solar powered HDH systems have the constraint of periodic operation. This limitation is due to the availability of solar irradiation during the sunshine

hours. In order to tackle this issue, Yuan and Zhang [14] have introduced an HDH system that can operate continuously. They developed a mathematical model to study the system under different operating conditions. The system works on a closed air loop and powered by solar energy. They found that increasing the flow rate of saline water without changing the solar collector size would decrease the productivity of potable water. In another paper by the same authors [15], they found that their system can produce 2.7 kg/m^2-day in winter and 5.2 kg/m^2-day in summer.

Zhang et al. [16] have studied solar powered HDH system with air bubble humidifier. The results showed that in order to enhance the effectiveness of the humidification process more heat input is required in the air bubbling stage. Another compact HDH system has been examined by Ghazal et al. [17] in which they used sieves to modify the air bubbles size to enhance the heat transfer process. They replaced both the evaporator and solar heater with a modified solar collector which reduced the size of the conventional HDH system. Air is passed to the humidifier as bubbles through it. These modifications allowed improving the humidification process by 32%. In addition, the effect of configurations on the performance of HDH systems that can be driven by solar energy has been reviewed by Narayan et al. [18]. They found that the production cost of the multi-effect closed-air open-water (CAOW) water heated system to be $ 3 to 7/m^3. This system was considered to be the most effective in terms of energy consumption.

Müller–Holst stated that CAOW arrangement has the least energy consumption among other HDH configurations [19]. In an effort to optimize solar collectors that are used in HDH systems, many studies concentrated on using parabolic trough solar collector [3,

20,21]. They used solar collector that incorporates synthetic oil and water as heat carrying fluids. They reported a thermal efficiency of 69.73-72.24 % in Algeria [21]. Furthermore, the effect of using external reflector has been studied theoretically and experimentally by Elminshawy et al. [22]. This study found an enhancement in evaporation process and the system productivity as a result of using the external reflector and water heaters. They reported an efficiency of 0.77. The production cost was found to be USD 0.035/Litre.

The potential of linking HDH systems to geothermal energy as a renewable energy source has been investigated by Ghalavand et al. [23]. They used geothermal energy as a heat source to power the desalination process. Another researcher studied this configuration analytically and experimentally [24]. They tried to optimize the water to air mass flow rate ratio and the temperature difference between the cooling water in the condenser and the heated water to enhance the system productivity. They found the optimum range for saline water to air mass flow rate ratio to be 1.5-2.5.

Many studies have focused on the optimization of each component of the HDH systems. They tried to come up with innovative designs to improve the performance of HDH systems [25,26]. Innovative designs to reduce the dehumidifier size by the employment of direct contact HDH process has been studied by Niroomand et al. [27]. They indicated that a direct contact dehumidifier has a higher impact on the productivity than the direct contact humidifier. The feasibility of this method is further assured by the work of many researchers [28,29]. They found this process resulted in marginal humid air pressure loss

and increased the heat transfer efficiency in the dehumidifier. They recommended this design be used in small-scale water production.

The potential of replacing air with another carrier gas has also been investigated by many researchers [30,31]. They found that carbon dioxide as a carrier gas instead of air offered a good solution to calcium scaling and more fresh water can be produced. Hydrogen and helium gasses performed better in terms of achieving high rates of heat transfer, while carbon dioxide was better for high mass transfer rates.

The major drawback of HDH system is its high-energy consumption compared to the conventional desalination plants. To tackle this issue, researchers came up with different solutions [32–34]. The integration of vapor compression, desiccant air dehumidification and membrane air with HDH systems has been investigated among these solutions. However, the mechanical vapor compression solution may end up to be more energy consuming if it is not addressed carefully. The use of either solid (zeolite) or liquid (lithium bromide solution) desiccant to dry the air has been investigated as another possible solution to reduce energy consumption. Though the use of this design adds to the complexity of the HDH system which is not desirable [33].

Further investigation has been carried out on using a membrane to dry a compressed humid air that passes through it. In this design, they compressed the air in an air compressor. The membrane properties allowed only humid air to pass through to the permeate side [34]. Zhang et al. [35] have investigated humidification process analytically and experimentally through an air membrane system. They reported a decrease in the performance of the HDH system as a result of employing a membrane

module made from fiber. A novel mechanical compression HDH system has been introduced by Ghalavand et al. [23]. The system was more energy efficient and has higher recovery rate when compared to the conventional HDH systems. Gao et al. [36] designed another HDH system that has a mechanical vapor compression (MVC) pump. They reported a production of 60 kg/day of potable water at an electrical energy consumption rate of 500 W (compressor rated power). In comparison with conventional HDH configurations, the MVC HDH system was more energy efficient [37]. Furthermore, it has a higher gained output ratio (GOR) when compared to the conventional water-heated HDH system.

Another alternative system to the traditional HDH configuration was the use of a thin wall to transfer heat between the humidifier and the dehumidifier. As the humid air condenses on this wall and loses its heat through it to be used in the evaporation process in the humidifier. This system combined the humidifier and the dehumidifier in a single unit which is separated by a wall [37]. Saline water is sprayed to form a thin film on the humidifier side of the wall and as vapor condenses on the other side, heat is gained by this film. This configuration enhanced the evaporation process. They reported a GOR of 9.6 for seawater and 16.8 for brackish water [38]. This design could compete with the conventional desalination plants in terms of energy consumption [38,39]. Hamieh and Beckman [39] have examined this design experimentally and economic analysis has also been Presented. This system proved to have the best salt rejection when compared to other HDH systems.

Heating and dehumidification of air in series is another system that has been investigated in the literature. These sequential processes can be done in 4 to 5 stages. The basic concept behind this system is increasing the humidity of the air at the exit of the dehumidifier, which can increase the productivity of the system [40]. Kang et al.[41] proposed a multi-effect HDH desalination system. They varied the operating parameters to investigate the performance of this design. Experimental work was carried out on this system to validate the mathematical model. They reported a GOR of 2.44 and up to 72.6 kg/h of potable water was reported. In this design, a heat recovery process was obtained by making use of the latent heat of condensation and the brine residual heat.

Another multi-effect HDH system with two stages was introduced by Hou [42]. A pinch temperature model has been followed. Tests have been conducted for a higher and lower temperature ranges 60-80 °C and 30-60 °C, respectively. The system is solar driven that employs a solar evacuated tube to heat the air. A higher GOR has been reported for the two-stage compared to single stage HDH process. Another experimental study was carried out for a two-stage multi-effect HDH system by Zamen et al. [43]. This system has been used to treat brackish water and produce drinkable water. They built a pilot system that has a solar collector with a total area of 80 m^2. The tests have been carried out for both summer and winter operating conditions. The produced fresh water in winter was less than half of the amount produced in summer. Their results also showed a significant improvement with two stages. The total heat input was reduced for the double stage HDH process; thus the cost per unit of water produced is reduced for this configuration. An increase of 20% in productivity was observed for the double stage relative to the single stage system.

A hybrid system consisting of HDH cycle and air conditioning cycle has been examined by Nada et al. [44]. They evaluated the performance of this system experimentally by varying the operating conditions and observing their relevant effect. An increase in potable water production has been reported for increasing air mass flow rate and specific humidity. A combined system between two-stage HDH cycle and cooling cycle has been investigated [45]. The cooling system was basically a vapor absorption refrigeration (VAR) system with a solar concentrator, while the HDH system used a flat plate solar collector. This integration was based on the idea of increasing the energy utilization factor (EUF), which is the ratio of the maximum load consumed to the rated capacity of the system. An enhancement in the EUF was reported at high effectiveness humidifier. This integration resulted in an increase from 270 liters per hour to 400 liters per hour. Further increase in the amount of produced potable water was reported. A value of 0.33 and 0.58 of the EUF was reported for the plant and the cycle respectively [45].

The problem of increasing the size of HDH systems for commercial applications is mainly limited by high energy consumption. This fact motivated the idea of hybridization with the conventional desalination plants. Plenty of work in the literature was devoted to this issue [37,46,47]. For example, Nada et al. [48] have investigated the HDH system coupled with air conditioning system. For hot climate regions, the performances of many hybrid configurations have been evaluated in terms of fresh water production and the reduction in required thermal energy. In general, an increase in the amount of produced potable water was reported when the supplied air temperature was increased.

In addition, Yildirim et al. [47] have investigated another type of combined system between HDH cycle and thermoelectric cooling cycle. They developed a pilot set-up to evaluate the performance of this integration. The HDH configuration was the open-air open-water system. They reported a potable water mass flow rate of 0.1346 kg/day and a 0.78 for the cooling unit coefficient of performance. They found that total amount of produced freshwater was a weak function of the mass flow rate of the water for the tested values. However, the COP of the cooling cycle was increased as the mass flow rate of the water decreased. In an attempt to reduce the energy consumption of a combined system between HDH and reverse osmosis was proposed by Narayan et al. [46]. The GOR of this combined system was 20, which is a significant increase when compared to traditional HDH systems.

The system that integrates HDH system with the single stage flash desalination system has been studied in the literature [49,50]. The HDH configuration used for this design was air-heated, which is coupled to the evaporator where flash evaporation process took place. The heat input was generated from a solar collector that used to heat both air and water [50,51]. The economic feasibility of this system was evaluated in a separate work [52]. Based on the economic model they have found that the combined system had a better productivity and was more economically than the standalone system. Furthermore, Eslamimanesh and Hatamipour [53] have conducted a study to compare the performance of a pilot HDH set-up to a reverse osmosis system from an economic point of view. They suggested to couple HDH system with the reverse osmosis plant in order to obtain the optimum performance. Recent studies have focused on the integration of HDH systems

with waste water treatment plants [54–57]. This combination provides HDH with another advantage to serve in a wide range of water process applications.

2.2 Thermal Balancing and Extraction

Müller–Holst proposed to vary the water to air mass flow rate ratio continuously in order to achieve thermal balancing of HDH systems [58,59]. This variation will decrease stream to stream temperature difference. They make use of natural convection to circulate the moist air stream through ports in both the humidifier and the dehumidifier. This circulation will result in a variation of the water to air mass flow rate ratio. After optimization, the system has 120 kWh/m^3 (≈450 kJ/kg) as total heat input. Another novel approach to varying the water to air mass flow rate ratio was introduced by Zamen et al. [60]. They designed a multi-stage process, in which, humidification and dehumidification processes are executed in sequence. The brine flow was common for all stages, while the air flow was separate for each stage. Schlickum [61] and Hou [42] reported a similar design. Zamen et al. [60] have defined the system by the temperature pinch approach. The total heat consumed by this system was about 800 kJ/kg. The humidifier and dehumidifier both have a temperature pinch of 4 °C, at a top cycle temperature of 70 °C and bottom cycle temperature of 20 °C.

A novel HDH system driven by forced convection was invented by Brendel [62], [63]. Under balanced temperature profiles, forced convection was used to extract water from the dehumidifier and was injected in the dehumidifier. This extraction process was executed at several points in both the humidifier and the dehumidifier. Thiel and Lienhard [64] have stated that the optimization of heat and mass transfer exchanger

(HME) devices thermodynamically require considering both temperature and concentration profiles. They have shown that balancing humidity profile have more significance in the optimization of the system than balancing the temperature profile. Forced convection driven HDH systems with air extraction and injection have also been investigated by Younis et al. [65]. They have succeeded to increase the system efficiency as the energy consumption decreased to 800 kJ/kg. In their system, the air was extracted from two points in the humidifier and injected to the dehumidifier. They followed enthalpy-temperature diagrams, as in several other publications [58,60,62,66] to illustrate the extraction impact on the design of HDH system.

Thermal balancing by extracting air or water from the humidifier and injected it into the dehumidifier or vice versa has been investigated by Narayan et al. [67]. Mistry et al. [68] found that reducing the specific entropy would result in minimizing the GOR. Miller and Lienhard [69] studied the effects of extraction on balancing enthalpy rates in HDH systems. They followed an effectiveness-based methodology. Their main conclusion was that extractions are better for systems that have a high effectiveness in both humidifier and dehumidifier.

The variation of temperature pinch effect on both recovery ratio (RR) and GOR has been studied by McGovern et al. [66]. They showed an increase in GOR from 3.5 to 14 by incorporating single water extraction. That increase was achieved by using bottom cycle temperature of 25 °C and top cycle temperature of 70 °C and assuming effective heat and mass transfer area to be very large. Furthermore, for single water extraction and under same operating conditions they reported an increase in RR from 7% to 11%.

Despite all of the above publications on this subject, still, there are concepts remained unclarified. In an attempt to clarify these concepts, Narayan et al. [70] defined a novel parameter called the enthalpy pinch. They used this parameter to balance HME devices since this parameter takes into account both heat and mass transfer processes that are occurring in HDH systems. Balanced systems that have zero extraction, one extraction and an infinite number of extractions were defined using the enthalpy pinch approach. An increase in the GOR from 2.6 to 4.0 for a system with single air extraction has been reported in an experimental study by Narayan et al. [71]. In this experimental study, the enthalpy pinch was 19 kJ/kg of dry air. Bottom and top cycle temperature were 25 °C and 90 °C, respectively.

Chehayeb et al. [72] in continuation of the previous work by Narayan et al. [70] have investigated the effect of extractions on the GOR, RR, and the total heat input to the cycle. They examined a finite number of extractions and found that the smaller the enthalpy pinch the larger the impact of balancing. That is, when the heat and mass transfer areas decrease (large enthalpy pinch), the balancing loses its significance. Furthermore, they found that the balancing effect on water recovery is not significant compared to its effect on energy efficiency. Chehayeb et al. [73] in another investigation studied the effect of extraction on a fixed-size HDH system with the double stage of HDH processes. They proposed generalized energy effectiveness for HME devices. Their model was constructed from a multi-tray bubble column dehumidifier and a packed-bed humidifier. Their results pointed out that thermodynamic balancing maximizes both the GOR and water recovery while keeping entropy generation at minimum levels. Furthermore, they indicated that the direction of extraction should always be from the

humidifier to the dehumidifier to reach a balanced system. It was stated that total balancing can be difficult to achieve at all locations, hence the location of extractions can be vital in the effort to attain complete thermal balancing.

Thermal balancing is a well-known concept in heat exchangers devices. To develop a basic understanding of this concept we take the limiting case where heat transfer area approaches infinity. For such a device the rate of entropy generation is mainly because of 'thermal imbalance' or what also called 'remanent irreversibility' [70]. When the streams in this device have a different capacity rate value this contribute to the so-called 'thermal imbalance' [74]. Thus, for the thermally balanced heat exchangers, the ratio of the heat capacity rate (HCR) must equal unity. Recently this concept has been applied to HME devices [67]. Narayan et al.[67] modified this ratio to suit the HME devices, and it was defined as the cold stream maximum enthalpy rate change to the maximum enthalpy rate change of the hot one. To obtain the maximum change the ideal exit states for each stream should be defined. Thiel and Lienhard [75] fixed the size of the HME device, the rate of heat transfer and the rate of condensation and observed that the minimum entropy generation in the dehumidifier occurred at HCR equals unity. In this case, one could claim that the balanced state occurs when the value of HCR approaches unity regardless of fixing device size or effectiveness. Theoretically, the complete balanced HME device has a constant temperature and humidity difference along the length of it [76]. The non-linear relation between humidity and temperature saturation curve proved that it is impossible to achieve this equipartition for both humidifier and dehumidifier simultaneously [70], [75]. The extraction arose as a good solution to this issue, though it cannot achieve zero entropy generation [70].

2.3 Thesis Overall Objectives

The struggle to improve HDH system has been discussed in the literature review. Part of these studies has focused on improving the thermodynamic performance of the HDH system through thermal balancing. Thermal balancing through extraction of one of the flowing fluids from one component and injecting it to the other has proved to be one of the vital solutions to the basic drawback of the HDH systems, i.e., efficient utilization of energy input. In this work, several studies of modified HDH cycles analytically and experimentally are carried out.

2.3.1 Performance Evaluation of a Modified Closed-Water Open-Air (CWOA) System

This objective mainly consists of an experimental investigation of the performance of a modified CWOA HDH system. An experimental set-up is constructed, which is equipped with a data acquisition system to record readings from thermocouples on a real-time basis. The results of different parameters then are analyzed and compared with the model results. The analytical model for this system is implemented on an EES software and validated against the experimental results.

2.3.2 Performance Evaluation of The Basic Open-Water Open-Air and The Modified Closed-Water Open-Air (CWOA) Systems

In this objective, a thermodynamic study for 0% brine recirculation at the humidifier exit for an OWOA cycle and 100% brine recirculation (modified CWOA cycle) is conducted from an energy perspective first. Further analysis is then presented in an exergo-

economic study of these cycles, also an alternative option to the modification which is basically a heat recovery process are explored through coupling the HDH system with an RO module.

2.3.3 Performance Evaluation of the Basic and Modified Closed-Air Open-Water (CAOW) HDH System with and without Air Extraction

The work in the literature regarding air extraction has focused on water heated CAOW cycle as a basic configuration. In this objective, an analysis for this cycle combined with two modifications to close the water loop is presented. In this regard, a proposal to modify the CAOW arrangement by using heat recovery process is made. The heat recovery process is executed through two approaches, a mixing chamber, and a heat exchanger. Furthermore, the use of single and double air extraction and injection to thermodynamically balance the system following the enthalpy pinch model is carried out. Zero, single and double extraction models are evaluated for conventional CAOW water heated cycle as well as the modified cycles. The basic aim of this analysis is to generate an operating scheme that helps to identify the optimum performance region for each of these arrangements.

CHAPTER 3

Theoretical and Experimental Study of Modified Closed Water Open Air HDH System

In this chapter, two studies are carried out the first one is an experimental investigation and the second study is an analytical investigation of the modified water heated CWOA HDH system and the basic OAOW HDH system.

3.1 System Description

In this section, a detailed description of the basic and modified cycles is presented.

3.1.1 Open Water Open Air HDH system

This is a basic cycle which consists of an open-air loop and open-water loop as shown in Figure 3.1. The saline water is passed through the dehumidifier and then heated in the heater before it is sprayed in the humidifier. The sprayed saline hot water is then evaporated partially and the rest is then thrown away as rejected brine. The evaporated water is then carried with the dry air coming from the blower and leaves the humidifier as a hot and humid air. This air is then passed to the dehumidifier where it condenses and the condensate water is collected as fresh water, while the air leaves the system.

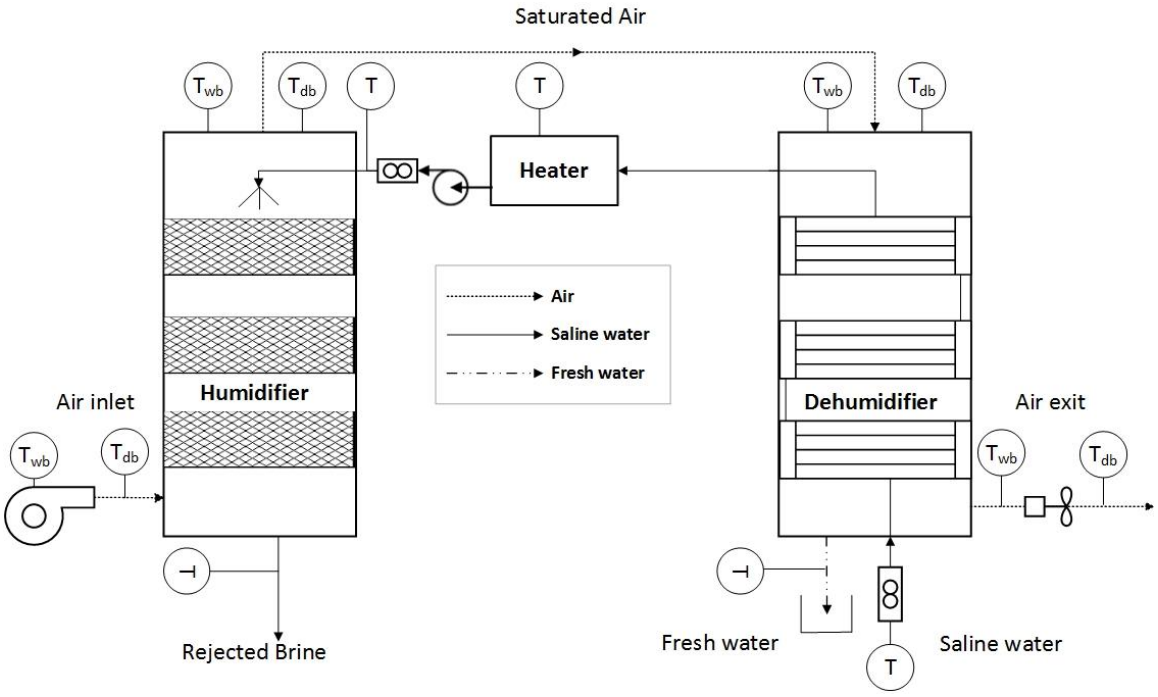

Figure 3.1 Open-Air Open-Water HDH System.

3.1.2 Modified Closed Water Open Air HDH System

As illustrated in Figure 3.2 this system consists of the same components as the previous system. The modification is basically in the water loop which is closed. The saline water enters the dehumidifier and absorbs heat from the hot humid air and partially admitted to a tank as make-up water and the rest is thrown away. The water from the tank is then sprayed in the humidifier and evaporates. The portion which is not evaporated is then collected and circulated back to the tank to close the water loop.

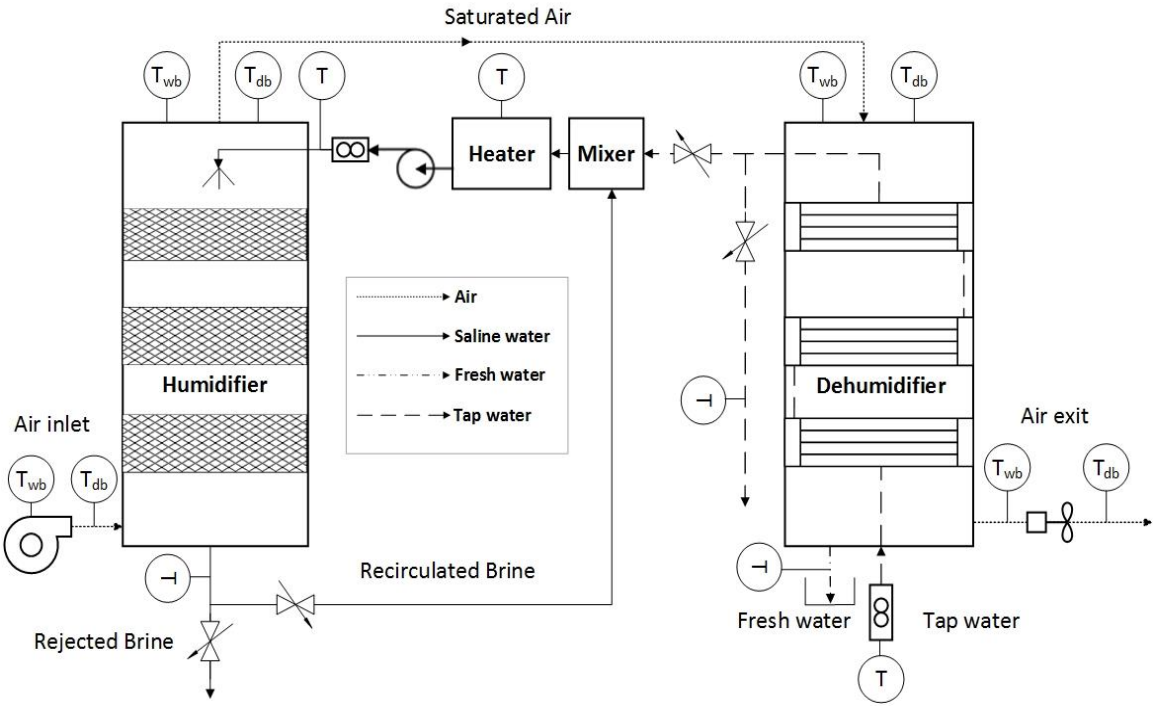

Figure 3.2 Modified Closed-Water Open-Air HDH System.

3.2 Performance Metrics and Modelling

The GOR is the ratio of the latent heat of vaporization of fresh water to the amount of heat utilized to produce it.

$$GOR = \frac{\dot{m}_{fw} \times h_{fg}}{\dot{Q}_{in}} \quad (3.1)$$

The effectiveness of the dehumidifier is defined as [77]:

$$\varepsilon_{deh} = \max \left\langle \frac{h_{a,in} - h_{a,out}}{h_{a,in} - h_{a,out,ideal}}, \frac{h_{w,out} - h_{w,in}}{h_{w,out,ideal} - h_{w,in}} \right\rangle \quad (3.2)$$

The ideal enthalpy of the outlet air is taken at the temperature of the inlet water, while the ideal enthalpy of the outlet water is measured at the inlet air temperature [77].

The effectiveness of the humidifier is expressed as [77]:

$$\varepsilon_{hum} = \max\left\langle \frac{h_{a,out} - h_{a,in}}{h_{a,out,ideal} - h_{a,in}}, \frac{h_{w,in} - h_{w,out}}{h_{w,in} - h_{w,out,ideal}} \right\rangle \quad (3.3)$$

Similarly the ideal enthalpy of the outlet air is taken at the temperature of the inlet seawater, while the ideal enthalpy of the outlet seawater is measured at the inlet air wet bulb temperature since the air loop is open, and wet bulb temperature is less than the dry bulb temperature; therefore, the water can be cooled further [77].

Another metric used in this study is water to air mass flow rate ratio (MR), and the modified heat capacity rate as defined in Narayan et. al [67]:

$$MR = \frac{\dot{m}_w}{\dot{m}_a} \quad (3.4)$$

$$HCR = \frac{\Delta H_{\max,cold}}{\Delta H_{\max,hot}} \quad (3.5)$$

An EES code is written based on a set of governing equations, which is basically mass and energy balance for each component. Then the effectiveness equations for both humidifier and dehumidifier are added to complete this set of equations [77].

Dehumidifier mass and energy balance equations:

$$\dot{m}_{fw} = \dot{m}_a(\omega_{in} - \omega_{out}) \quad (3.6)$$

$$\dot{m}_w(h_{w,out} - h_{w,in}) = \dot{m}_a(h_{a,in} - h_{a,out}) - \dot{m}_{fw}h_{fw} \quad (3.7)$$

Heater energy balance equation (for the basic cycle):

$$\dot{Q}_{in} = \dot{m}_w(h_{w,out} - h_{w,in}) \quad (3.8)$$

Heater mass and energy balance equations (for the modified cycle):

$$x = \frac{\dot{m}_w - y\dot{m}_b}{\dot{m}_w} \quad (3.9)$$

where x presents the fraction of mass flow rate which is used as a makeup and y is the fraction of rejected brine mass flow rate which is recirculated to the tank (heater).

$$\dot{m}_w h_{w,out} = \dot{Q}_{in} + y\dot{m}_b h_b + x\dot{m}_w h_{w,in} \quad (3.10)$$

The humidifier mass and energy balance equations, give

$$\dot{m}_b = \dot{m}_w - \dot{m}_{fw} \quad (3.11)$$

$$\dot{m}_w h_{w,in} - \dot{m}_b h_b = \dot{m}_a (h_{a,out} - h_{a,in}) \quad (3.12)$$

The above equations are the key equations used in the model and certain assumptions are followed which can be summarized as follows:

- Steady state conditions.
- Heat input is taken to be 4.5 kW.
- Properties are evaluated at atmospheric pressure and use for sea water are based on Sharqawy et al. [78] work.
- Air inlet temperature is at 26 °C and 50% relative humidity.
- Air leaves both the humidifier and dehumidifier at 90% relative humidity.
- The feed water mass flow rate of 0.07 kg/s with salinity 35 g/kg.
- Water inlet temperature is at 21 °C.

3.3 Experimental Investigation

Desalination is basically a process of producing fresh water out of the saline water through various techniques. One of these methods is the HDH system, which is the

system under study in this work. The set-up is constructed earlier as a term project in the department. After an initial run for the system, the results obtained were not satisfying so certain modifications and calibrations are carried out to obtain reliable and repeatable results. In this chapter, a comprehensive description of the system and the modification done are presented. Furthermore, the results obtained are presented and discussed.

3.3.1 Set-up Description

The system under consideration is a modified water heated closed-water open-air CWOA. Figure 3.3 illustrates the system configuration. Raw water is used as cooling water from a tap in the lab. This water is passed through a flowmeter then into a dehumidifier, which has dimensions of (122x30.5x30 cm^3). It consists of three condensers. After that, the warm raw water is partially passed to the tank as make-up in the first configuration, the rest is thrown away. The tank is filled with this raw water, which has a salinity of 2500 ppm and is equipped with 4 electrical heaters (1.2 kW, 1.2 kW, 1.2 kW and 2 kW).

A pump is then used to draw the hot raw water and pass it through a valve and a flowmeter to control the flow rate of the feed to the humidifier. After that, the hot water is sprayed in the humidifier. The humidifier acts basically as a cooling tower with dimensions of (122x30.5x30 cm^3) and has a packing material to increase the contact area. Water coming out of the humidifier (rejected brine) is then circulated back to the tank.

The forced air stream is provided by an air fan with three speeds i.e. three air mass flow rates (0.055, 0.066 and 0.08 kg/s). The dry air is then moved in a counter flow manner from the bottom of the humidifier through the packing material and carries the water

vapor and leaves as a hot humid air. It is then ducted in the dehumidifier where it passes through the condensers where the water is condensed and the cold air is rejected to the atmosphere. The distilled water is then collected and measured to calculate the flow rate of the product.

The set-up is equipped with K-type thermocouples that are connected to a data acquisition system to record temperatures of both water and air streams on a real-time base as shown in Figure 3.3. LabVIEW software is used to run the data acquisition system and the results are then recorded on a Microsoft Excel file.

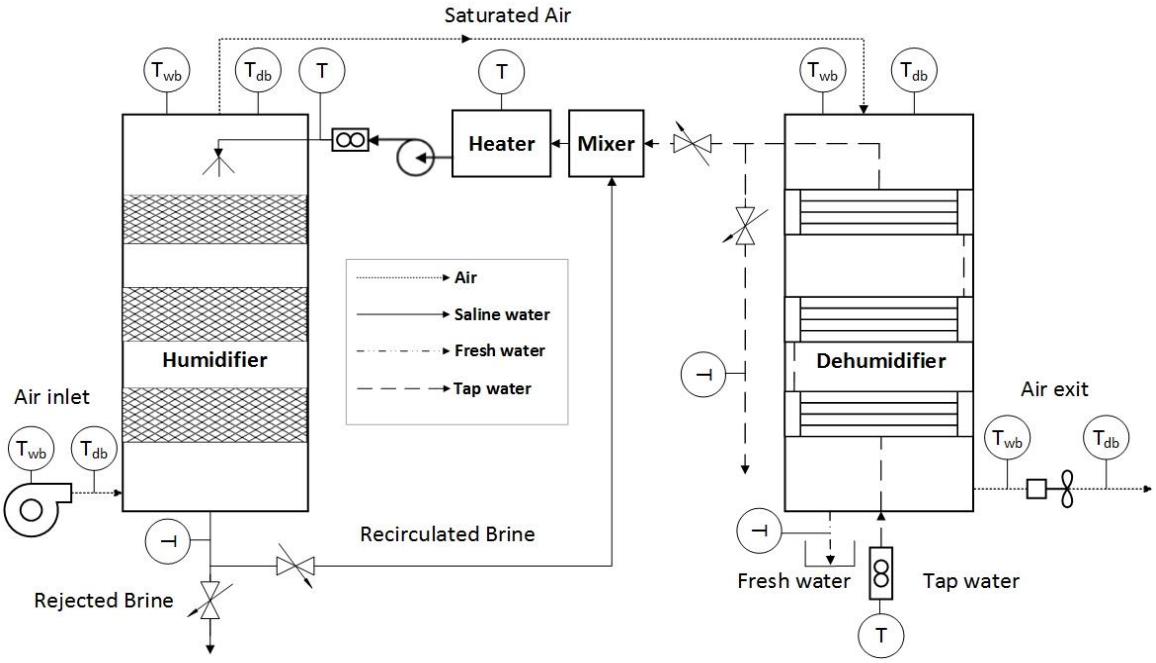

Figure 3.3 Experimental set-up description.

3.3.2 Modifications and Calibration of the Set-up

Based on previous recommendations several modifications have been done to calibrate the system to ensure reliable results.

3.3.2.1 Humidifier

The packing material, cellulose pads, was consisting of 3 pieces of 10 cm each in height. The height of the packing material was originally 30 cm in total which resulted in low effectiveness. Some pieces of 10 cm height are replaced with 15 cm thick pieces to increase the height of the packing material to 65 cm in total. At the exit of the humidifier, there was a small fan which has been replaced with a mesh from the humidifier side to act as a demister. A piece of Lofa is also placed at the inlet of the dehumidifier to serve the same purpose. A flowmeter to control and measure the flow rate of the feedwater to the humidifier is also installed after the pump and before the humidifier. These modifications are shown in Figure 3.4.

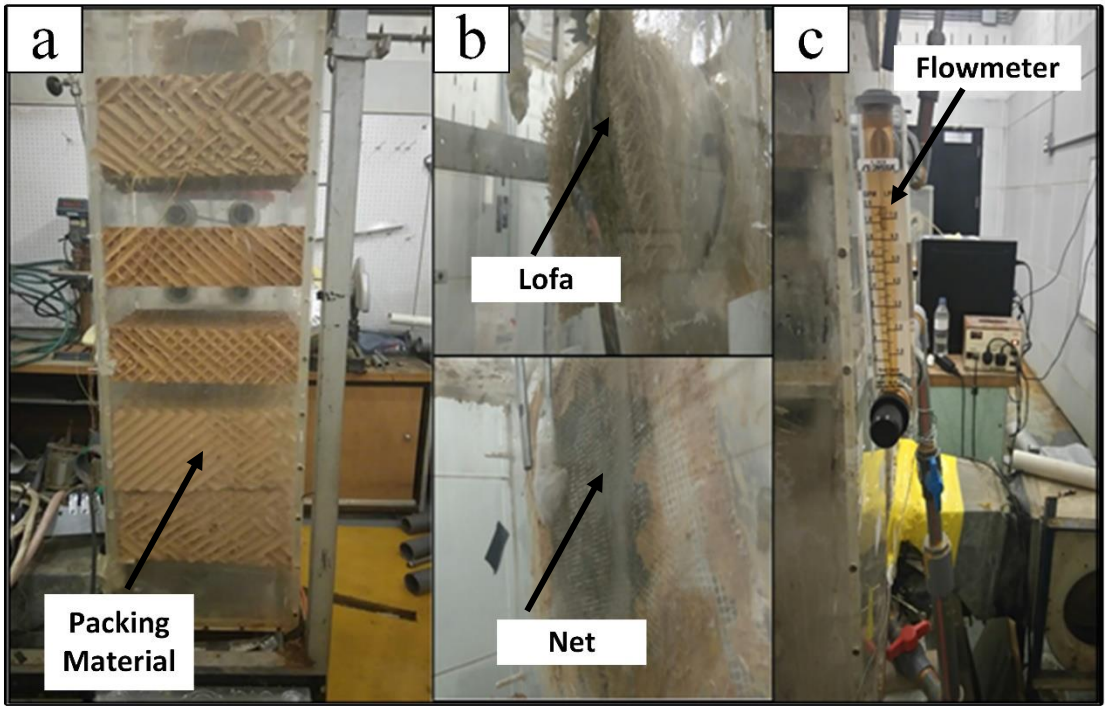

Figure 3.4 Humidifier modifications and calibration: (a) packing material; (b) net and Lofa; (c) flowmeter.

3.3.2.2 Heater

The heater is basically a tank (62x36x43 cm^3) equipped with 4 electric heaters. It was made of fiberglass which deforms with heat and then leaked. In order to tackle this issue, the tank is reconstructed from metal sheets. Another problem arose which is heat loss because of the use of metal, which transfers heat to the surroundings. Glass wool blanket batts insulation is then applied to cover the tank from all sides but the top. A cover made of Polystyrene foam is then placed on the top to complete the insulation. This work is shown in Figure 3.5.

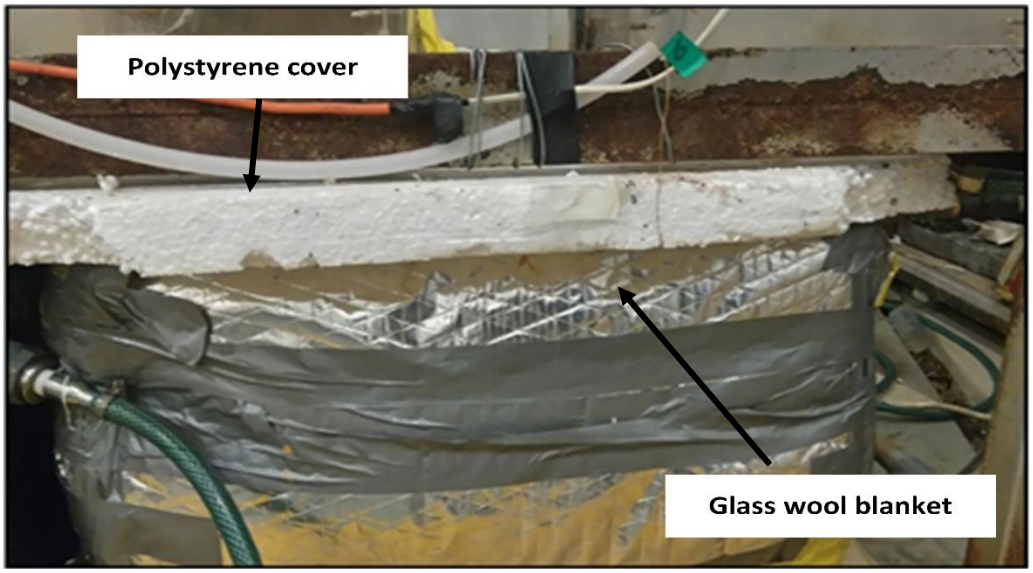

Figure 3.5 Insulated tank.

3.3.2.3 Dehumidifier

A flowmeter is installed before the dehumidifier to measure and control the flow rate of the cooling water as it passes through it. Figure 3.6 illustrates the location of the flowmeter.

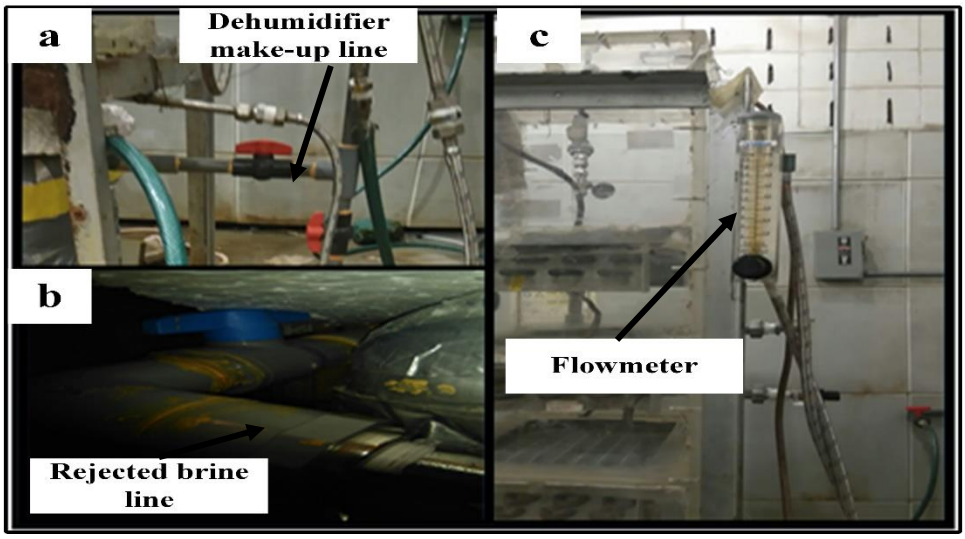

Figure 3.6 Dehumidifier modification and calibrations: (a) make-up water line; (b) rejected brine line; (c) flowmeter.

3.3.2.4 Piping and Electrical wiring

Pipe connections from the dehumidifier to the tank are constructed in a way to allow some of the water coming out of the dehumidifier to be admitted to the tank as make-up water with the help of a float valve, which is installed inside the tank. To run another configuration of the system, an additional valve is installed to make sure that all water coming out of the dehumidifier is directed back to the tank. These connections are illustrated in Figure 3.6. The electrical components (heaters, air fan, and the pump) were connected to electrical sources, separately. An electrical box is installed to combine all of them in one unit which can be controlled easily through switches. This modification is exhibited in Figure 3.7.

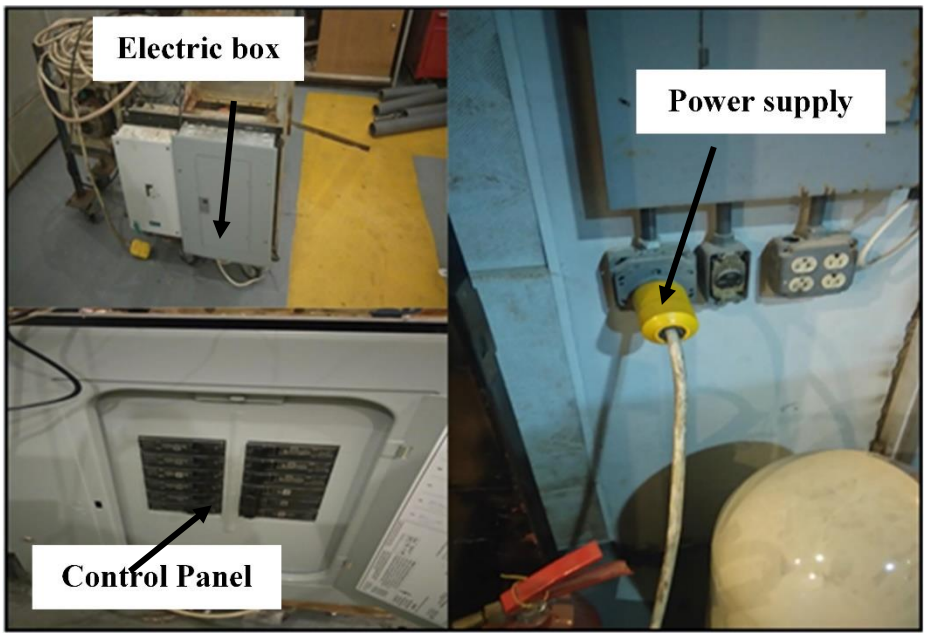

Figure 3.7 Electrical box connections.

3.3.3 Uncertainty Analysis

Since we are measuring temperatures and volumetric flow rates it is necessary to evaluate the effect of these measured values on the system performance parameter GOR. EES provide this tool to perform the sensitivity analysis. K-type thermocouples have an uncertainty of ±0.1 °C. Flowmeters are of type FL50000, which have an uncertainty of ±5%. Air flowmeter is used to measure the speed of air and then the mass flow rate of air is calculated, which has an uncertainty of ±0.5%. The GOR calculated from the experiment is dependent only on the temperature and flow rate of the potable water. This flow rate is calculated from the produced fresh water over a 1 hour period, which is collected in a graduated cylinder with an accuracy of ±12 ml. The maximum uncertainty is then calculated for the experimental GOR, which is found to be ±2.22%. Additional

details with regard to the uncertainty analysis for the effectiveness and GOR is presented in Appendix A.

3.4 Experimental Results

In this section, the experimental results are compared with the analytical results. These results are presented in a graphical form to help validate the analytical model. It is found that the maximum GOR was 0.4 on a total heat input of 4.4 kW and under two different water-to-air mass flow rate ratios (MR) of 1.81 and 2.27. The minimum GOR was 0.23 and found under total heat input of 3.2 kW and MR of 1.36.

Figure 3.8 presents the effect of changing MR by varying the water mass flow rate on the GOR at 5.6 kW heat input. As expected, the trend indicates the increase in GOR as the MR increases, which is associated with increasing the amount of water supplied to the system. As the mass flow rate of the water increases that means more vapor is generated in the humidifier. Thus more condensate water is extracted in the dehumidifier. The difference between the experimental and analytical GOR is within ±5% deviation which indicates that the analytical code is validated for design and performance evaluation purpose. The computer code showed that the GOR increased from 0.35 to 0.38, while the experimental values from 0.33 to 0.37 for changing MR from 1.36 to 2.27, respectively.

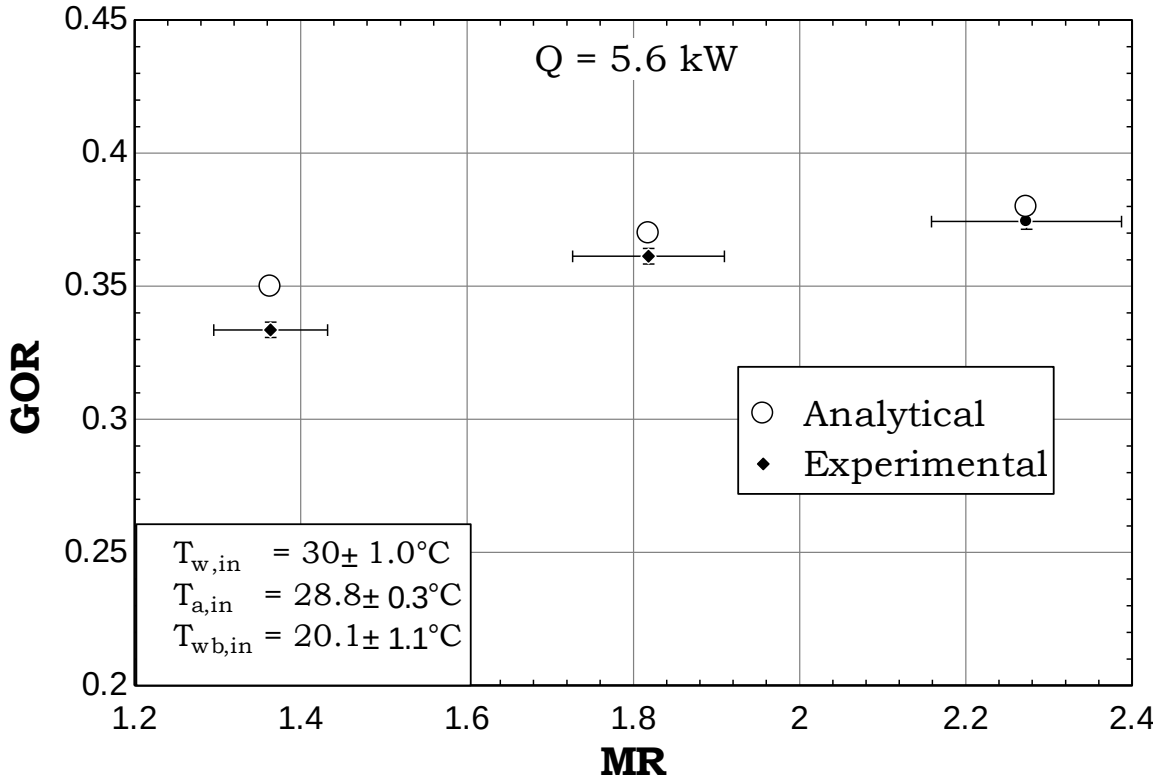

Figure 3.8 Effect of water to air mass flow rate ratio on the GOR.

The effect of MR on the GOR at 4.4 kW heat input is illustrated in Figure 3.9. The deviation between the analytical and experimental GOR values is also under ±5%. The experimental GOR shows an increasing trend as MR increases, which is due to the increased amount of evaporation. The analytical GOR reaches a maximum of 0.42 at MR equal to 1.81 and then drops slightly to 0.41 due to the increase of temperature of the water that enters the dehumidifier. This increase affects the capacity to condensate more distillate and consequently results in the slight reduction of GOR. The experimental GOR reaches a maximum of 0.4 at MR equals 1.81 and decrease to a value slight below 0.4 as MR increases to 2.27 which are similar to the analytical behavior.

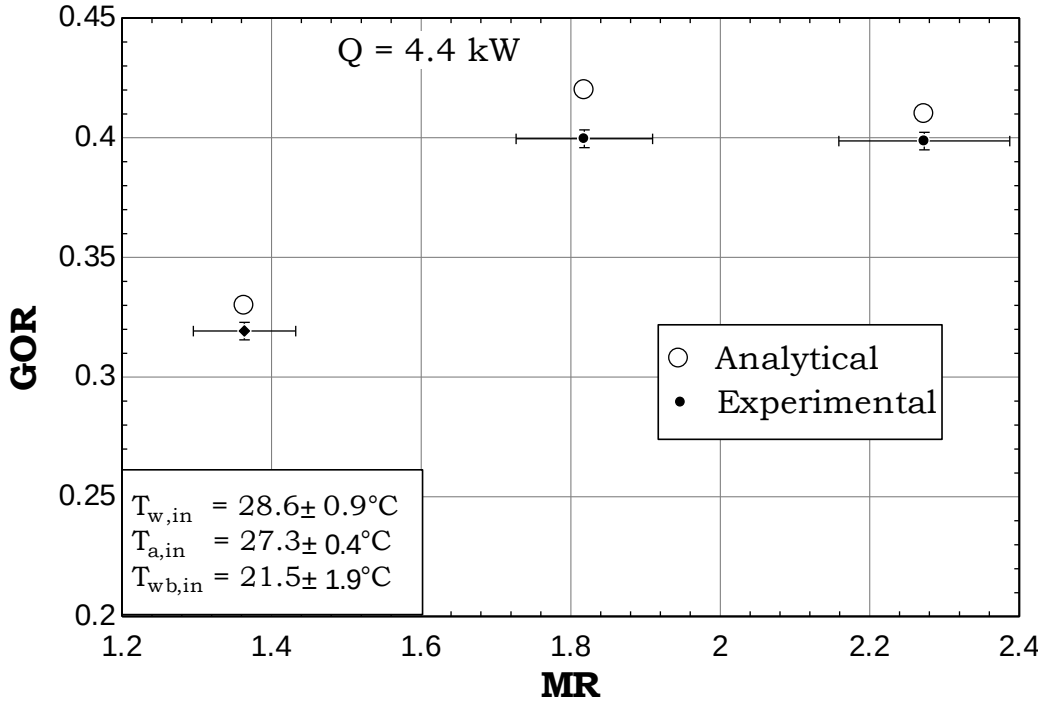

Figure 3.9 Effect of water to air mass flow rate ratio on the GOR.

At total heat input of 3.2 kW, the effect of MR on GOR is shown in Figure 3.10. The deviation between the analytical GOR and the experimental one is also under ±5%. The analytical GOR increases as MR increases to reach a peak of 0.34 at MR= 1.81 and then drops to 0.29 at MR= 2.27. The experimental GOR has the same behavior, it reaches the peak of 0.32 at MR=1.81 and then drops to 0.28 at MR=2.27. Increasing MR through water mass flow rate increases the amount of generated vapor which means more product and consequently higher GOR. At MR =2.27 the GOR (both analytical and experimental) decreases compared to the GOR at MR=1.81. This is basically due to the cooler water through the condenser which results in a better condensation rate. It is important to note that the GOR at different operating conditions is low, this is due to the low humidifier effectiveness (refer to Figure 3.11) which results in a poor evaporation rate and consequently lower GOR values.

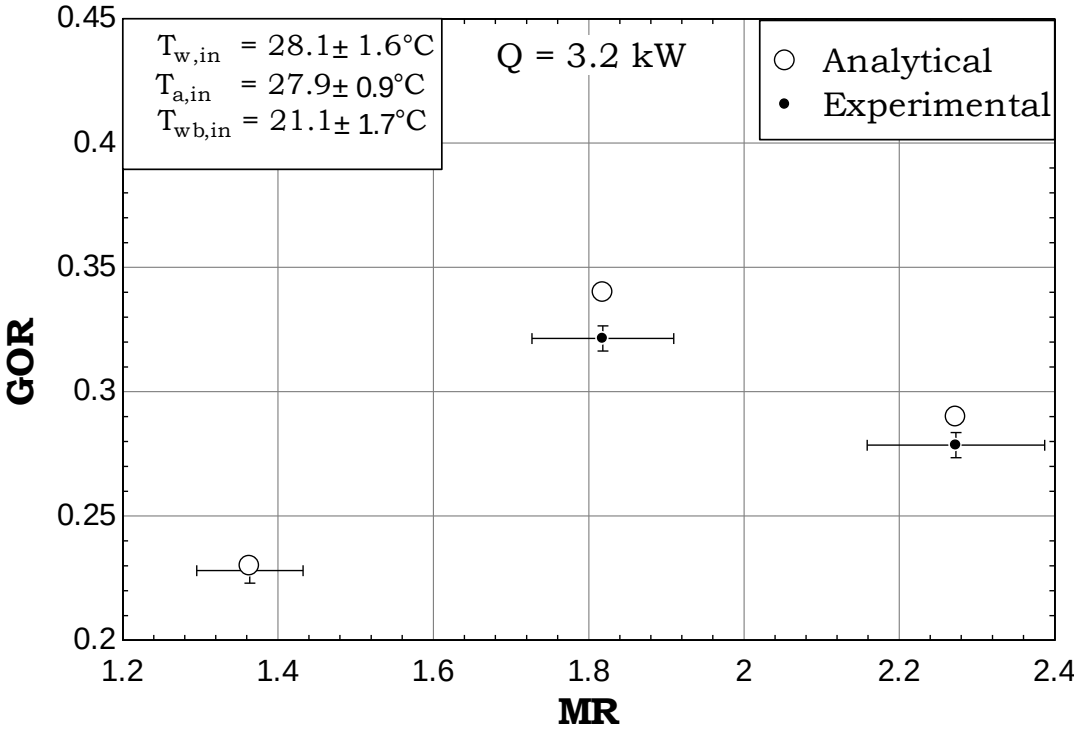

Figure 3.10 Effect of water to air mass flow rate ratio on the GOR.

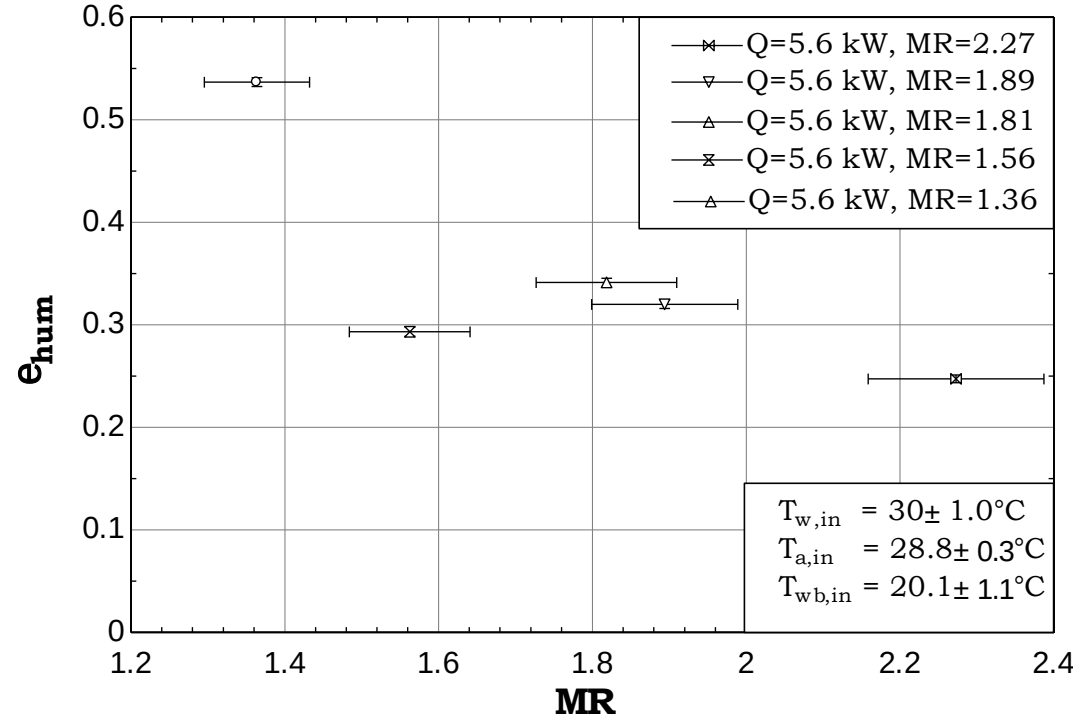

Figure 3.11 Variation of humidifier effectiveness versus MR at a heat input of 5.6 kW.

3.5 Results and Discussion of the Modified CWOA HDH System

After the code is validated against experimental results, a parametric study on the modified system is conducted which is presented in this section.

3.5.1 Valid Effectiveness Ranges for the Parametric Study

To perform the analysis of the modified cycle and to compare it with the basic cycle, the limits of components effectiveness are defined. The limits then are defined through basic condition, which is, the temperature of water recirculated back to the heater (T_{w4}) to be greater than that of make-up water coming from the dehumidifier (T_{w2}). This process is conducted for MR range from 1 to 3 with a step of 0.5 and then the working range of effectiveness is determined. Tables 3.1 through 3.5 illustrate the outcomes of this process. From this study, the following is observed: for the MR in between 1 to 3, the working range of humidifier effectiveness for a dehumidifier with the effectiveness of 0.5 is 0.4 to 0.6. Also for a dehumidifier effectiveness of 0.6 and 0.7, the humidifier effectiveness is 0.4 to 0.53, and for a dehumidifier effectiveness of 0.8 and 0.85, the humidifier effectiveness is 0.4 to 0.47.

Table 3.1 Components effectiveness valid for recirculation system at MR=1.

MR	ε_{deh}	ε_{hum}	T_{w2}	T_{w4}	Observation
1	0.5	0.40	24	31	MR = 1, ε_{deh} = 0.5, 0.4 < ε_{hum} < 0.6
1	0.5	0.47	25	30	
1	0.5	0.53	26	29	
1	0.5	0.60	27	28	
1	0.6	0.40	25	32	MR = 1, ε_{deh} = 0.6, 0.4 < ε_{hum} < 0.53
1	0.6	0.47	26	31	
1	0.6	0.53	28	30	
1	0.7	0.40	26	32	MR = 1, ε_{deh} = 0.7, 0.4 < ε_{hum} < 0.53

1	0.7	0.47	28	32	
1	0.7	0.53	29	31	
1	0.8	0.40	27	33	MR = 1, ε_{deh} = 0.8, 0.4 < ε_{hum} < 0.47
1	0.8	0.47	29	32	
1	0.85	0.40	28	33	MR = 1, ε_{deh} = 0.85, 0.4 < ε_{hum} < 0.47
1	0.85	0.47	30	33	

Table 3.2 Components effectiveness valid for recirculation system at MR = 1.5

MR	ε_{deh}	ε_{hum}	T_{w2}	T_{w4}	Observation
1.5	0.5	0.45	24	32	MR = 1.5, εdeh = 0.5, 0.45 < εhum < 0.67
1.5	0.5	0.47	24	32	
1.5	0.5	0.53	25	31	
1.5	0.5	0.60	26	30	
1.5	0.5	0.67	28	28	
1.5	0.6	0.40	24	33	MR = 1.5, εdeh = 0.6, 0.4 < εhum < 0.6
1.5	0.6	0.47	26	32	
1.5	0.6	0.53	27	31	
1.5	0.6	0.60	29	30	
1.5	0.7	0.40	25	33	MR = 1.5, εdeh = 0.7, 0.4 < εhum < 0.53
1.5	0.7	0.47	27	33	
1.5	0.7	0.53	29	32	
1.5	0.8	0.40	26	34	MR = 1.5, εdeh = 0.8, 0.4 < εhum < 0.47
1.5	0.8	0.47	29	33	
1.5	0.85	0.40	27	34	MR = 1.5, εdeh = 0.85, 0.4 < εhum < 0.47
1.5	0.85	0.47	30	33	

Table 3.3 Components effectiveness valid for recirculation system at MR = 2.0

MR	ε_{deh}	ε_{hum}	T_{w2}	T_{w4}	Observation
2	0.5	0.40	23	34	MR = 2, ε_{deh} = 0.5, 0.4 < ε_{hum} < 0.86
2	0.5	0.47	23	33	
2	0.5	0.53	24	32	
2	0.5	0.60	24	32	
2	0.5	0.67	25	31	
2	0.5	0.73	26	30	
2	0.5	0.80	27	30	
2	0.5	0.87	27	29	
2	0.6	0.40	23	34	MR = 2, ε_{deh} = 0.6, 0.4 < ε_{hum} < 0.8
2	0.6	0.47	24	33	
2	0.6	0.53	25	33	
2	0.6	0.60	26	32	

2	0.6	0.67	26	32	
2	0.6	0.73	28	31	
2	0.6	0.80	29	30	
2	0.7	0.40	24	34	MR = 2, ε_{deh} = 0.7, 0.4 < ε_{hum} < 0.73
2	0.7	0.47	25	34	
2	0.7	0.53	26	33	
2	0.7	0.60	27	33	
2	0.7	0.67	28	32	
2	0.7	0.73	30	31	
2	0.8	0.40	24	35	MR = 2, ε_{deh} = 0.8, 0.4 < ε_{hum} < 0.67
2	0.8	0.47	26	34	
2	0.8	0.53	27	34	
2	0.8	0.60	29	33	
2	0.8	0.67	31	33	

Table 3.4 Components effectiveness valid for recirculation system at MR = 2.5

MR	ε_{deh}	ε_{hum}	T_{w2}	T_{w4}	Observation
2.5	0.5	0.40	22	34	MR = 2.5, ε_{deh} = 0.5, 0.4 < ε_{hum} < 1
2.5	0.5	0.47	23	34	
2.5	0.5	0.53	23	33	
2.5	0.5	0.60	24	33	
2.5	0.5	0.67	24	33	
2.5	0.5	0.73	24	32	
2.5	0.5	0.80	25	32	
2.5	0.5	0.87	25	31	
2.5	0.5	0.93	26	30	
2.5	0.5	1.00	27	30	
2.5	0.6	0.40	23	34	MR = 2.5, ε_{deh} = 0.6, 0.4 < ε_{hum} < 1
2.5	0.6	0.47	23	34	
2.5	0.6	0.53	24	34	
2.5	0.6	0.60	24	33	
2.5	0.6	0.67	25	33	
2.5	0.6	0.73	25	33	
2.5	0.6	0.80	26	32	
2.5	0.6	0.87	27	31	
2.5	0.6	0.93	28	31	
2.5	0.6	1.00	29	30	
2.5	0.7	0.40	23	35	MR = 2.5, ε_{deh} = 0.7, 0.4 < ε_{hum} < 0.87
2.5	0.7	0.47	24	34	
2.5	0.7	0.53	24	34	
2.5	0.7	0.60	25	34	
2.5	0.7	0.67	26	33	

2.5	0.7	0.73	27	33	
2.5	0.7	0.80	28	33	
2.5	0.7	0.87	29	32	
2.5	0.8	0.40	24	35	$MR = 2.5, \varepsilon_{deh} = 0.8, 0.4 < \varepsilon_{hum} < 1$
2.5	0.8	0.47	24	35	
2.5	0.8	0.53	25	35	
2.5	0.8	0.60	26	34	
2.5	0.8	0.67	27	34	
2.5	0.8	0.73	29	34	
2.5	0.8	0.80	30	33	

Table 3.5 Components effectiveness valid for recirculation system at MR = 3.

MR	ε_{deh}	ε_{hum}	T_{w2}	T_{w4}	Observation
3	0.5	0.40	22	35	$MR = 3, \varepsilon_{deh} = 0.5, 0.4 < \varepsilon_{hum} < 1$
3	0.5	0.47	22	34	
3	0.5	0.53	23	34	
3	0.5	0.60	23	34	
3	0.5	0.67	23	33	
3	0.5	0.73	24	33	
3	0.5	0.80	24	33	
3	0.5	0.87	24	32	
3	0.5	0.93	25	32	
3	0.5	1.00	25	31	
3	0.6	0.40	22	35	$MR = 3, \varepsilon_{deh} = 0.6, 0.4 < \varepsilon_{hum} < 1$
3	0.6	0.47	23	35	
3	0.6	0.53	23	34	
3	0.6	0.60	24	34	
3	0.6	0.67	24	34	
3	0.6	0.73	24	33	
3	0.6	0.80	25	33	
3	0.6	0.87	25	33	
3	0.6	0.93	26	32	
3	0.6	1.00	27	32	
3	0.7	0.40	23	35	$MR = 3, \varepsilon_{deh} = 0.7, 0.4 < \varepsilon_{hum} < 1$
3	0.7	0.47	23	35	
3	0.7	0.53	24	35	
3	0.7	0.60	24	34	
3	0.7	0.67	25	34	
3	0.7	0.73	25	34	
3	0.7	0.80	26	34	
3	0.7	0.87	27	33	
3	0.7	0.93	28	33	
3	0.7	1.00	29	32	
3	0.8	0.40	23	35	$MR = 3, \varepsilon_{deh} = 0.8, 0.4 < \varepsilon_{hum} < 1$

3	0.8	0.47	24	35	
3	0.8	0.53	24	35	
3	0.8	0.60	25	35	
3	0.8	0.67	26	35	
3	0.8	0.73	26	34	
3	0.8	0.80	27	34	
3	0.8	0.87	28	34	
3	0.8	0.93	30	33	
3	0.8	1.00	32	33	
3	0.85	0.40	23	35	$MR = 3$, $\varepsilon_{deh} = 0.85$, $0.4 < \varepsilon_{hum} < 1$
3	0.85	0.47	24	35	
3	0.85	0.53	24	35	
3	0.85	0.60	25	35	
3	0.85	0.67	26	35	
3	0.85	0.73	27	35	
3	0.85	0.80	28	34	
3	0.85	0.87	29	34	
3	0.85	0.93	31	34	

3.5.2 Basic Cycle (OAOW) Performance

After determining the working range of effectiveness, the analysis for system performance of the basic cycle (0% rejected brine circulation) is conducted.

Figure 3.12 shows the effect of MR on the performance of basic cycle at different humidifier effectiveness (0.4 to 0.6), which is the working range for a dehumidifier with 0.5 effectiveness. As the MR increases, GOR increases until it reaches a peak and then starts to drop. This is due to the fact that the definition of maximum effectiveness of the humidifier changes from effectiveness of water to effectiveness of air, this indicates lower water temperatures at the inlet of the humidifier and thus lower evaporation and GOR. As expected, the GOR increases as the effectiveness of the humidifier increases since higher effectiveness means high evaporation and consequently higher GOR. Figures 3.13 through 3.16 replicate the same behavior with a higher GOR since the dehumidifier effectiveness increases from 0.6 to 0.85.

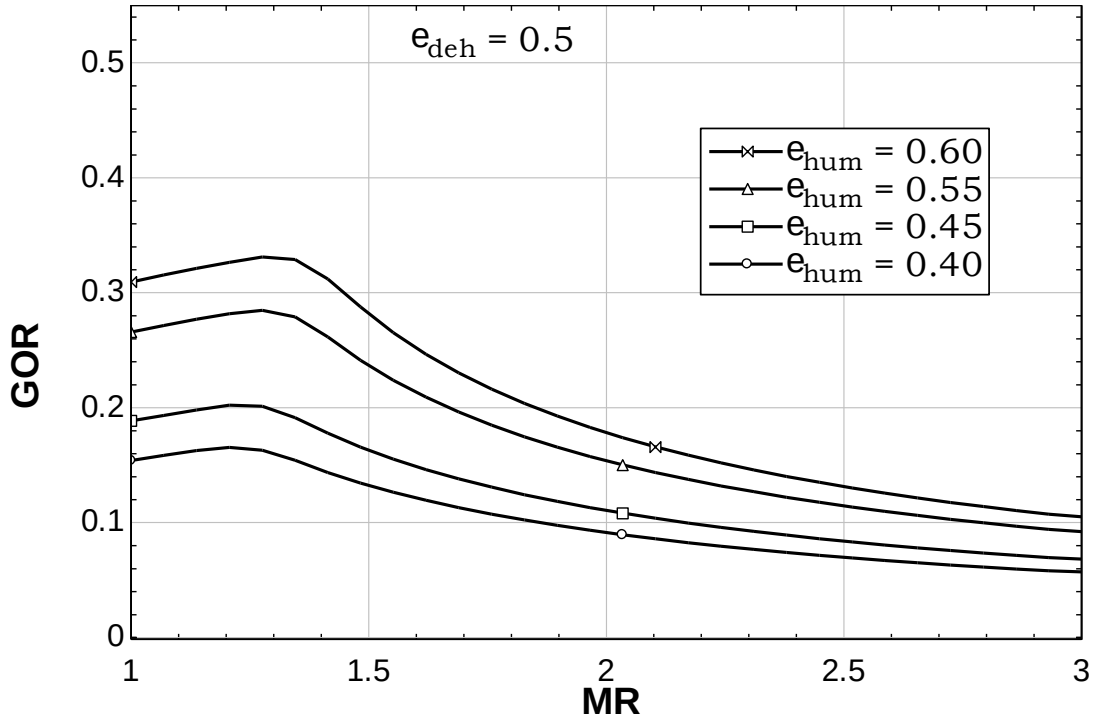

Figure 3.12 Effect of varying MR on the GOR for (OAOW) HDH system at ε_{deh}=0.5.

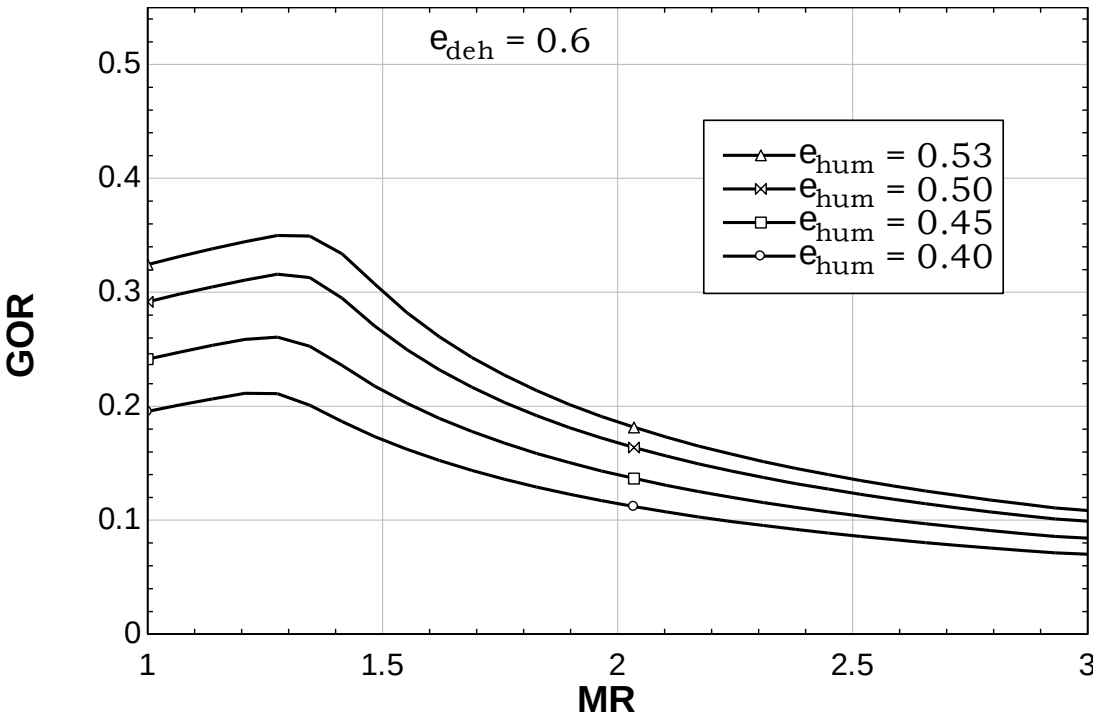

Figure 3.13 Effect of varying MR on the GOR for (OAOW) HDH system at ε_{deh}=0.6.

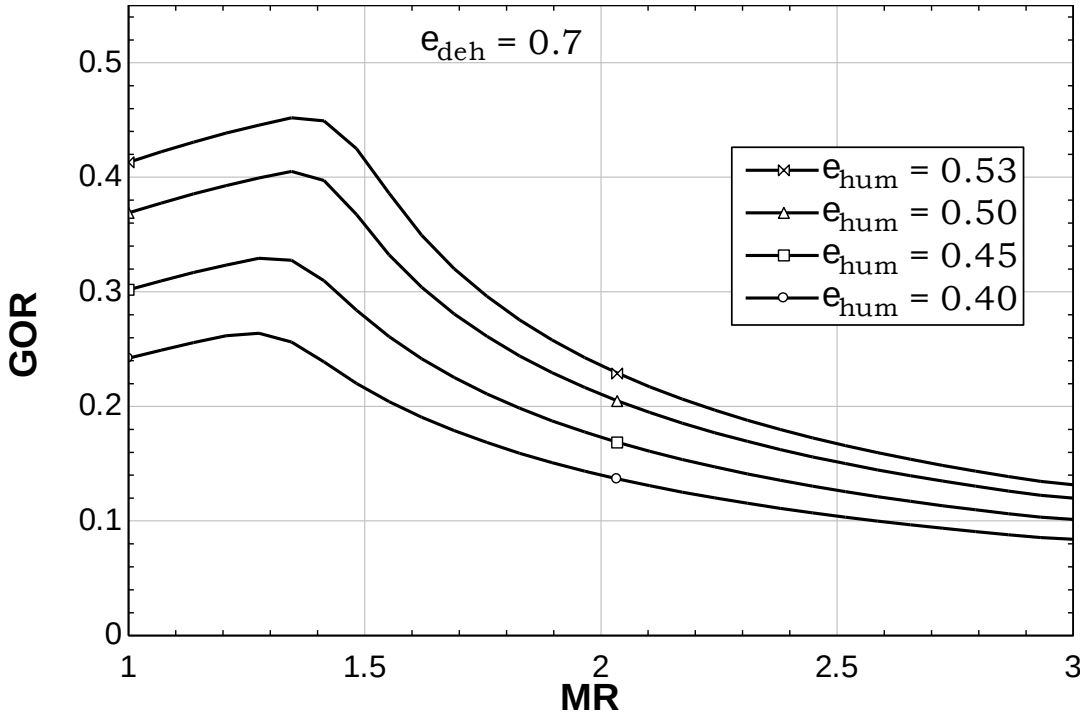

Figure 3.14 Effect of varying MR on the GOR for (OAOW) HDH system at ε_{deh}=0.7.

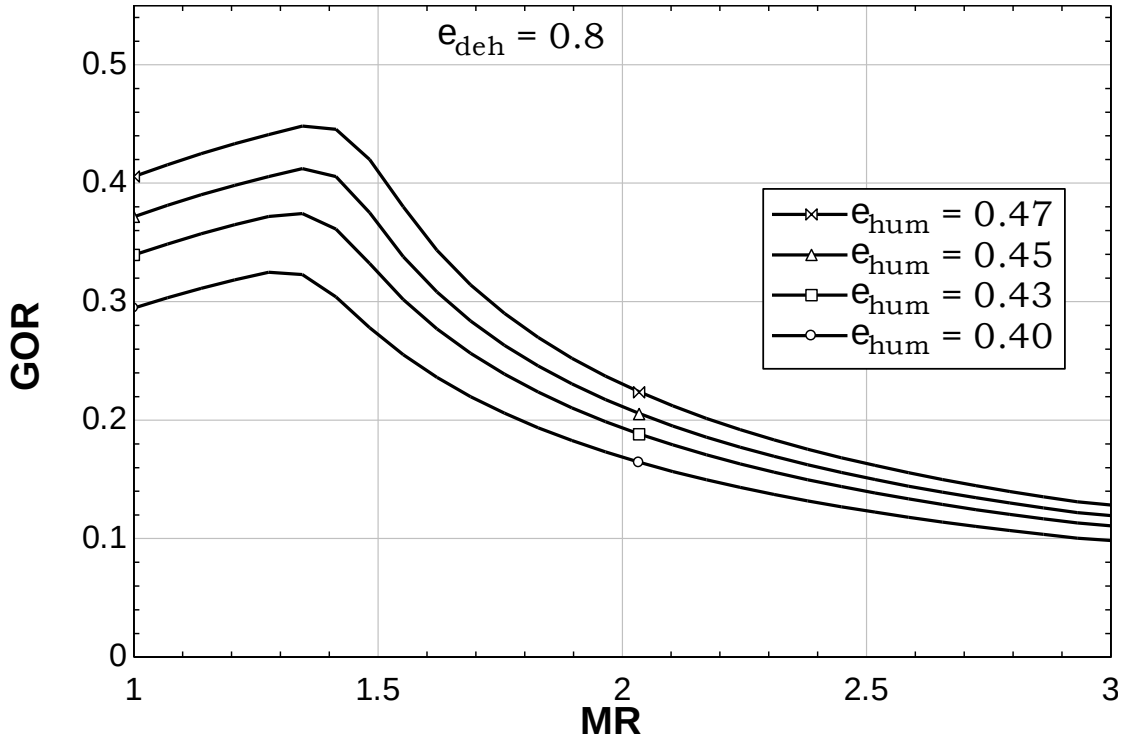

Figure 3.15 Effect of varying MR on the GOR for (OAOW) HDH system at ε_{deh}=0.8.

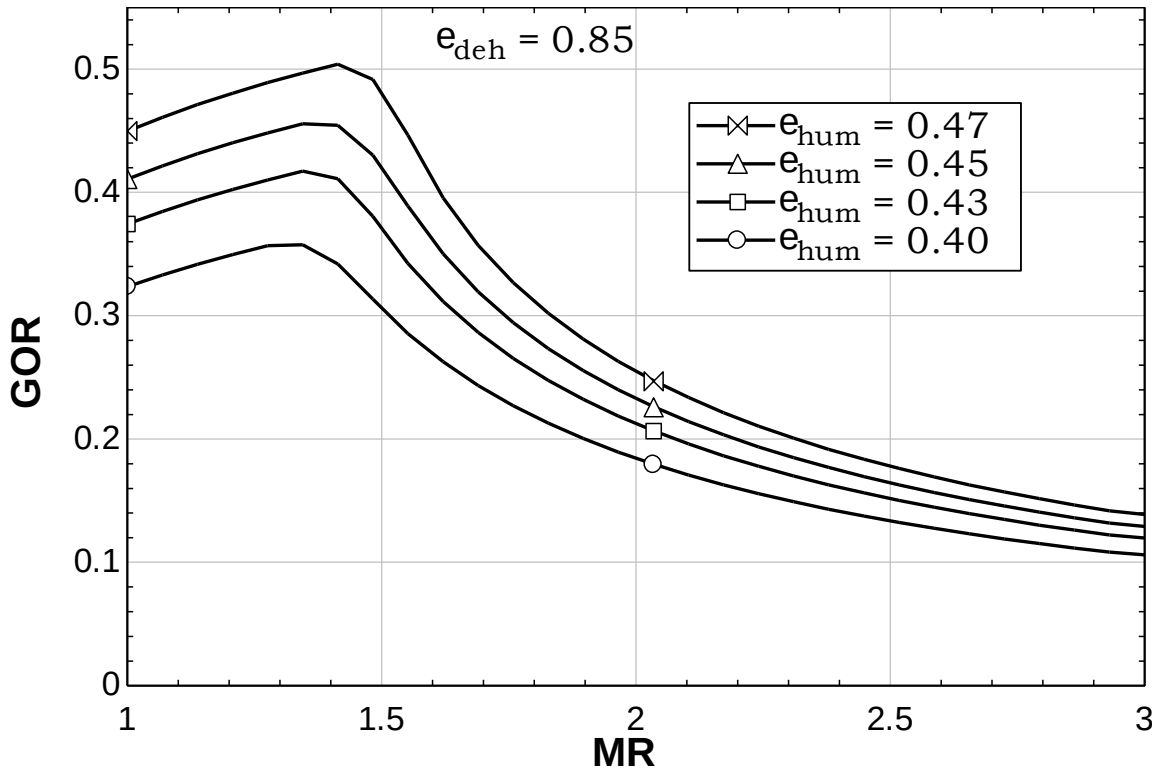

Figure 3.16 Effect of varying MR on the GOR for (OAOW) HDH system at ε_{deh}=0.85.

Figure 3.17a illustrates the effect of varying MR on the system performance as the effectiveness of the humidifier is kept constant at 0.4, while the effectiveness of dehumidifier is increased from 0.5 to 0.85. Similar to the behavior of Figures 3.12 through 3.16, the GOR increases to a peak value. As described earlier, at this point, the maximum effectiveness definition changes from water to air, the GOR drops. The GOR increases as the dehumidifier effectiveness increase, which is due to the better condensation process. This behavior is replicated through Figures 3.17b, 3.17c, and 3.17d.

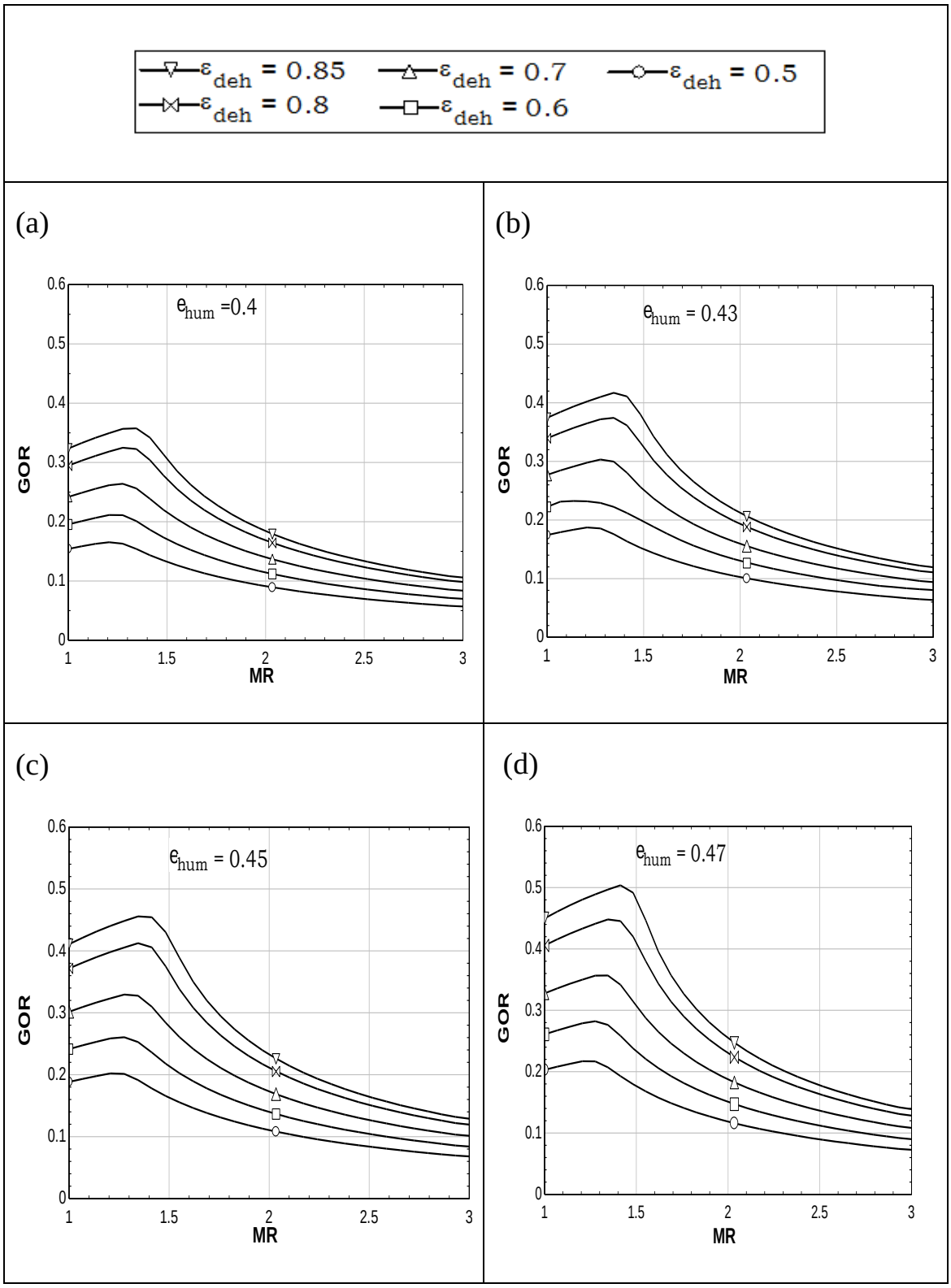

Figure 3.17 Effect of varying MR on the GOR for OAOW HDH system at (a) ε_{hum}=0.4; (b) ε_{hum}=0.43; (c) ε_{hum}=0.45; (d) ε_{hum}=0.47.

3.5.3 Modified CWOA Cycle Performance

In this section, the modified cycle performance is examined by varying MR while holding the effectiveness of humidifier constant and varying the dehumidifier effectiveness since the dehumidifier has a greater influence on GOR as stated by Narayan et. al [79]. Figure 3.18 presents the effect of varying MR on the GOR of the modified cycle as the effectiveness of the humidifier is held constant at 0.4 and the dehumidifier effectiveness is varied from 0.5 to 0.85.

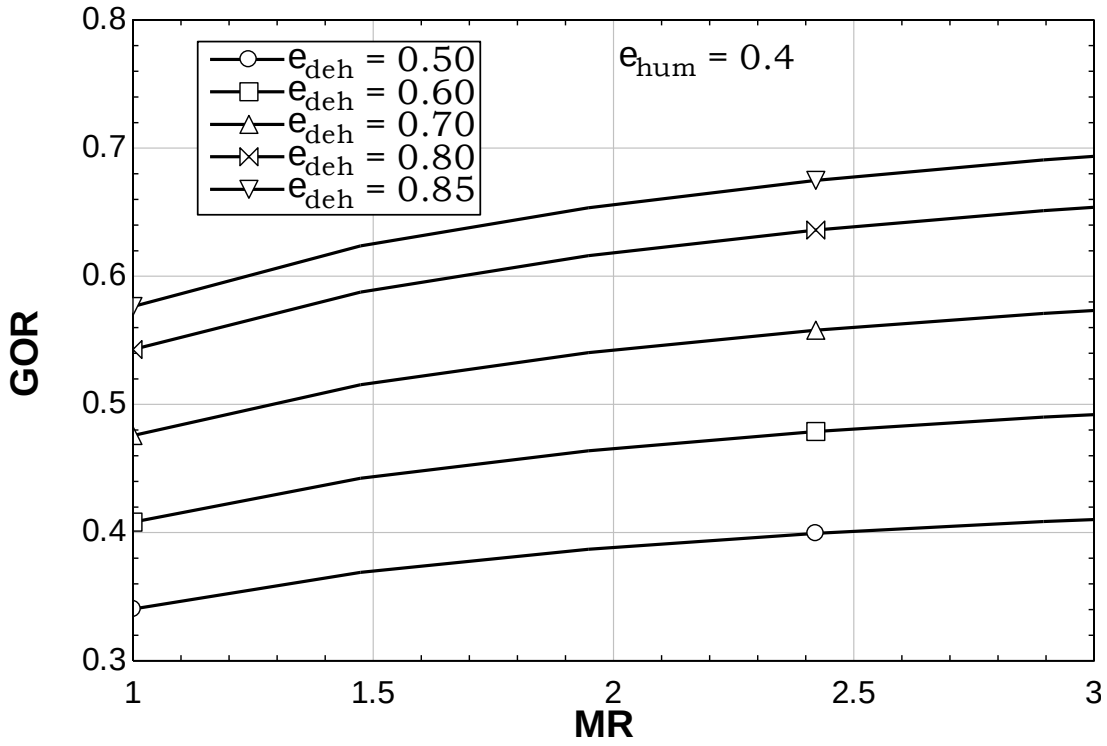

Figure 3.18 Effect of varying MR on the GOR for Modified CWOA HDH system at ε_{hum}= 0.4.

It can be seen from the figure that increasing MR increases the GOR, the MR is increased either the air mass flow rate is decreased which leads to a better evaporation and hence increase in GOR or increasing water mass flow rate which means an increase in

evaporation and consequently high GOR. As noticed from Figure 3.18 the GOR increased at MR=3 to almost 0.7 by increasing dehumidifier effectiveness from 0.5 to 0.85. Increasing the dehumidifier effectiveness increases the GOR since it reflects a better condensation process and is more sensitive to the system performance as also noted by Narayan et. al [79].

3.5.4 Effect of Rejected Brine Recirculation on Performance

In this section, the effect of circulating the rejected brine from the humidifier back to the heater on the performance is examined. Figure 3.19 illustrates the limiting case 0% brine recirculation which is the basic cycle (OAOW) and 100% is the modified cycle CWOA. As explained in the previous sections, the GOR increases for the modified cycle as MR increases, while it has a peak and then drops for the basic cycle. The modified cycle has a higher GOR when the system is operating at humidifier effectiveness of 0.4 and dehumidifier effectiveness of 0.85. This range of MR and effectiveness fulfills the condition that the temperature of the water coming from the humidifier is higher than the makeup water temperature. As a result, the maximum temperature is higher and better evaporation is achieved and consequently an increase in GOR.

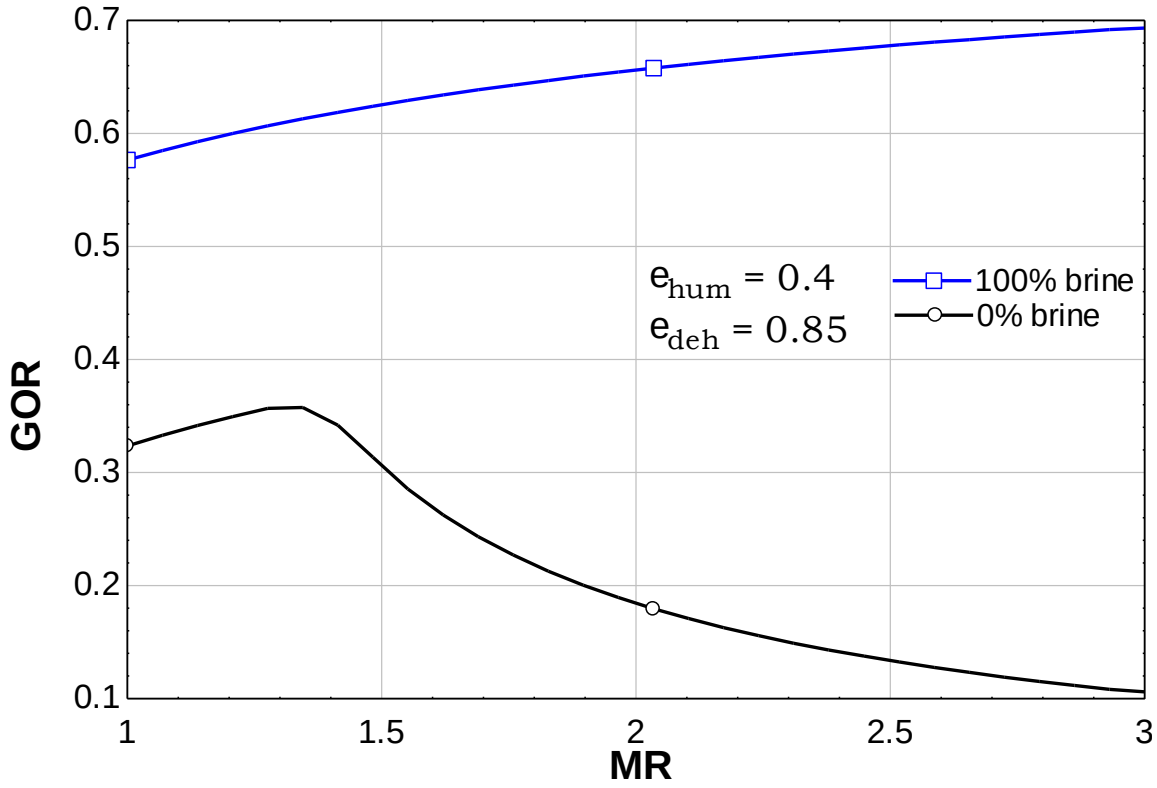

Figure 3.19 The performance of the basic and modified cycles (0% and 100% rejected brine at humidifier exit) at ε_{hum}=0.4 and ε_{deh}=0.85.

Figure 3.20 presents the effect of recirculation of rejected brine at the humidifier exit on the performance of the modified system by varying MR at humidifier effectiveness of 0.4 and dehumidifier effectiveness of 0.85. At 95% and 90% rejected brine recirculation, the behavior mimic that of 100% (the modified system), as the increase in MR increases the GOR since the air mass flow rate decreases. After that (80% to 10%) the system starts to act as the basic cycle by reaching a peak and then drops since the effect of makeup starts to outplay the effect of recirculated brine and the definition of maximum effectiveness changes from water to air. As explained earlier, the definition change indicates a decrease in water temperatures of water at the humidifier inlet, thus one would expect less

evaporation and hence the GOR. This is expected as the recirculated brine contains a considerable amount of heat and now its contribution to the mass flow rate that finally enters the humidifier is reduced. This explains the reduction in performance as the percentage of circulated brine reduced from 95% to 10%, i.e., as the system moves from the modified cycle towards the basic cycle. Figures 3.21 through 3.23 replicate the same behavior as all these runs considered the effectiveness range that results in a brine temperature higher than the makeup temperature.

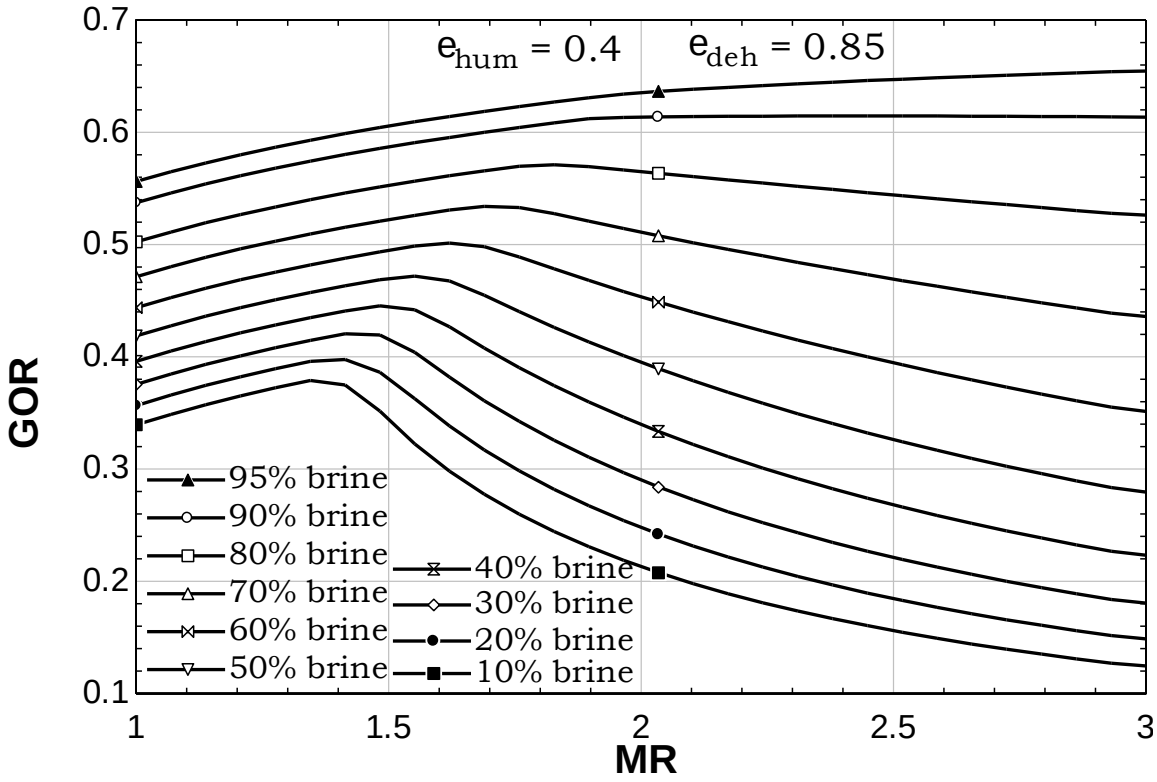

Figure 3.20 Effect of rejected brine recirculation on the performance of the system at ε_{hum}=0.4 and ε_{deh}=0.85.

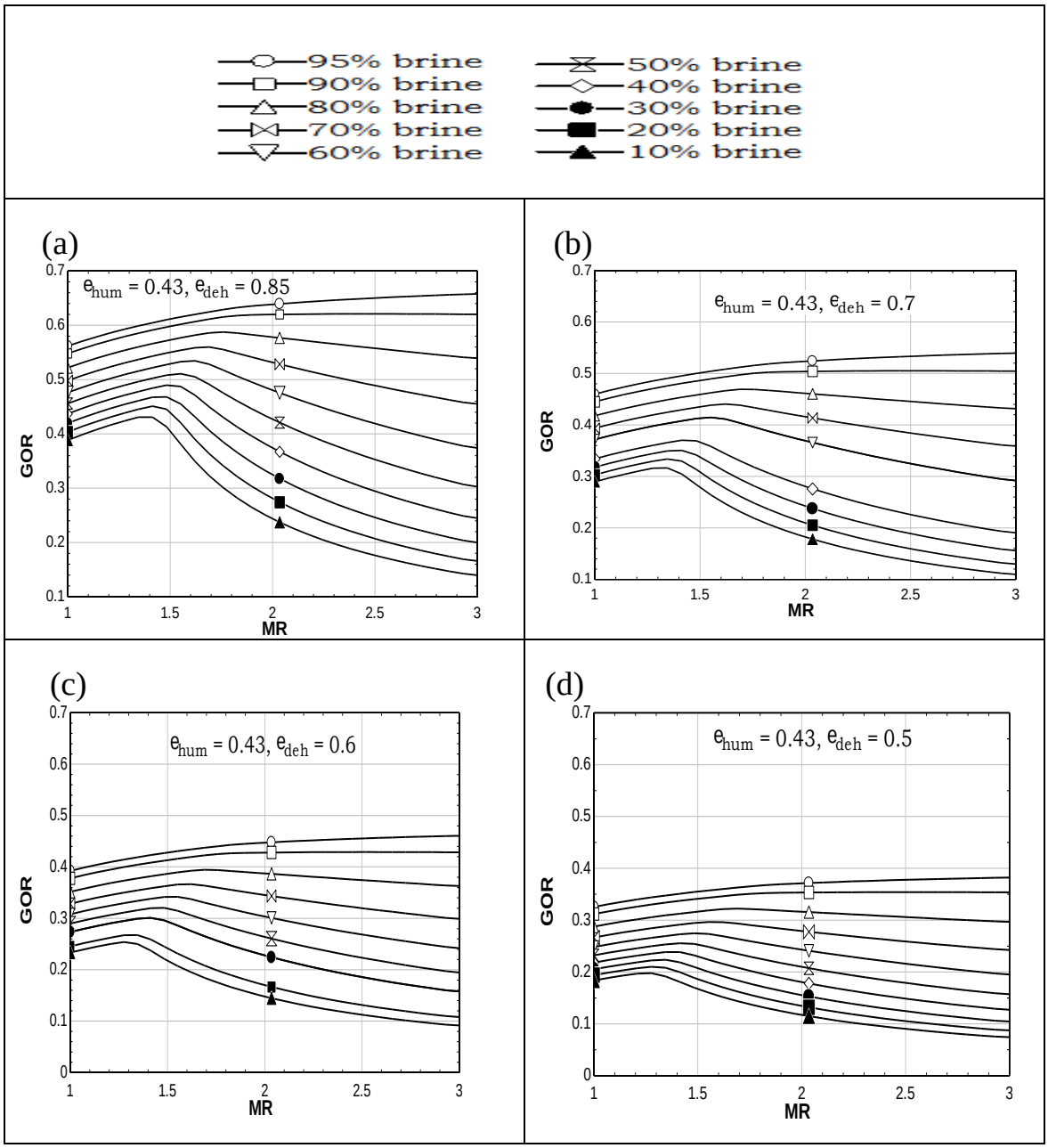

Figure 3.21 Effect of rejected brine recirculation on the performance of the system at ε_{hum}=0.43 and (a)ε_{deh}=0.85; (b) ε_{deh}=0.7; (c) ε_{deh}=0.6; (d)ε_{deh}=0.5.

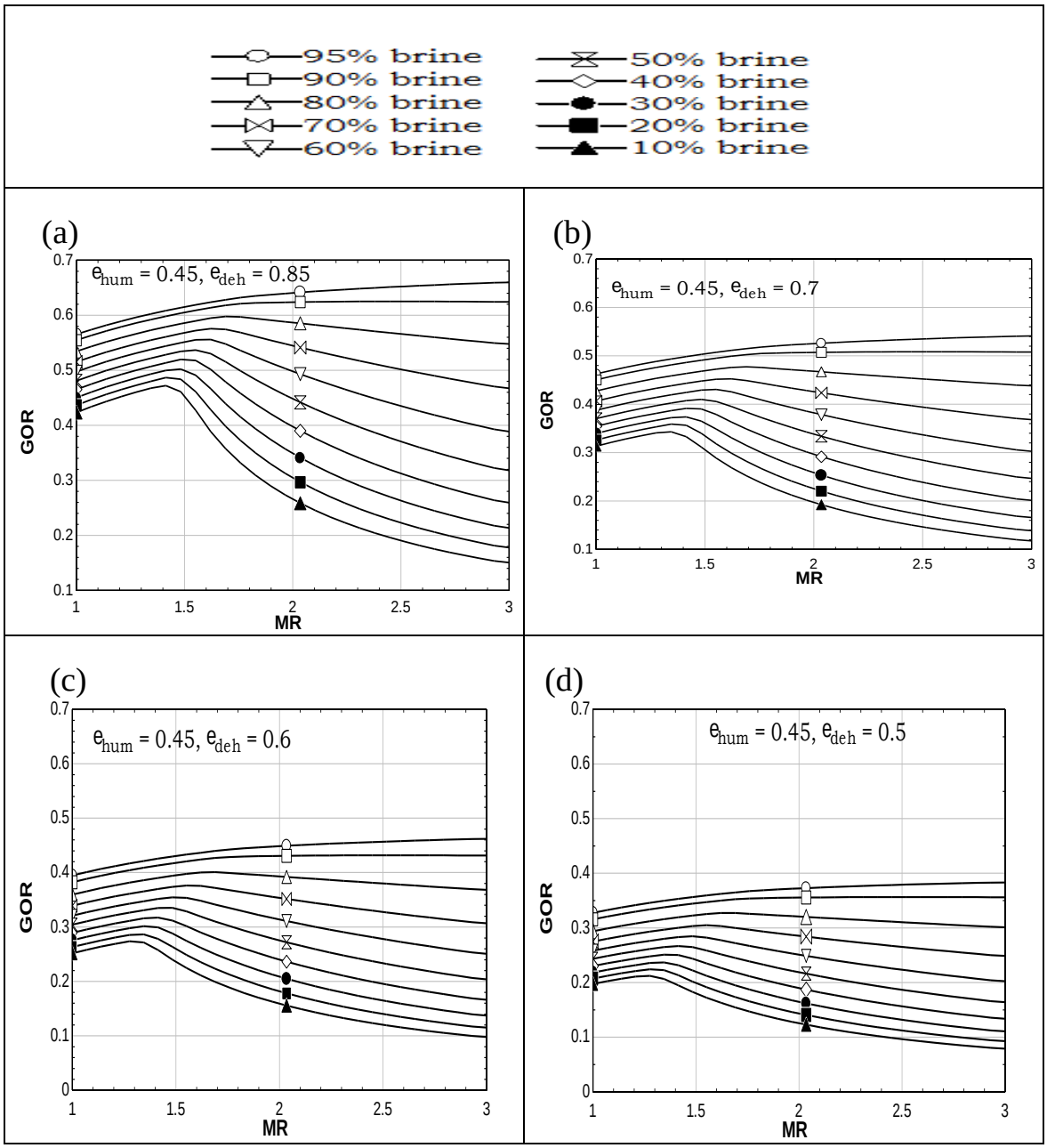

Figure 3.22 Effect of rejected brine recirculation on the performance of the system at ε_{hum}=0.45 and (a)ε_{deh}=0.85; (b) ε_{deh}=0.7; (c) ε_{deh}=0.6; (d)ε_{deh}=0.5.

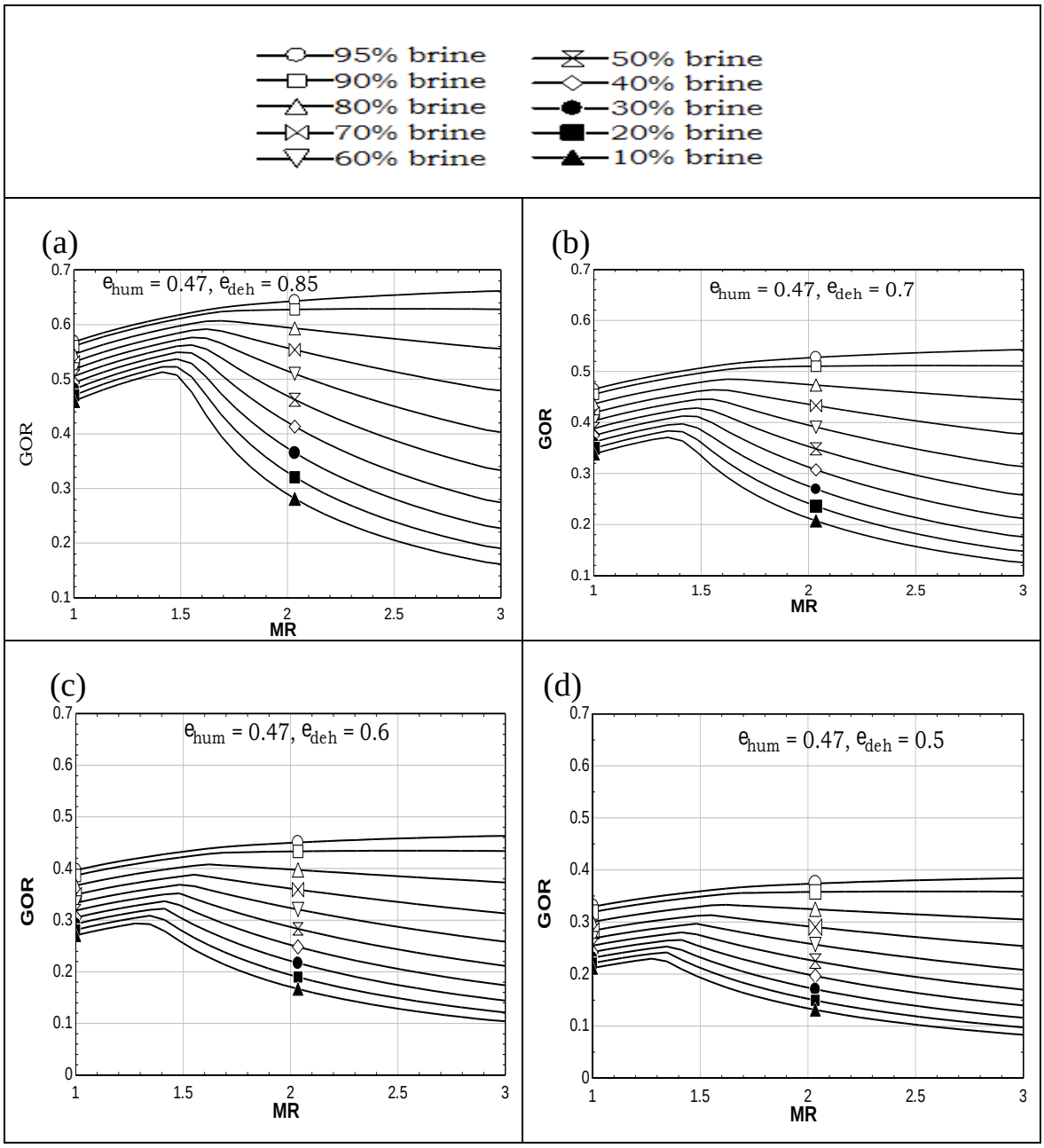

Figure 3.23 Effect of rejected brine recirculation on the performance of the system at ε_{hum}=0.47 and (a)ε_{deh}=0.85; (b) ε_{deh}=0.7; (c) ε_{deh}=0.6; (d)ε_{deh}=0.5.

The performance of the system is replicated for the range of effectiveness that justifies the idea of modification that is the brine recirculation as a heat recovery process. In Figure 3.24 the limiting case (0% and 100%) is explored at effectiveness that falls out of the valid effectiveness range i.e. the range that fulfills the basic condition mentioned

earlier. At the humidifier effectiveness of 0.6 and dehumidifier effectiveness of 0.85, The basic and modified cycle is examined by varying MR.

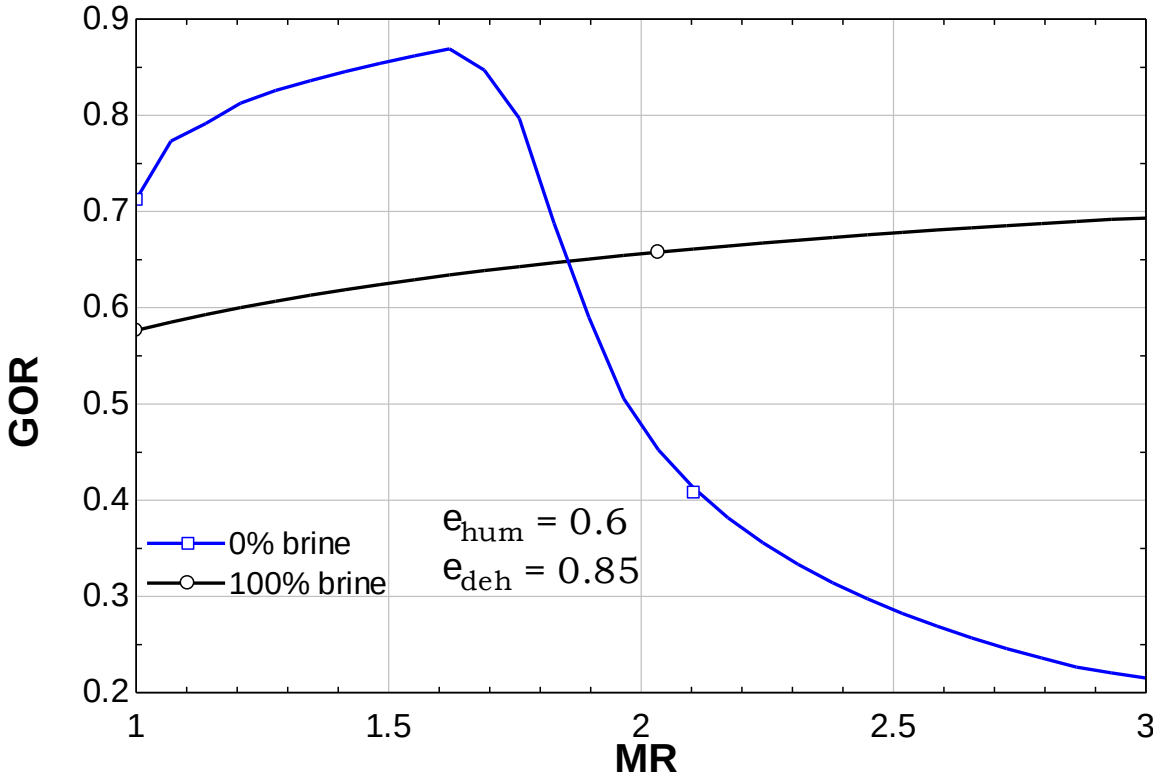

Figure 3.24 The performance of the basic and modified cycles (0% and 100% rejected brine at humidifier exit) at ε_{hum}=0.6 and ε_{deh}=0.85.

The basic cycle GOR starts to increase until it reaches the peak where after it the GOR drops as the definition of effectiveness changes. The modified cycle also increased as the air mass flow rate decreases. The same behavior is noticed; however, the basic cycle has a higher GOR at the beginning and even after the peak till a certain point. This is due to the fact that a high dehumidifier effectiveness will result in a higher makeup temperature which is directly induced to the heater without mixing with the rejected brine. For the modified cycle, the mixing will result in a reduced temperature of the water that needs to

be heated, thus reduced the temperature of water entering the humidifier. This reduction will reduce the evaporation and GOR of the system.

The basic cycle performance after the peak starts to drop as the temperature of water reduces until a certain point at which the performance of the modified cycle exceeds that of basic cycle. After this point, the temperature of water at humidifier inlet is higher for the modified cycle than the basic cycle, thus the modified cycle has a better performance. Decreasing air mass flow rate by increasing MR affects the heating of makeup water at the dehumidifier inlet, which is more dominant for the basic cycle than for the modified cycle.

In Figure 3.25a the effect of rejected brine recirculation on the performance of the system is shown at a humidifier effectiveness of 0.6 and dehumidifier effectiveness of 0.85 which falls outside the valid range that discussed earlier. Similar to Figure 3.20 here also the behavior at 95% and 90% rejected brine recirculation mimics that of 100% (the modified system in Figure 3.24), as the MR increases the GOR since the air mass flow rate decreases and the definition of effectiveness doesn't change. After that (80% to 10%) the system starts to act as the basic cycle (as in Figure 3.24) by reaching a peak and then drops since the effect of makeup starts to outplay the effect of recirculated brine and the definition of maximum effectiveness changes. The main difference here is that the system has moved outside the range of effectiveness that fulfills the condition at which mixing is justifiable. This created a point at certain MR at which all curves intersect which means the brine recirculation has no effect on the GOR. At this point, a sort of balancing occurs and the system becomes insensitive to the circulation. This point then can be used as an

indicator of the range of MR that allows a better performance for recirculation and where to shift towards the basic cycle (0% circulation).

Figures 3.25b and 3.25c exhibits the same behavior and the same point of intersection occurred at different heat capacity rate ratios and a different value of MR. As the dehumidifier effectiveness decreases, as shown in these figures, the point of intersection occurs at lower MR which shows a region at which the basic cycle has a higher performance than the modified cycle. This indicates that this region is sensitive to the dehumidifier effectiveness as it increases and decreases accordingly. As explained earlier, the heating of makeup water occurs at the dehumidifier which makes the dehumidifier effectiveness more dominant factor for the basic cycle than for the modified cycle as the modified cycle utilizes less makeup water. Figure 3.25d illustrates that when the system returns to the working range this point disappears.

Figures 3.26a through 3.25d show the same behavior when humidifier effectiveness is fixed at 0.8, which does not fulfill the valid range condition for recirculation. The dehumidifier effectiveness is changed from 0.85 at Figure 3.26a to 0.5 at Figure 3.26d. The point of intersection also moved from higher MR to lower MR as the dehumidifier effectiveness decreases, which support the argument that this point marks the region of dominance of the basic cycle, to the left of this point, and proportional to the dehumidifier effectiveness accordingly.

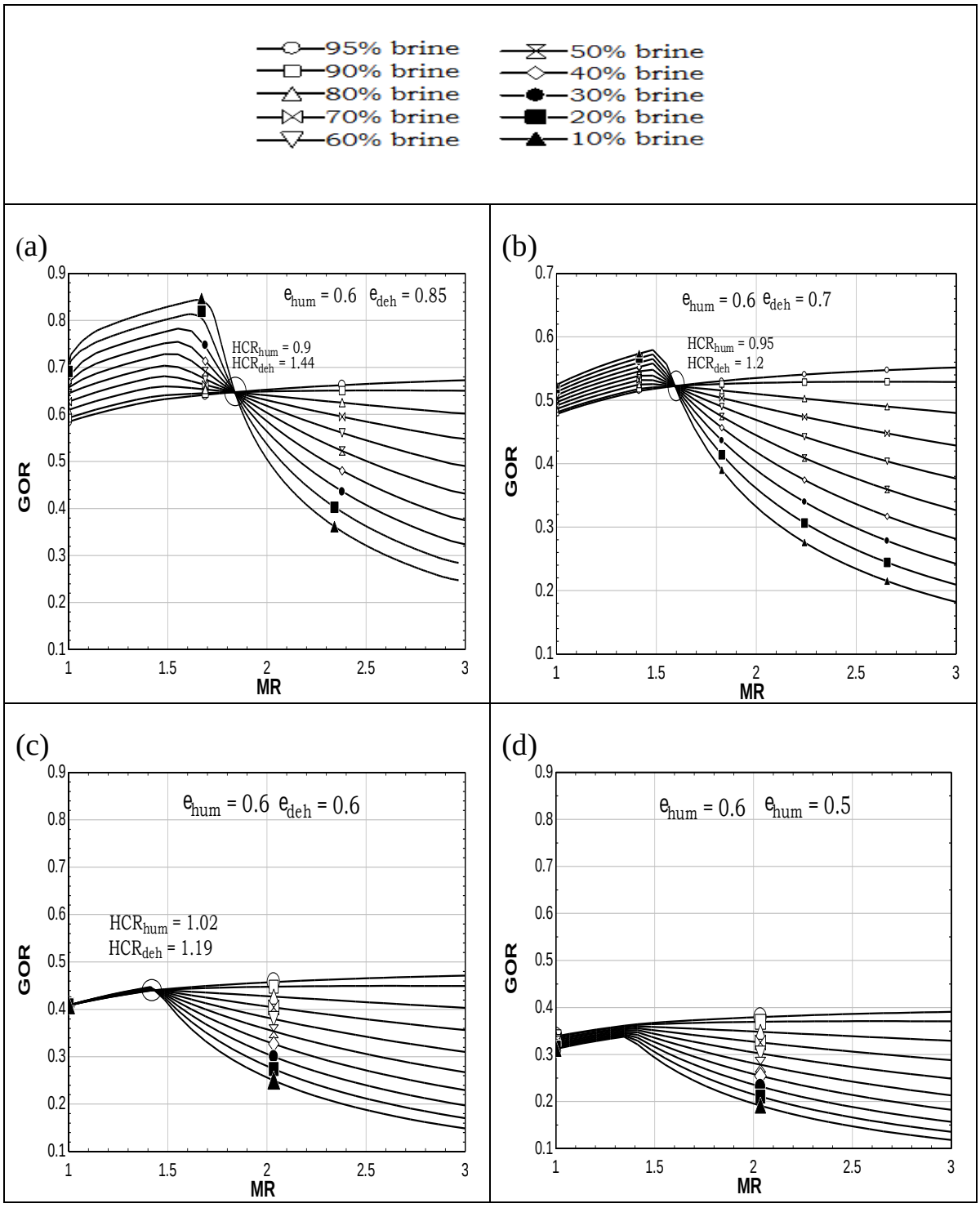

Figure 3.25 Effect of rejected brine recirculation on the performance of the system at ε_{hum}=0.6 and (a) ε_{deh}=0.85; (b) ε_{deh}=0.7;(c) ε_{deh}=0.6; (d) ε_{deh}=0.5.

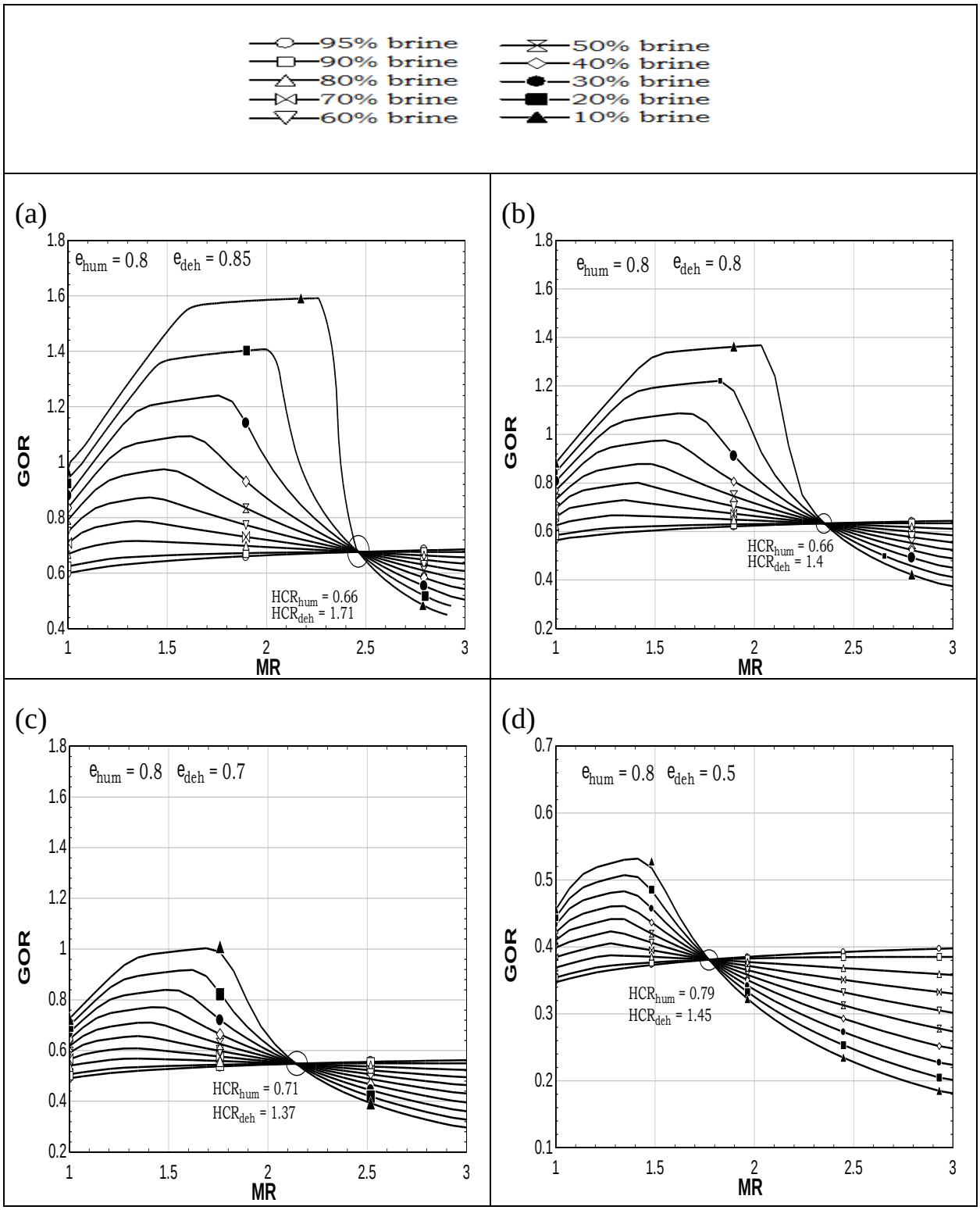

Figure 3.26 Effect of rejected brine recirculation on the performance of the system at ε_{hum}=0.8 and (a) ε_{deh}=0.85; (b) ε_{deh}=0.8; (c) ε_{deh}=0.7; (d) ε_{deh}=0.5.

CHAPTER 4

Exergo-economic Analysis of Modified Closed-Water Open-Air HDH System

In this chapter, an extended analysis of the modified CWOA cycle that considers second law analysis of the basic OAOW and modified CWOA cycles is presented. The possibility of coupling RO with the basic cycle as an alternative to the recirculation option is also explored. In addition, exergo-economic analysis of these systems is also executed.

4.1 Alternative Systems Description

The basic and modified systems have already been described in Chapter 3 and illustrated in Figures 4.1 and 4.2. In this chapter, the alternative option that includes RO coupled with the basic cycle is described.

There are basically 3 RO systems suggested being coupled with the OAOW HDH system as alternative options to the circulation of rejected brine (the modified cycle) . The rejected brine is utilized in an RO module with a pump which is the first option, as illustrated in Figure 4.3. The pump will drive the saline water across the module to separate fresh and saline water as it passes through it. The second option is shown in Figure 4.4 that is to equip the RO module with Pelton turbine to recover the high pressure of the rejected brine from the RO as an energy recovery unit. The recovered energy is

utilized in the high-pressure pump. The other option is to equip the RO with pressure exchanger to exchange the pressure from the high pressure rejected brine stream exiting the RO module to the rejected brine exiting the humidifier before it enters the high-pressure pump as shown in Figure 4.5.

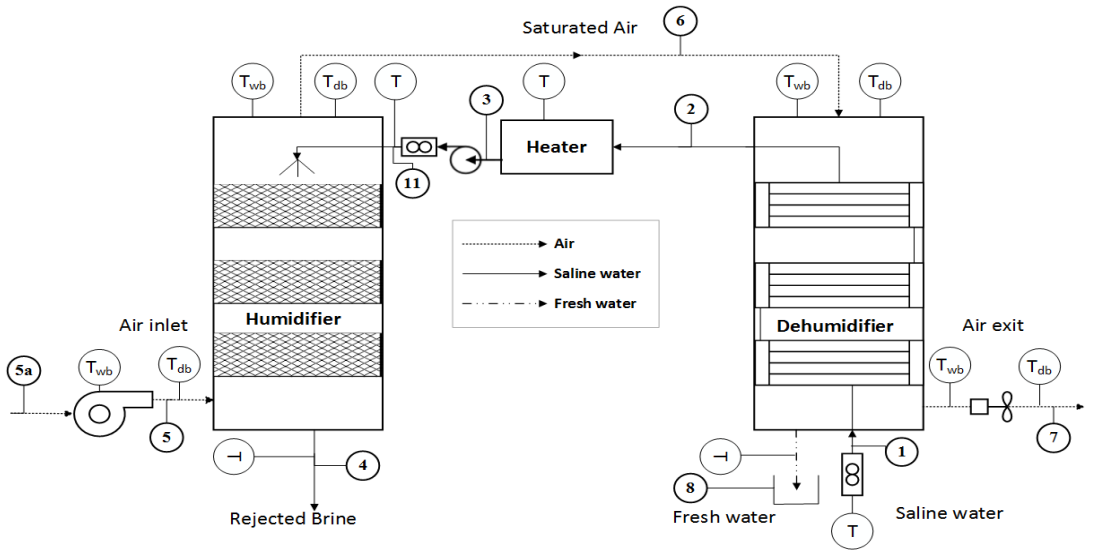

Figure 4.1 The basic Open-Air Open-Water HDH system.

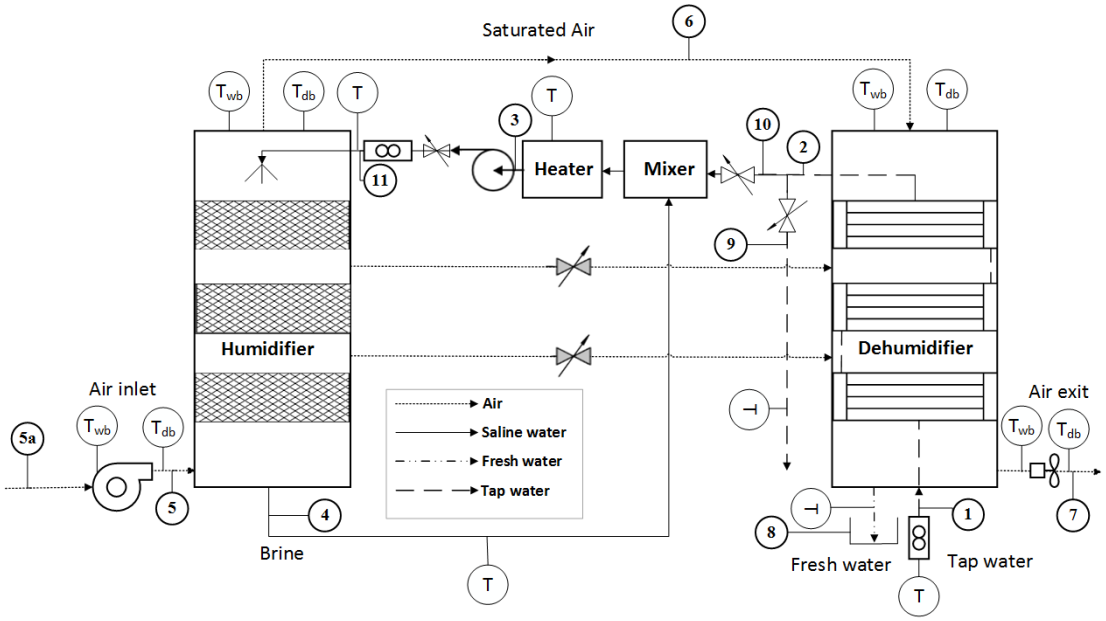

Figure 4.2 The Modified Closed-Water Open-Air HDH system.

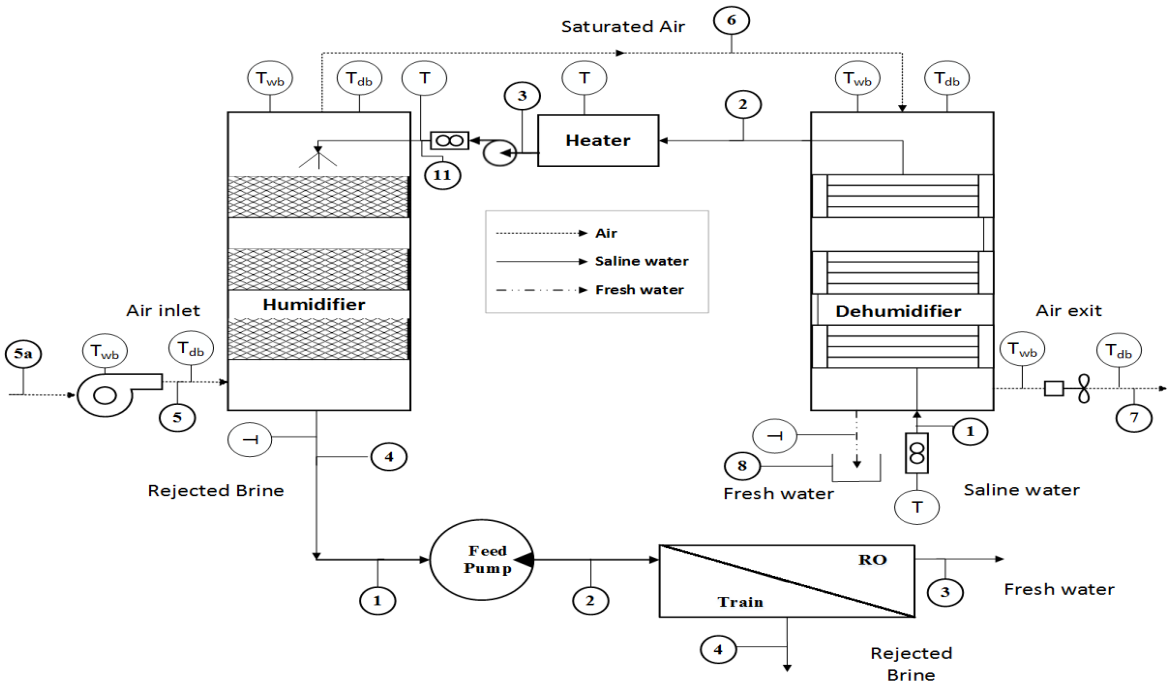

Figure 4.3 The basic Open-Air Open-Water HDH system coupled with RO system.

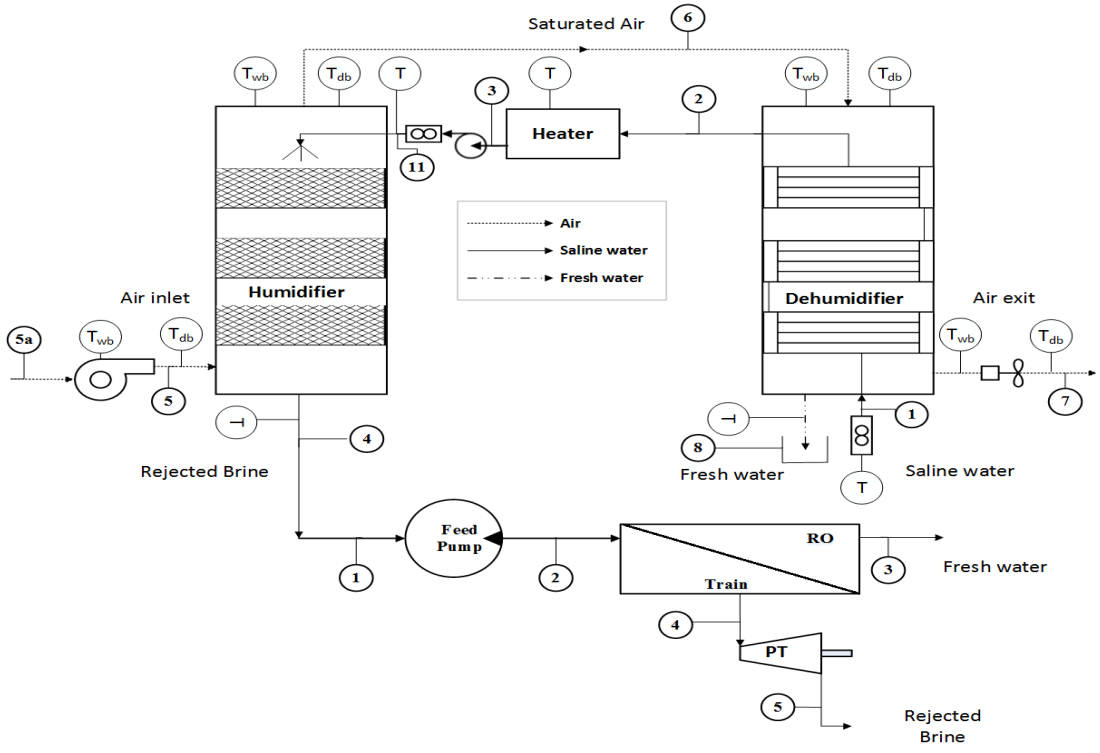

Figure 4.4 The basic Open-Air Open-Water HDH system coupled with an RO system with a Pelton turbine.

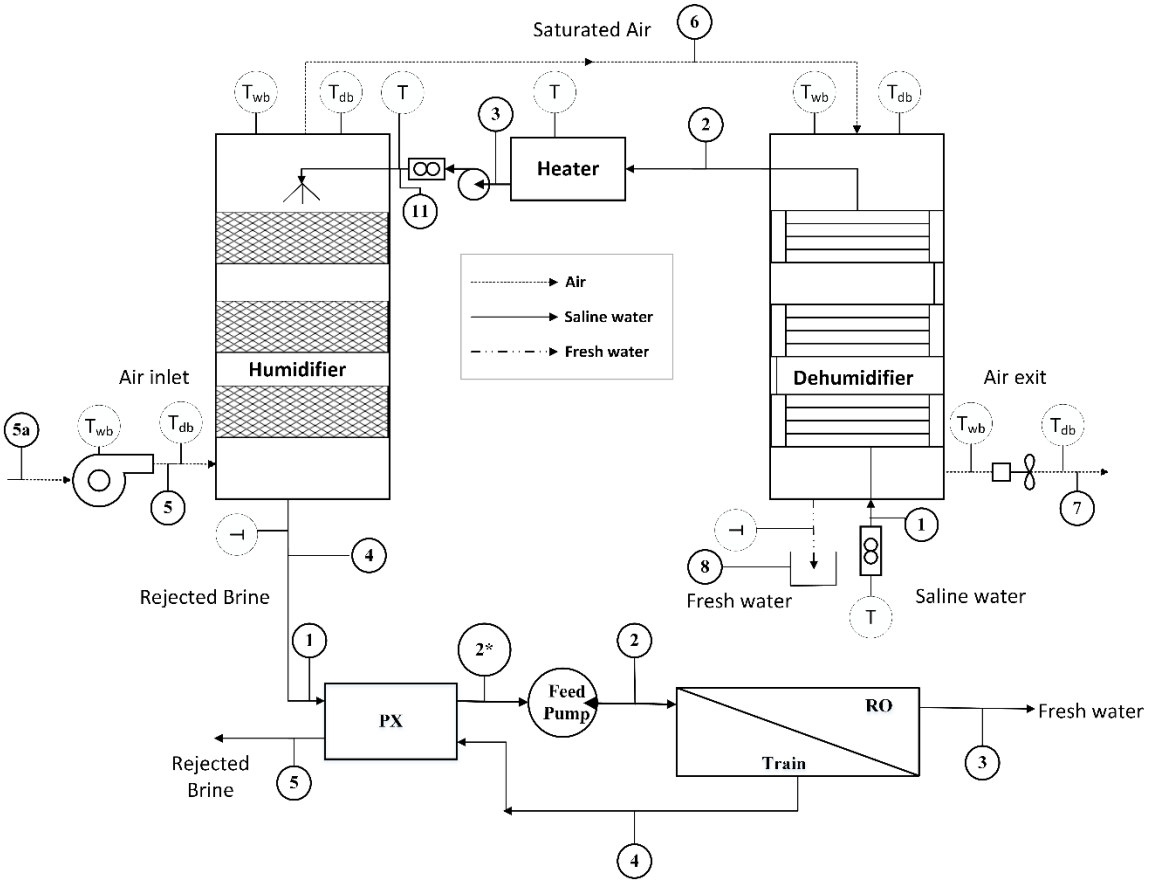

Figure 4.5 The basic Open-Air Open-Water HDH system coupled with an RO system with Pressure exchanger.

4.2 Performance Metrics and Modelling

The HDH system model and performance metrics are explained in Chapter 4. In this section, the first law equations of the RO system are presented along with the second law equations for all systems (HDH and coupled systems). The key exergo-economic model equations are then presented. These equations are used in the EES code to enable the calculation of both the second law efficiency and exergo-economic analysis.

4.2.1 Reverse Osmosis First Law Analysis

The Reverse Osmosis (RO) system analysis is illustrated in [80] and the key equations and performance metrics that are utilized in the EES code are presented in this section.

The steady-state mass and solution balance equations can be written as:

$$\sum_{in} \dot{m} = \sum_{out} \dot{m} \quad (4.1)$$

$$\sum_{in} \dot{m}X = \sum_{out} \dot{m}X \quad (4.2)$$

The actual high-pressure pump work and the turbine work can be written in terms of the respective isentropic efficiencies as,

$$\dot{W}_p = \frac{\dot{W}_{is,p}}{\eta_{is,p}} = \frac{\dot{V}\ \Delta P_p}{\eta_{is,p}} \quad (4.3)$$

$$\dot{W}_{PT} = \eta_{is,PT}\dot{W}_{is,PT} = \eta_{is,PT}\ \dot{V}\ \Delta P_{PT} \quad (4.4)$$

While the pressure exchanger efficiency is calculated as [81].

$$\eta_{PX} = \frac{\sum_{out}(\dot{V}P)}{\sum_{in}(\dot{V}P)} \quad (4.5)$$

The recovery ratio (RR) is defined as the ratio of mass flow rate of fresh water produced to feed water mass flow rate, which can be written as,

$$RR = \frac{\dot{m}_{fw,RO}}{\dot{m}_{w,RO}} \quad (4.6)$$

And finally the specific energy consumption (SEC) is given by,

$$SEC = \frac{\dot{W}_{in}}{3600\dot{V}_{fw,RO}} \quad (4.7)$$

4.2.2 Second Law Analysis

The second-law analysis of both HDH systems (basic and modified) and the coupled systems (HDH and RO) with its three configurations is conducted through the balance equations. These equations are basically exergy balance through each component and then the second-law efficiency is defined.

Bejan et al.[82] defined the second law (exergetic) efficiency as the ratio of useful exergy output to the inlet exergy to the system.

$$\eta_{II} = \frac{\dot{X}_{out,useful}}{\dot{X}_{in}} \quad (4.8)$$

The exergy destruction is calculated at each component by the following equation [80].

$$\dot{X}_D = \sum_{in} \dot{X} - \sum_{out} \dot{X} \quad (4.9)$$

For the HDH system, the assumptions that are mentioned in Chapter 3 is also used here. While for the RO system, the following assumptions are followed.

- Dead state for feedwater is taken at the condition of inlet feedwater at atmospheric pressure, the temperature of 21°C and salinity of 35 g/kg [83].
- Dead state for air is taken at standard conditions of air at atmospheric pressure and temperature of 25°C.
- Pressure drops and leakages are negligible in lines and pressure exchanger [80].
- Recovery ratio is fixed at 50% and produced pure water (permeate) with 0 g/kg salinity [83].

- Pump supply the feed to the RO module at 6 MPa and has an efficiency of 85% [83].
- The pressure drop across RO module is assumed to be 100 kPa.
- Pressure exchanger efficiency is assumed to be 96% [80] and efficiency of Pelton turbine fixed at 85% [84].

4.2.3 Cost Calculations

The economic analysis requires an evaluation of specific economic parameters, which is illustrated in the following subsections.

4.2.3.1 Fixed costs

This basically presents the capital costs Z ($). It consists of both purchasing cost and running cost. The fixed cost for each component is determined and summarized in Table 4.1 from the literature [52,85] and the direct cost of the components that are used in the experimental setup. It is important to notice that heat input is either presented through electrical heater as used in the experimental work or a solar heater whose cost is taken from [85]. The size of heater is assumed to provide the needed 5.6 kW, which is supplied by the electrical heater.

Table 4.1 Capital investment cost for stand-alone HDH and combined HDH-RO systems.

Item	Investment cost	
	HDH	HDH-RO
Humidifier	133$	133$

Dehumidifier	500$	500$
Tank	200$	200$
Electrical Heater	48$	48$
Flowmeters	230$	230$
Blower	250$	250$
Solar Heater	4267$	4267$
Miscellaneous	573$	573$
RO module	-	900$

The cost equations that are used to determine the capital cost of some of the components are summarized in this section. For example, the pump cost that is used to circulate the saline water from the tank to the humidifier [86]:

$$Z_P = 13.92\ \dot{m}_w\ \Delta P^{0.55}\ e^{1.05} \qquad (4.10)$$

The high-pressure pump used in the coupled system to drive the RO module and Pelton turbine fixed cost is, respectively, calculated from [87].

$$\log_{10}\left(Z_{RO,P}\right) = 3.3892 + 0.05361 \times \log_{10}\left(\dot{W}_{RO,P}\right) + 0.1538\left[\log_{10}\left(\dot{W}_{RO,P}\right)\right]^2 \qquad (4.11)$$

$$\log_{10}(Z_{PT}) = 2.2476 + 1.4956 \times \log_{10}(\dot{W}_{PT}) \\ -0.1618\left[\log_{10}(\dot{W}_{PT})\right]^2 \quad (4.12)$$

These capital costs are then multiplied by capital recovery factor (CRF) to calculate the annual capital cost (Z_{Annual}) of each component [82].

$$Z_{Annual} = CRF \times Z \quad (4.13)$$

where CRF is determined by this equation in which i and n presents interest rate and amortization period, respectively, and multiplied by an index factor 1.2 (20%) to accommodate the effect of an increase in the fixed cost over the years:

$$CRF = \left\langle \frac{i(1+i)^n}{(1+i)^n - 1} \right\rangle 1.2 \quad (4.14)$$

Finally, the model that is used to calculate the rate of capital investment $\dot{Z}$ ($/s) is given by

$$\dot{Z} = \frac{Z_{\text{Annual}}}{365 \times 24 \times 3600 \times Availability} \quad (4.15)$$

4.2.3.2 Stream's Cost Balance

Equation 4.16 presents a cost balance for each component which is used to determine the cost of output stream cost (in $/s) by applying it [82]. The cost of each stream is equal to the sum of the costs of working fluid exergy streams and fixed cost of the components producing it. Which is used to calculate the final product cost $\dot{C}_{fw}$ (in $/s) as well.

$$\dot{C}_{output} = \Sigma \dot{C}_{fluid} + \dot{Z} \qquad (4.16)$$

In addition to this balance a supplementary equation is needed to solve the balance when needed, which is given by,

$$\frac{\dot{C}_{fluid,in}}{\dot{X}_{fluid,in}} = \frac{\dot{C}_{fluid,out}}{\dot{X}_{fluid,out}} \qquad (4.17)$$

It is important to emphasize that El-Dessouky et al [1] assumed operation and maintenance cost ($\dot{C}_{OM}$) to be 20% of the total annual cost of the unit. The cost of intake water is assumed to be 4.6 $/hr. The electricity cost is calculated from the equation given below,

$$\dot{C}_{electricity} = C_{electricity}\ SEC\ \dot{V}_{fw} \qquad (4.18)$$

El-Dessouky et al. [1] method to calculate the final product can be expressed as,

$$\dot{C}_{fw} = \dot{Z}_{total} + \dot{C}_{OM} + \dot{C}_{intake} + \dot{C}_{electricity} \qquad (4.19)$$

Thus, the product cost by the cost flow method [82], C_{fw} (in $/m^3) and El-Dessouky et al. [1] approach is calculated by the below equation.

$$C_{fw}(\text{in } \$/\text{m}^3) = \frac{\dot{C}_{fw}}{\dot{V}_{fw}} \qquad (4.20)$$

The assumptions that are used in the cost section, is summarized below.

- The cost of intake water is assumed to be 4.6 $/hr.

- The cost of electricity $C_{electricity}$ is 0.09 $/kWhr.
- Pretreatment costs are neglected and plant availability is assumed to be 90% with a life expectancy of 20 years [1].
- The interest rate (i) is 5%.
- Operation and maintenance cost ($\dot{C}_{OM}$) is assumed to be 20% of the total annual cost of the unit [1].
- The pressure exchanger capital investment is assumed to be the same cost as that of Pelton turbine.

4.3 Results and Discussion

In this section, the results of the second-law analysis are presented and discussed for HDH system with both basic OAOW and modified CWOA cycles. Furthermore, the alternative option of coupling HDH with an RO module is evaluated from exergetic perspective. Then the cost analysis for all aforementioned systems is presented and discussed.

4.3.1 Basic OAOW and Modified CWOA Cycles

Emrah and Serkan [88] reported a second-law efficiency of a CWOA solar driven air heated and water heated varied between 0.03% and 1.867%. From second law analysis, the second-law efficiency of the modified CWOA varies from 0.05% to 0.077% which falls the same region that is reported in [88].

Figure 4.6 illustrates the effect of dehumidifier effectiveness on the exergetic efficiency of the HDH system. The system is operating in the range of component effectiveness that

meets the condition of brine recirculated temperature to be higher than the makeup temperature. The modified cycle (100% brine recirculation) has almost five times higher exergetic efficiency than the basic cycle (0% brine recirculation), which shows the close relation between the GOR and second-law efficiency. As the effectiveness of dehumidifier increases the exergetic efficiency increases, which can be explained by Equation 4.8. The useful exergy, in this case, is the exergy of produced fresh water. It should be noted that an increase in the dehumidifier effectiveness increases by means of better condensation, thus the exergetic efficiency also increases.

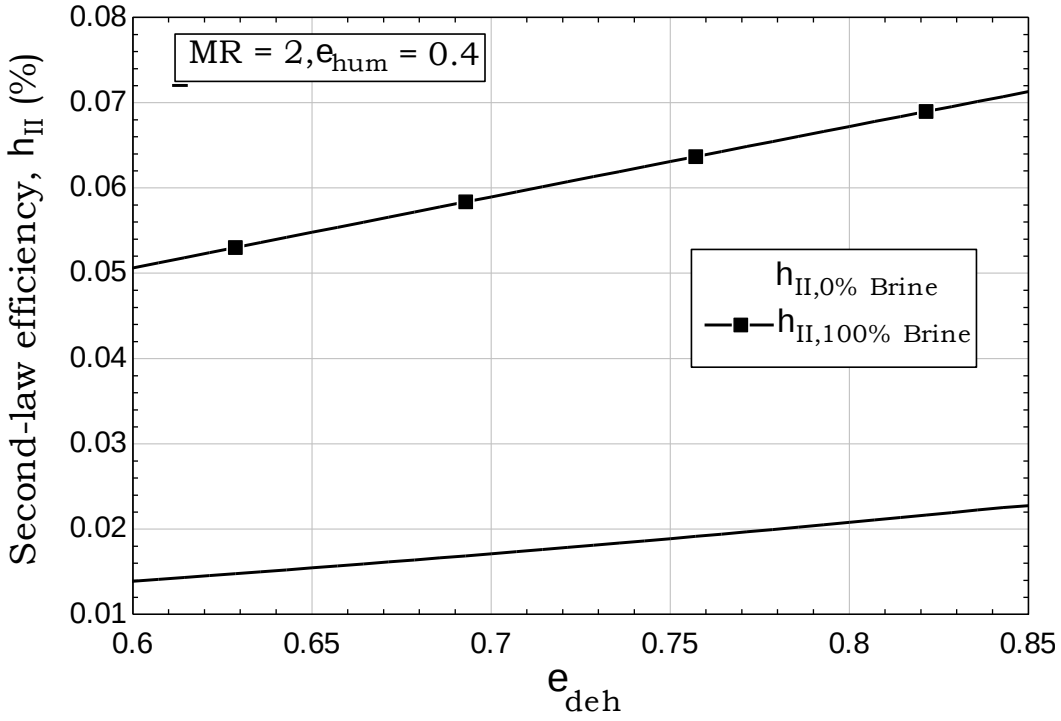

Figure 4.6 Effect of dehumidifier effectiveness on the second-law efficiency for HDH cycles.

Figure 4.7 shows the effect of increasing mass flow rate ratio on the exergetic efficiency of both the HDH cycles. As the basic cycle reaches a peak of 0.04% second-law efficiency at MR=1.45 and then start to drop which occurs due to the definition of

maximum effectiveness change from water to air in the humidifier. This definition change indicates lower water temperature at the humidifier inlet and consequently less evaporation; therefore, the product as well as the exergetic efficiency is also low.

The modified CWOA cycle exergetic efficiency increases along with an increase in MR from slightly above 0.06% to 0.077% for 1-3 MR range. The increase in MR means a decrease in air mass flow rate which provides a better evaporation process due to more time available for air to absorb water vapor. Thus, there is improved product and second-law efficiency. Another possibility is that the saline water mass flow rate is increased, which leads also to more water available for evaporation and consequently more product and improved exergetic efficiency.

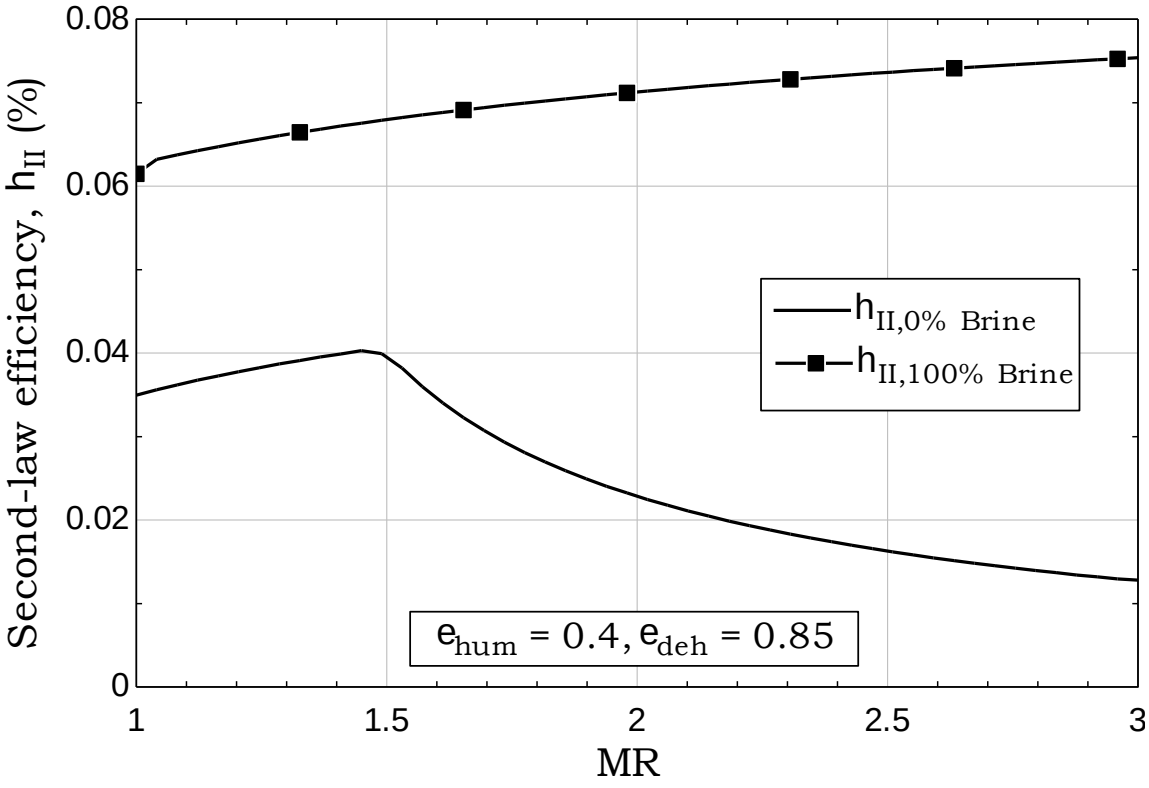

Figure 4.7 Effect of mass flow rate ratio (MR) on the second-law efficiency for HDH cycles.

The percentage of exergy destroyed in each component of the HDH system that operates on basic and modified cycles, having same input conditions that are used in Figure 4.7 is presented in Figure 4.8. The exergy destruction in heater for both the cycles dominates the scene, as expected in thermal processes. In the modified cycle with brine recirculation, the heater has slightly less percentage due to the heat recovery process which explains the better exergetic efficiency of the modified cycle at these input conditions. A humidifier in both cycles comes second in exergy destruction, this is partially due to the low effectiveness used here $\varepsilon_{hum} = 0.4$ compared to $\varepsilon_{deh} = 0.85$ effectiveness used in the dehumidifier. The other reason is that in the humidifier there is a high-temperature difference between the working fluids (ambient air and heated saline water). The humidifier in modified cycle experience a higher percentage since the temperature difference is expected to increase due to heat recovery process as the supplied amount of heat remains constant. In the dehumidifier, particularly due to less temperature difference and high effectiveness $\varepsilon_{deh} = 0.85$ the exergy destruction is almost negligible in both the cycles.

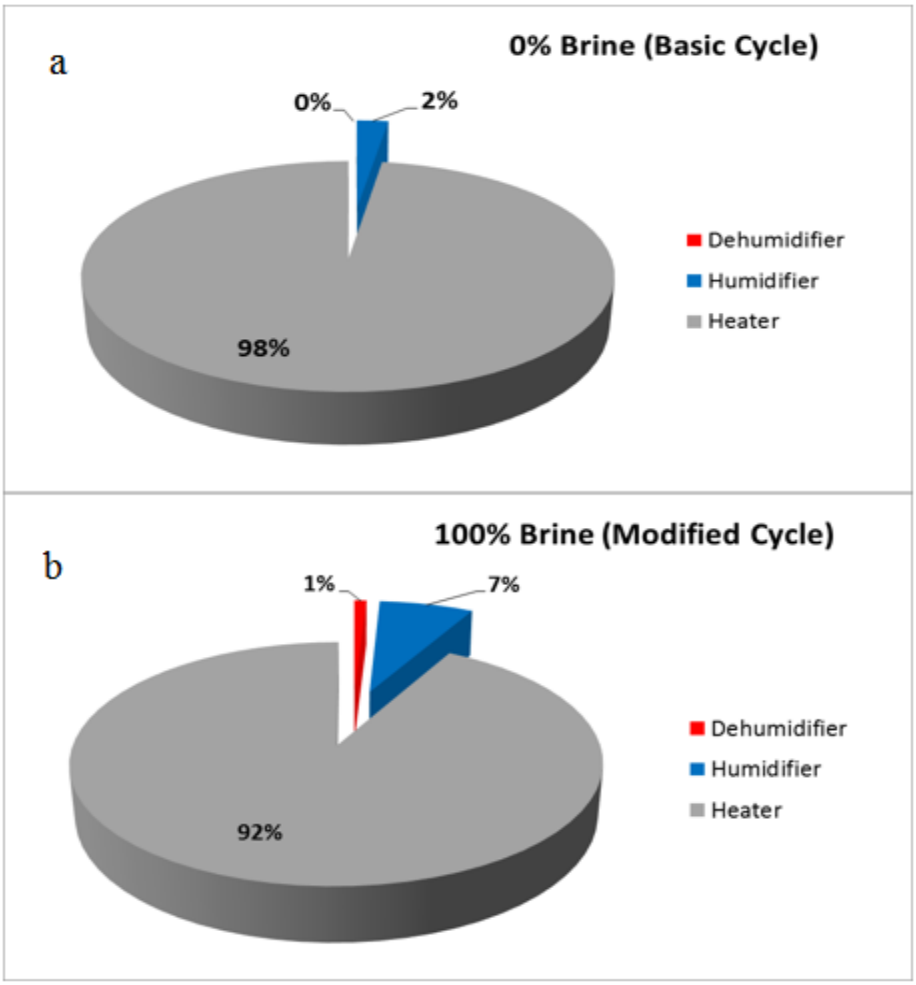

Figure 4.8 Exergy destruction by percentage in each component of (a) HDH (OAOW) basic cycle; (b) HDH (CWOA) modified cycle.

4.3.2 Coupled HDH (OAOW) with RO Module

The alternative approach to heat recovery process is to utilize the brine rejected from the humidifier in an RO system. The important issue to be noticed that the coupling of RO with HDH systems is only practical for Brackish water (<35 g/kg) and brine temperature less than 42 °C [89]. This limitation is basically due to the ability of RO module to withstand hot brine with high salinity coming out of the humidifier. The stand-alone HDH can work for wide range of saline waters, hence the coupling option is only viable

for certain operating conditions. The exergetic analysis has been validated for RO model and found to be in a good agreement with the literature [80].

This approach is analyzed in terms of GOR as shown in Figure 4.9, and in terms of exergetic efficiency as presented in Figure 4.10. The GOR for combined system has increased dramatically from less than 1 to around 16 which is basically due to less energy required in mechanical desalination systems as RO and more production rate at the assumed recovery ratio (50%). The effect of MR on the combined GOR is very small since it mainly affects the HDH system contribution to the final GOR which is very low in comparison to RO contribution.

The combined HDH-RO system with pressure exchanger has the highest GOR since using a pressure exchanger reduces the energy consumption, considerably. The combined HDH-RO with Pelton turbine comes next as the energy recovery reduces the energy required and thus enhances the GOR compared to HDH-RO system without energy recovery process.

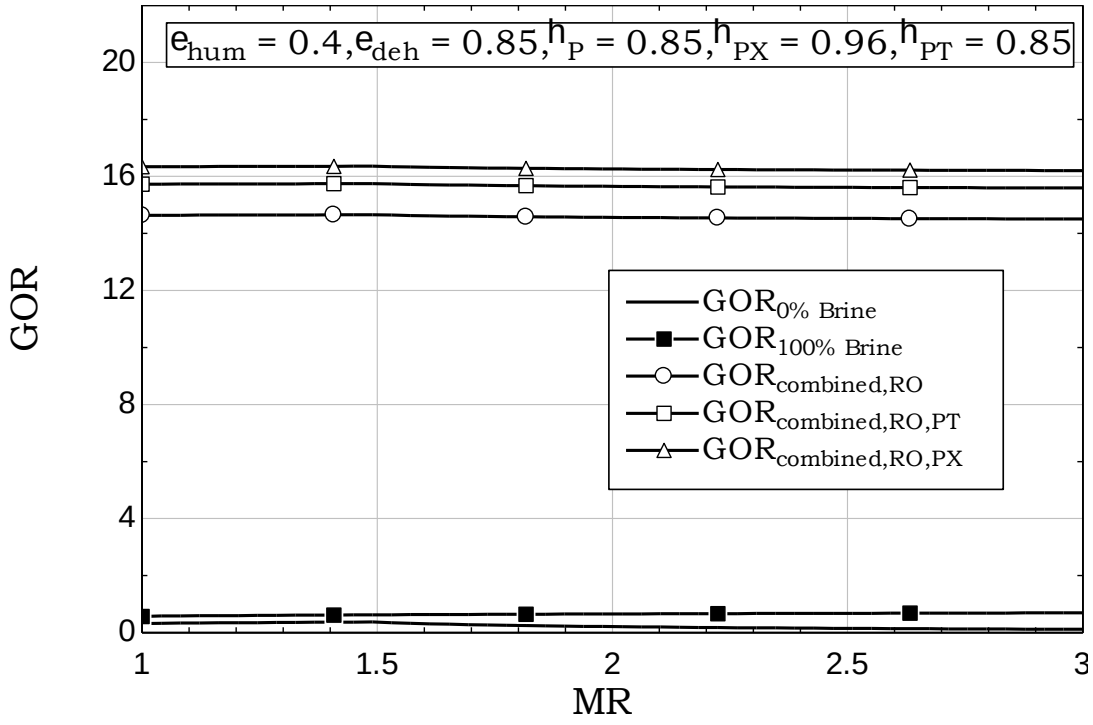

Figure 4.9 Effect of mass flow rate ratio on the performance of HDH cycles and combined HDH and RO systems.

Figure 4.10 illustrates the performance of all systems from exergetic standpoint. The combined system has a better second-law efficiency than the stand alone HDH systems (both basic and modified one). It increased the exergetic efficiency from less than 0.1% for both stand-alone HDH systems to a value around 3% for the combined systems. From the definition of second-law efficiency, this basically is related to the amount of produced fresh water and exergy input to run the system. The combined systems produces more and consume less energy, therefore it has higher exergetic efficiency. The increase in MR increases the second-law efficiency of the combined systems with the increasing MR, this results in higher product; that is, the potable water.

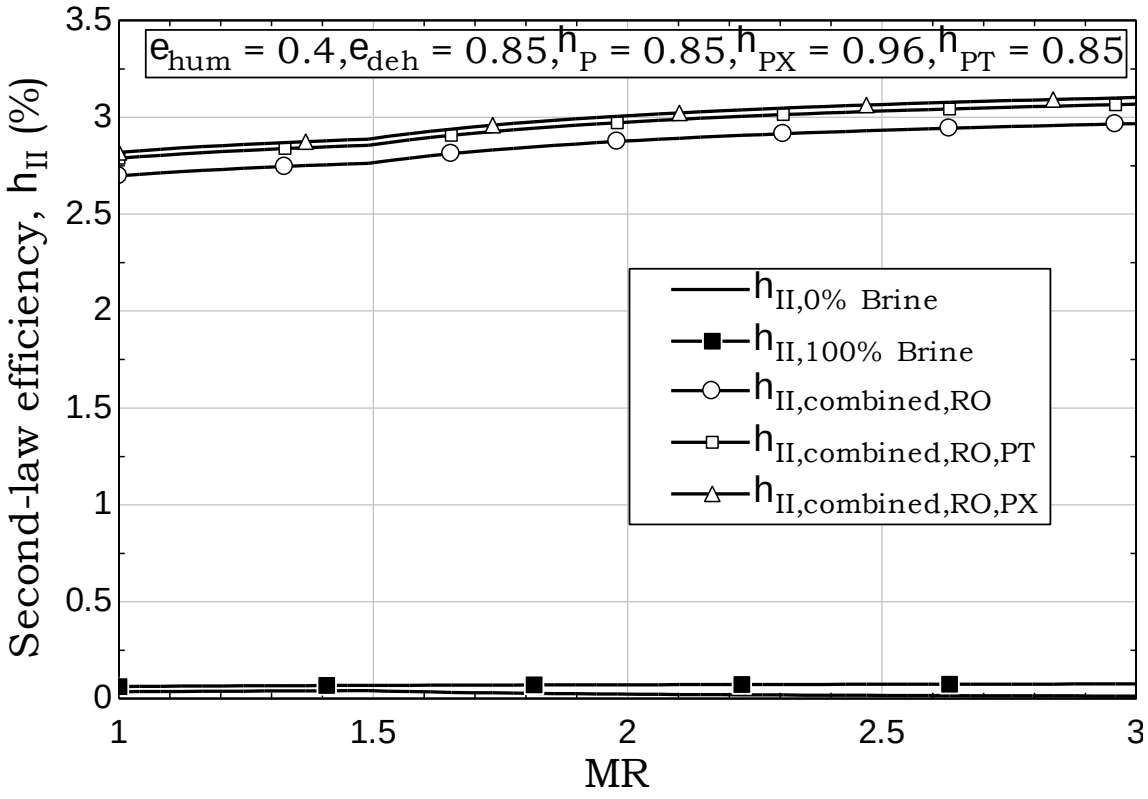

Figure 4.10 Effect of mass flow rate ratio on the exergetic efficiency of HDH cycles and combined HDH and RO systems.

The exergy destroyed, in terms of percentage, for each of the components of the combined HDH-RO systems is shown in Figure 4.11. For all the combined systems, the heater has the highest percentage of exergy destruction compared to other components, which is expected since this is main component where thermal energy is supplied.

For all the systems, dehumidifier contribution remained insignificant due to high effectiveness ε_{deh} = 0.85. The humidifier, which has a low specified effectiveness ε_{hum} = 0.4 and high temperature difference came second to the heater. Other components have small contributions to the total exergy destroyed since they are work-driven devices.

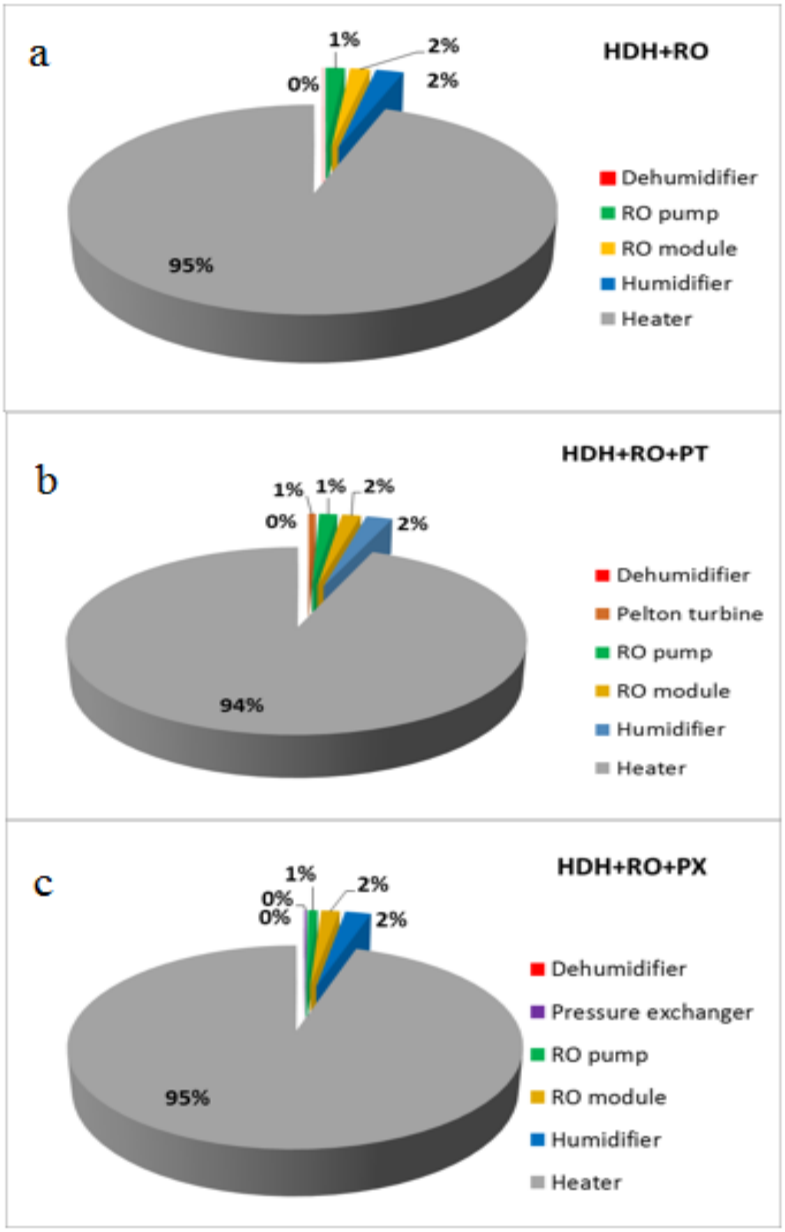

Figure 4.11 Exergy destruction by percentage in each component of (a) HDH with RO; (b) HDH with RO and Pelton turbine; (c) HDH with RO and pressure exchanger.

4.3.3 Parametric Study of Combined HDH-RO system

In this section, the specific energy consumption and exergetic performance of the combined HDH-RO system are studied by varying certain parameters for the RO section.

4.3.3.1 The Effect of High-Pressure Pump Efficiency

The high-pressure pump is used to increase the pressure of brine, leaving the humidifier to 6000 kPa. The effect of this pump efficiency, since it is the major work consuming device in the RO systems, on the overall second-law efficiency and specific energy consumption (SEC) is shown in in Figures 4.12 and 4.13, respectively. It can be seen from Figure 4.12 that the increase in pump efficiency from 0.70 to 0.85 increased the overall exergetic efficiency of all HDH-RO combined systems. Increasing pump efficiency decreases the actual work supplied to the high-pressure pump as can be seen from Equation 4.3. This decrease in work explains the increase in second-law efficiency of the combined systems as the exergy input is reduced.

This increase in pump efficiency increased the exergetic efficiency of HDH-RO without energy recovery from 2.82 to 2.88%, the HDH-RO with Pelton turbine from 2.91 to 2.97% and the HDH-RO with pressure exchanger from 2.97 to 3.1%. The pressure exchanger reduces the pressure needed by the high-pressure pump and hence its work, which justifies an increase in exergetic performance among all the combined systems. Pelton turbine recovers the mechanical energy, which is used to run the high-pressure pump. Thus, it reduces the energy needed from the external source and consequently improves the exergetic efficiency.

The effect of high-pressure pump efficiency on the specific energy consumption for the RO systems is shown in Figure 4.13. As expected, the amount of energy consumed is a minimum for the RO with pressure exchanger, which is then followed by the RO with Pelton turbine, and finally the maximum for the RO system without energy recovery unit.

This behavior is consistent with what has been explained in Figure 4.12; that is, the amount of work consumed by the RO systems is directly proportional to the second-law efficiency and inversely proportional to the specific energy consumption. Since the least amount of work consumed is for the system with the pressure exchanger, this justifies its lowest energy consumption.

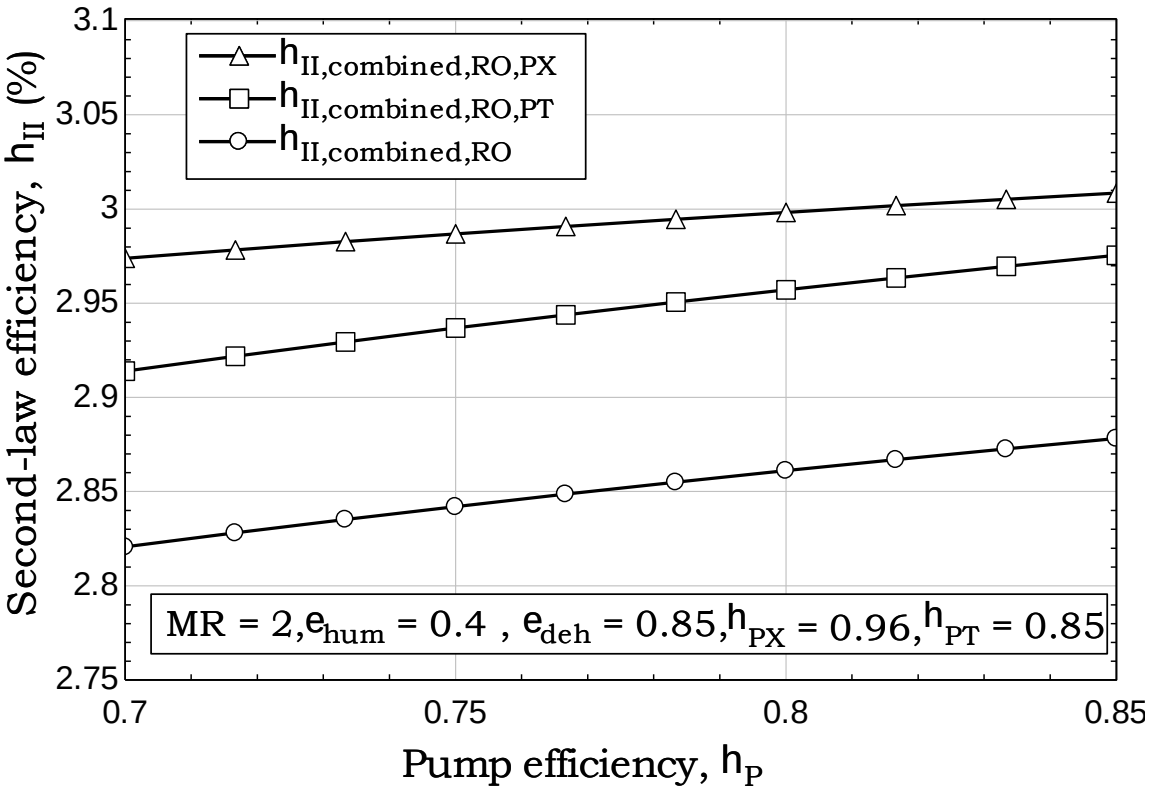

Figure 4.12 Effect of high-pressure pump efficiency on the exergetic efficiency of the combined HDH and RO systems.

The increase in pump efficiency decreases the actual work supplied and subsequently the specific energy consumption. As it increases from 0.70 to 0.85, the SEC decreases from 4.6 to 3.8 kWh/m^3 for the stand-alone RO system, 3.30 to 2.45 kWh/m^3 for the RO with Pelton turbine, and finally from 2.5 to 2.05 kWh/m^3 for the RO with pressure exchanger.

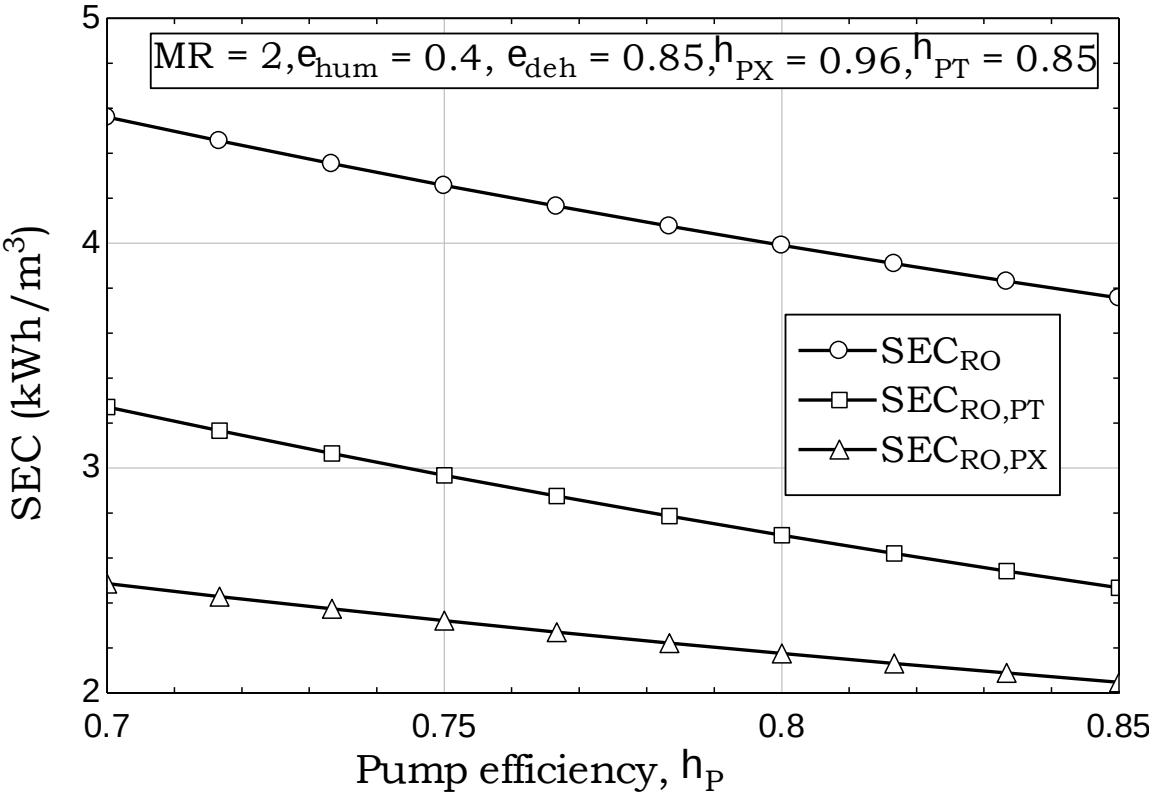

Figure 4.13 Effect of high-pressure pump efficiency on the specific energy consumption(SEC) of the RO systems.

The increase of pump efficiency from 0.70 to 0.85 has decreased the SEC of RO with Pelton turbine by 34.7% and the SEC of RO and RO with pressure exchanger by 21 and 22%, respectively. The effect of pump efficiency is more significant in RO with Pelton turbine since it decreases the amount of energy needed to be supplied from the external source.

4.3.3.2 The Effect of Pelton Turbine Efficiency

Figure 4.14 shows the effect of increasing Pelton turbine efficiency on the second-law efficiency at different values of high-pressure pump efficiencies. As discussed earlier, the

higher pump efficiency results in a higher exergetic efficiency. The figure shows that increasing Pelton turbine efficiency increases the second-law efficiency linearly. As the energy recovered increases, the exergy supplied from an external source decreases, thus the second-law efficiency increases.

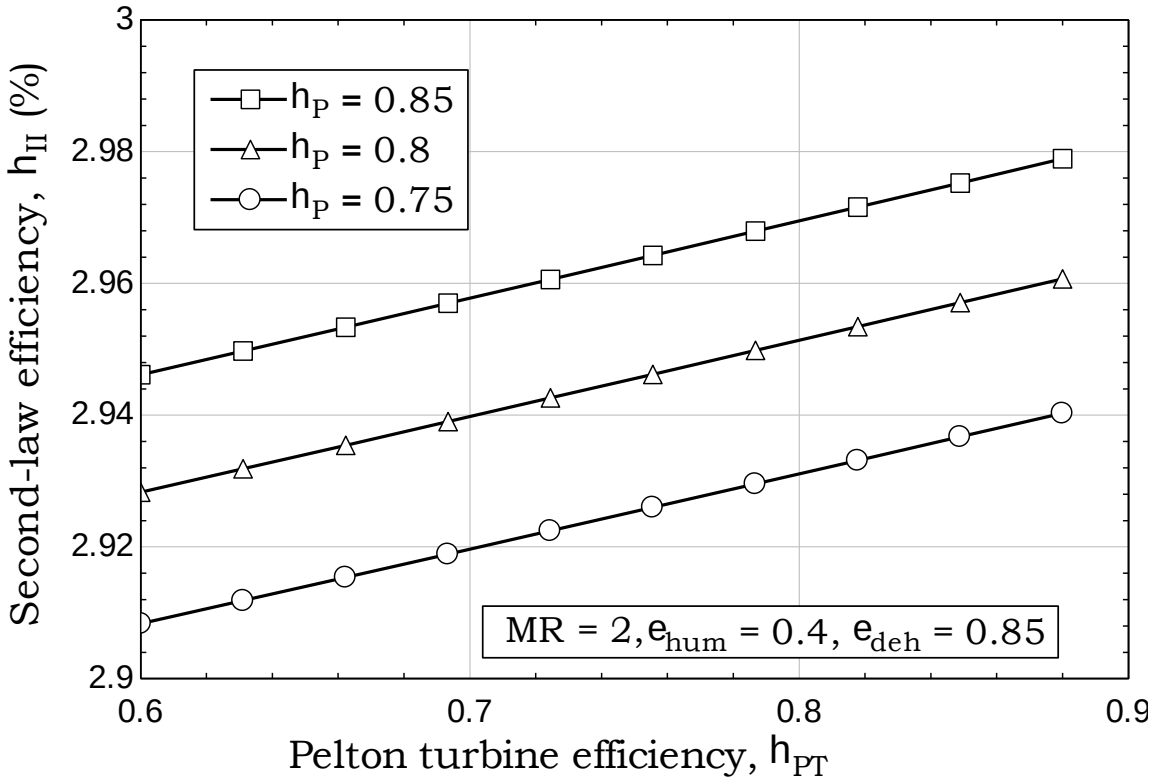

Figure 4.14 Effect of Pelton turbine efficiency on the exergetic efficiency of the combined HDH and RO system with Pelton turbine at different high-pressure pump efficiencies.

Increasing Pelton turbine efficiency from 0.60 to 0.88 increases the overall exergetic efficiency by 1.1% for combined HDH-RO system with pump efficiencies of 0.85, 0.80 and 0.75, respectively. The SEC of this system is decreased linearly as Pelton turbine efficiency increased from 0.60 to 0.88 as shown in Figure 4.15. The increase in Pelton turbine efficiency increases the amount of energy supplied (internally) to the high-

pressure pump and reduces the energy consumed externally. This explains the decrease in the SEC. Increasing Pelton turbine efficiency from 0.60 to 0.88, decreases the SEC by 17.5%,15.9% and 14.5% for combined HDH-RO system with pump efficiencies of 0.85, 0.8 and 0.75, respectively. As expected, the increase in high-pressure pump efficiency reduces the SEC.

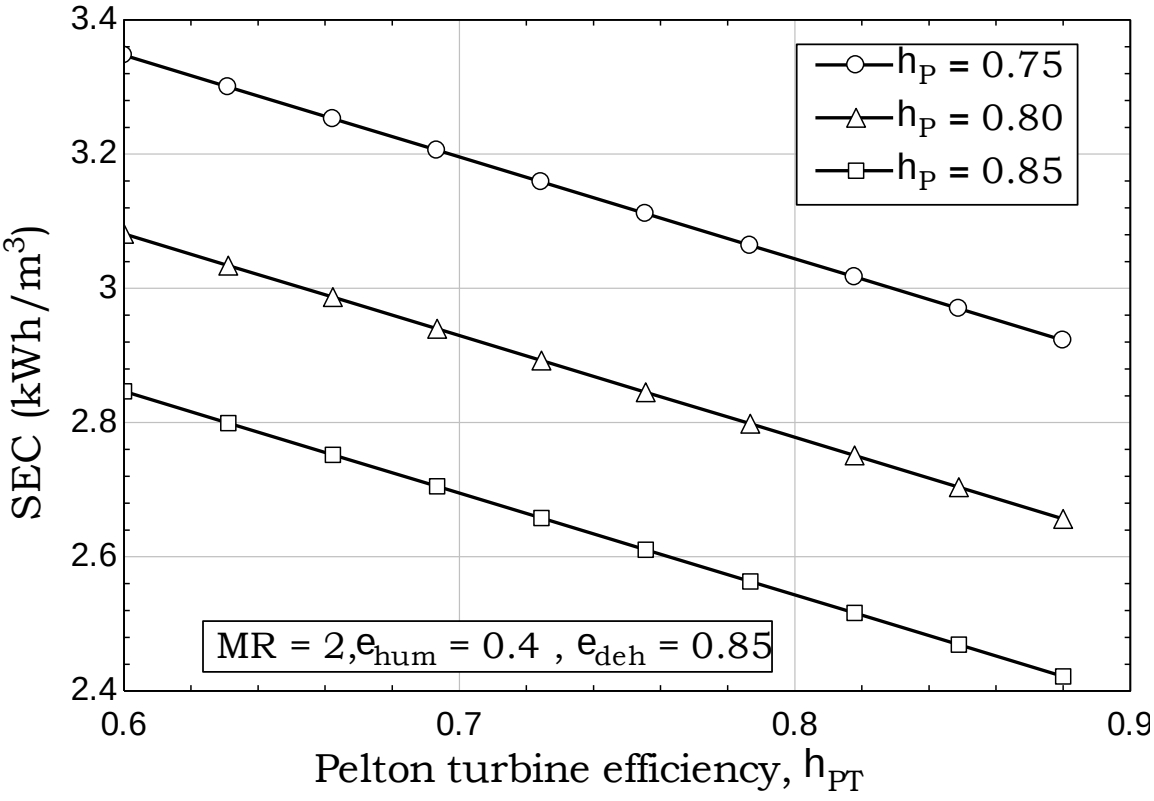

Figure 4.15 Effect of Pelton turbine efficiency on the specific energy consumption (SEC) of the RO system with Pelton turbine at different high-pressure pump efficiencies.

4.3.3.3 The Effect of Pressure Exchanger Efficiency

Increasing the pressure exchanger efficiency from 0.85 to 0.96 increased the overall second-law efficiency of the combined HDH-RO system linearly as shown in Figure 4.16. The increase in pressure exchanger efficiency results in a higher pressure of the

stream entering the high-pressure pump. This increase in pressure of the feed to the pump means the work required by the pump is reduced and hence the input exergy.

Increasing pressure exchanger efficiency from 0.85 to 0.96 increases overall exergetic efficiency by 1.9%, 0.6% and 0.5% for combined HDH-RO system with pump efficiencies of 0.75, 0.8 and 0.85, respectively. This suggests that the pump efficiency is more significant for the overall exergetic efficiency than the pressure exchanger or Pelton turbine efficiencies.

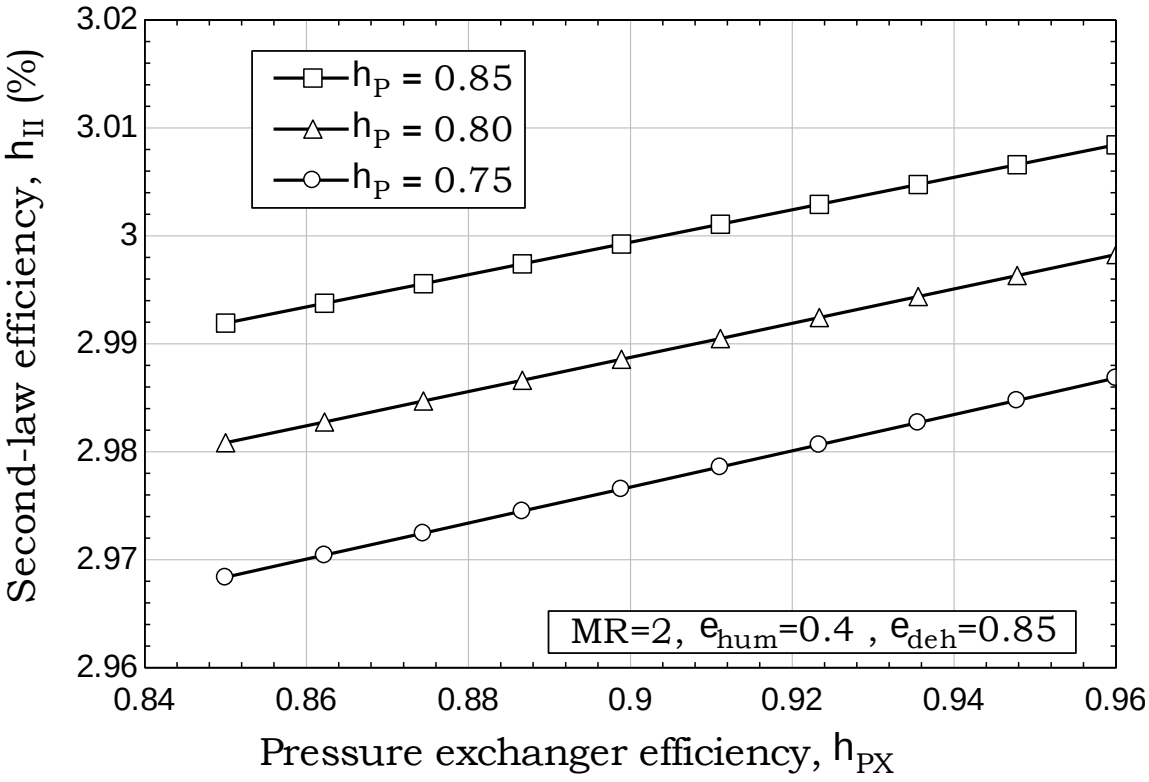

Figure 4.16 Effect of pressure exchanger efficiency on the exergetic efficiency of the combined HDH and RO system with pressure exchanger at different high-pressure pump efficiencies.

Figure 4.17 shows that increase in pressure exchanger efficiency is inversely proportional to the SEC of combined HDH-RO system with a pressure exchanger unit. The increase in pressure exchanger efficiency decreases the amount of work needed by the high-pressure

pump and thus decreases the SEC. Increasing pressure exchanger efficiency from 0.85 to 0.96 decreases SEC by 10.1% for combined HDH-RO system with pump efficiencies of 0.85, 0.8 and 0.75, respectively.

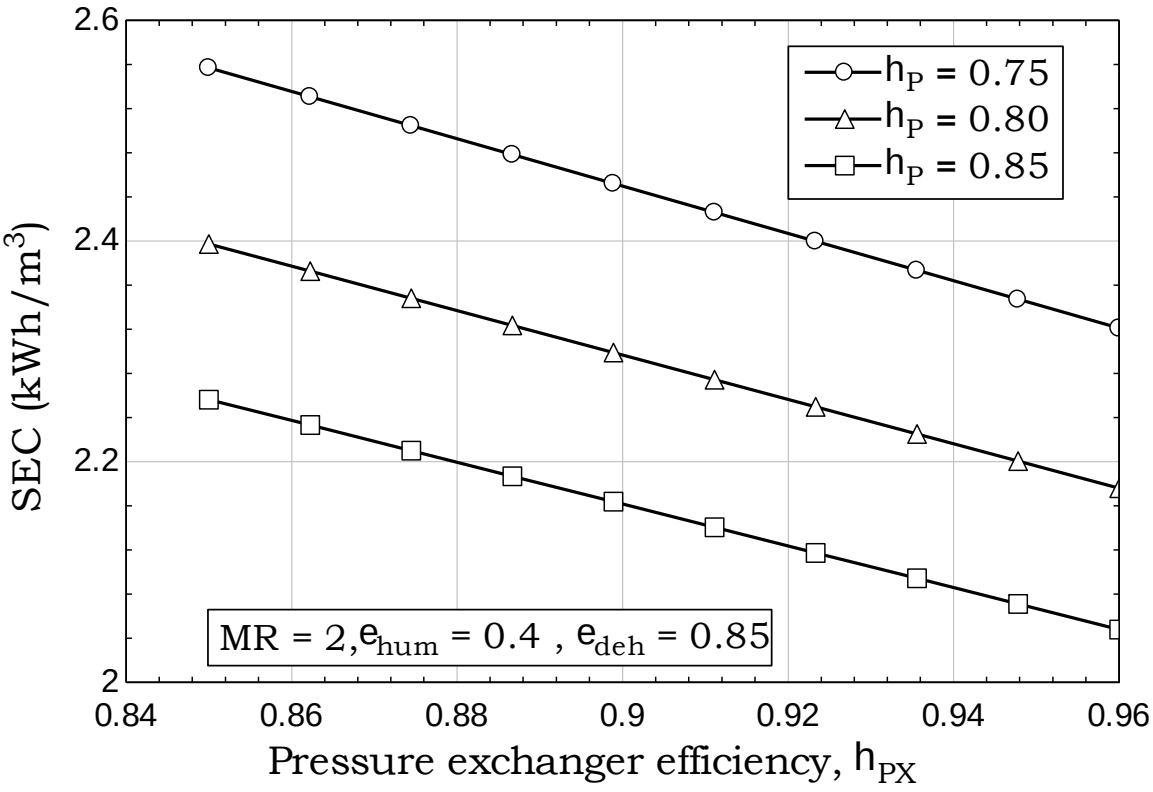

Figure 4.17 Effect of pressure exchanger efficiency on the specific energy consumption (SEC) of the RO system with pressure exchanger at different high-pressure pump efficiencies.

4.3.4 Economic Analysis

Two methods are applied to estimate the production cost of the HDH systems and HDH-RO combined systems. The first method is suggested by El-Dessouky et al. [1] in which the unit is considered as a closed box that has been invested in, then the cost of the output product is calculated. The other method which is the cost flow method, which is proposed by Bejan et al. [82]. In the later approach, the cost of each stream is calculated from cost balance equations and then the final production cost is obtained. In this method, the cost

of each component is defined and a clear picture can be seen; for example, which component is more sensitive to the overall cost. The most influential component of the final product cost, can be further investigated with an overall objective of reducing the product cost.

4.3.4.1 Economic Analysis of Basic (OAOW) and Modified (CWOA) Cycles

The basic input parameters that are assumed for both the basic and modified cycles is used with the humidifier effectiveness of $\varepsilon_{hum} = 0.4$ and dehumidifier effectiveness of $\varepsilon_{deh} = 0.85$ and MR = 2. The only input that has been changed is the total heat input which is increased from 4.5 to 5.6 kW (the amount used in the experimental work). The reported production cost for small-scale HDH systems in the literature ranges from 6.4 to 9.74 $\$/m^3$ [90,91].

The product cost for the basic OAOW cycle that uses electrical heater was 6.37 $\$/m^3$ (El-Dessouky method) and 6.56 $\$/m^3$ (cost flow method). The product cost when the system utilized solar heater was 5.81 $\$/m^3$ (El-Dessouky method) and 5.98 $\$/m^3$ (cost flow method). The second-law efficiency for this system was 0.033%. The high production cost is due to the small amount of produced water. It is clear from these results that using solar heater reduced the production cost by 9.6% (El-Dessouky method) and 9.7% (cost flow method) since it does not have a high running cost despite the huge difference in the investment cost.

The product cost for modified CWOA cycle that uses electrical heater was 2.82 $\$/m^3$ (El-Dessouky method) and 2.8 $\$/m^3$ (cost flow method). The product cost when the system

utilized solar heater was 2.57 $/m^3 (El-Dessouky method) and 2.54 $/m^3 (cost flow method). The second-law efficiency for this system was 0.074%. The production cost for this system is also high due to the low amount of produced fresh water and is also indicated by the low second-law efficiency. This result is highlighting the major problem of HDH systems, which is mentioned earlier in the introduction chapter; that is, the high-energy requirement of HDH systems for water production.

Also, here the utilization of solar heater reduces the production cost by 9.73% (El-Dessouky method) and 10% (cost flow method). The modified system has better second-law efficiency and subsequently a lower production cost as a result of the energy recovery process. It reduces the production cost of the systems with the electrical heater by 126% (El-Dessouky method) and by 134% (cost flow method). For the systems that utilized solar heaters, the production cost reduced by 126% (Dessouky method) and by 135% (cost flow method). This is basically due to energy recovery which enhanced the second-law efficiency by 124%.

The rate of investment cost for main components that are used on stand-alone HDH system is presented in Table 4.2. The solar heater has the highest investment cost rate of 0.052 $/hr and then comes the dehumidifier of 0.006 $/hr, while electrical heater has the lowest investment cost of 0.001 $/hr. The investment cost of the solar heater is higher when compared to the electrical heater but at the end of the day, the production cost is reduced by using the solar energy. As discussed in Chapter 2 the coupling of HDH systems with renewable energy enhanced its economic performance and tackled its main issue of high energy requirement.

Table 4.2 Rate of investment cost for main components of HDH system operates on basic and modified cycles.

Component	Rate ($/hr)	
	Basic and Modified Cycles	
	HDH (Solar heater)	HDH (Electrical heater)
Humidifier	0.002	0.002
Dehumidifier	0.006	0.006
Solar heater	0.052	-
Electrical heater	-	0.001
Tank	0.002	0.002
Pump	0.001	0.001
Blower	0.003	0.003

4.3.4.2 Economic Analysis of a Coupled HDH-OAOW with RO Module

The same analysis is repeated for the coupled system and the results by using both El-Dessouky method and cost flow method are reported in this section for the combined HDH-RO system. The option of using an electrical heater or solar heater is included in the analysis and the results are reported in this section. The reported production cost of RO systems ranges from 0.14 to 0.95 $/m^3$ [92].

The product cost for combined HDH-RO that used electrical heater was 0.11 $/m^3$ (El-Dessouky method) and 0.13 $/m^3$ (cost flow method). The product cost when the system utilized solar heater was 0.11 $/m^3$ (El-Dessouky method) and 0.12 $/m^3$ (cost flow method). The second-law efficiency for this system was 2.78%. The low production cost is due to a large amount of produced water and is also clear from the increase in second-law efficiency (83 times), which is considered as an economic index, compared to the basic OAOW stand-alone HDH system. The utilization of RO module reduced the production cost by almost 57 times for a system with electrical heater and 52 times for a system with solar heater. It is clear from these results that using solar heater has a negligible effect on this combined system since it will only affect the HDH unit and it has a little contribution to the amount of produced water.

The product cost for combined HDH-RO with Pelton turbine and used electrical heater were 0.11 $/m^3$ (El-Dessouky method) and 0.13 $/m^3$ (cost flow method). The product cost when the system utilized solar heater was 0.11 $/m^3$ (El-Dessouky method) and 0.12 $/m^3$ (cost flow method). The second-law efficiency for this system was 2.86%. The production cost for this system is also low due to the high amount of produced fresh

water, which is also indicated by the increase in second-law efficiency (85 times) compared to the basic cycle HDH system. It is clear from these results that using solar heater has a negligible effect on this combined system final product cost. The production cost of this combined system remained almost the same compared to simple HDH-RO combined system despite utilizing another component (Pelton turbine). This suggests a better exergetic performance resulting from adding Pelton turbine substitute for investment cost and additional operating and maintenance costs due to the addition of another component.

The product cost for combined HDH-RO with pressure exchanger and using an electrical heater were 0.11 $\$/m^3$ (El-Dessouky method) and 0.13 $\$/m^3$ (cost flow method). The product cost when the system utilized solar heater was 0.11 $\$/m^3$ (El-Dessouky method) and 0.12 $\$/m^3$ (cost flow method). The second-law efficiency for this system was 2.88%. The production cost for this system is also low due to the high amount of produced fresh water. It is also indicated by the increase in second-law efficiency (86 times) compared to the basic HDH cycle. Similar to a combined system with Pelton turbine using solar heater have a negligible effect on this combined system final product cost. Also, the production cost of this combined system remained almost the same compared to a simple HDH-RO combined system and HDH-RO with Pelton turbine. This suggests that better exergetic performance resulting from adding the pressure exchanger substitute for investment cost and additional operation and maintenance costs due to the addition. A conclusion can be drawn from all the above discussion is, the combined system with pressure exchanger has the best performance in terms of the GOR, second-law efficiency and production cost.

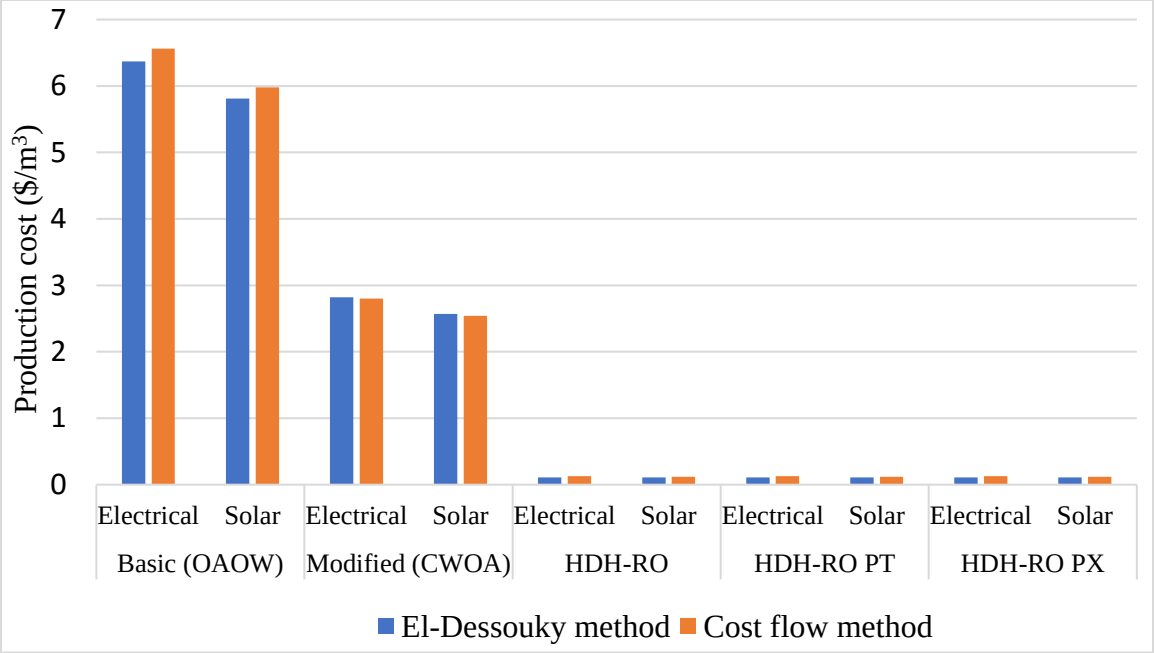

Figure 4.18 Production cost using both El-Dessouky and cost flow methods in each configuration of both stand-alone HDH and combined HDH-RO systems.

The rate of investment cost for main components that are used in RO section of the combined HDH-RO systems is presented in Table 4.3. RO module has the highest investment cost rate of 0.011 $/hr and then comes the Pelton turbine and pressure exchanger with fixed cost rate of 0.002 $/hr. The addition of RO systems adds a total investment rate of 0.0114 $/hr for the simple RO and 0.0134 $/hr for the RO with PT and RO with PX. The addition of recovery unit as discussed earlier improves the performance of the combined system significantly with just 17.5 % increase in the total investment cost rate of the RO section.

Table 4.3 Rate of investment cost for RO section main components in HDH-RO combined systems.

Component	Rate ($/hr)		
	Combined HDH-RO systems		
	HDH-RO (Simple)	HDH-RO (PT)	HDH-RO (PX)
High-pressure pump	0.0004	0.0004	0.0004
RO module	0.011	0.011	0.011
Pelton turbine	-	0.002	-
Pressure exchanger	-	-	0.002
Total RO section	0.0114	0.0134	0.0134

Chapter 5

Performance Evaluation of Conventional and Modified Closed-Air Open-Water HDH Systems with Extractions

The work in the literature regarding air extraction has focused on water heated CAOW cycle as a basic configuration. In this chapter, the closed-air open-water (CAOW) HDH arrangement is modified by incorporating heat recovery options. The heat recovery process is executed through two approaches, (i) a mixing chamber and, (ii) by a heat exchanger. Thermal balancing through air extraction is also evaluated for the basic as well as the modified cycles. Zero, single and double extractions models are evaluated for the conventional CAOW water heated cycle and both the modified cycles. An operating scheme is also developed to decide when to use the modified cycle or the basic cycle with or without extraction.

5.1 Performance and Operating Metrics

The GOR is the ratio of the latent heat of vaporization of fresh water to the amount of heat utilized to produce it.

$$GOR = \frac{\dot{m}_{fw} \times h_{fg}}{\dot{Q}_{in}} \qquad (5.1)$$

The effectiveness of the dehumidifier:

$$\varepsilon_{deh} = \max < \frac{h_{a2} - h_{a1}}{h_{a2} - h_{a1,ideal}}, \frac{h_{w1} - h_{w0}}{h_{w1,ideal} - h_{w0}} > \quad (5.2)$$

The ideal enthalpy of the outlet air is taken at the temperature of the inlet water, while the ideal enthalpy of the outlet seawater is measured at the inlet air temperature [77].

The effectiveness of the humidifier is expressed as:

$$\varepsilon_{hum} = \max < \frac{h_{a2} - h_{a1}}{h_{a2,ideal} - h_{a1}}, \frac{h_{w2} - h_{w3}}{h_{w2} - h_{w3,ideal}} > \quad (5.3)$$

Similarly, the ideal enthalpy of the outlet air is taken at the temperature of the inlet water, while the ideal enthalpy of the outlet seawater is measured at the inlet air temperature [77].

5.2 Conventional and Modified Cycles Description

The HDH systems are generally simple and cheap. In addition, they may be fabricated by a low-skilled labor which may result in low effectiveness humidifier. Thus, the hot brine coming out of the humidifier (refer to Figure 5.1) can be utilized to recover part of this heat instead of throwing it away. This recovery can be attained either through mixing part of the hot brine with the cooling water that leaves the dehumidifier in a mixing chamber before the heater or by installing a heat exchanger as illustrated in Figures 5.2 and 5.4. These modifications aim to reduce the heat input and increase the GOR of the system. In this study, zero, single and double air extractions are evaluated for both the conventional and modified CAOW water heated cycles.

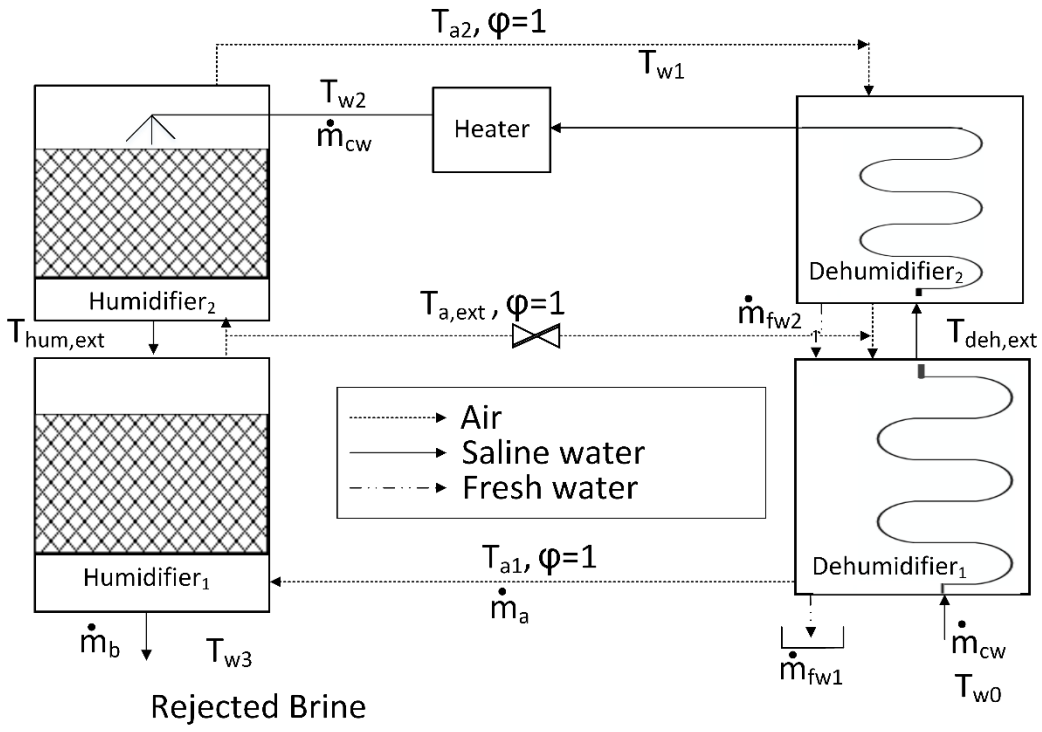

Figure 5.1 Water-heated CAOW HDH cycle with zero and single extraction.

5.2.1 Conventional Closed-Air Open-Water (CAOW), Water Heated Cycle

In this arrangement as illustrated in Figure 5.1 saline water enters the dehumidifier as cooling water and warms up before it is heated in a water heater or solar collector. The heated water is then sprayed in the humidifier which has a packing material to increase the heat and mass transfer area that enhances the evaporation process, the remaining unevaporated brine is rejected. The air loop in this cycle is closed, it enters the humidifier at low humidity and leaves as hot and humid air. Thereafter, it enters the dehumidifier where it undergoes a cooling and dehumidifying process. The condensate water is then collected as a fresh water at the bottom of the dehumidifier and air is circulated back to the humidifier to close the loop. In the case of single extraction, some of the air is extracted from the humidifier and injected into the dehumidifier by simply opening the

valve, as shown in Figure 5.1, while the double extractions cycle is illustrated in Figure 5.2 where there are two valves.

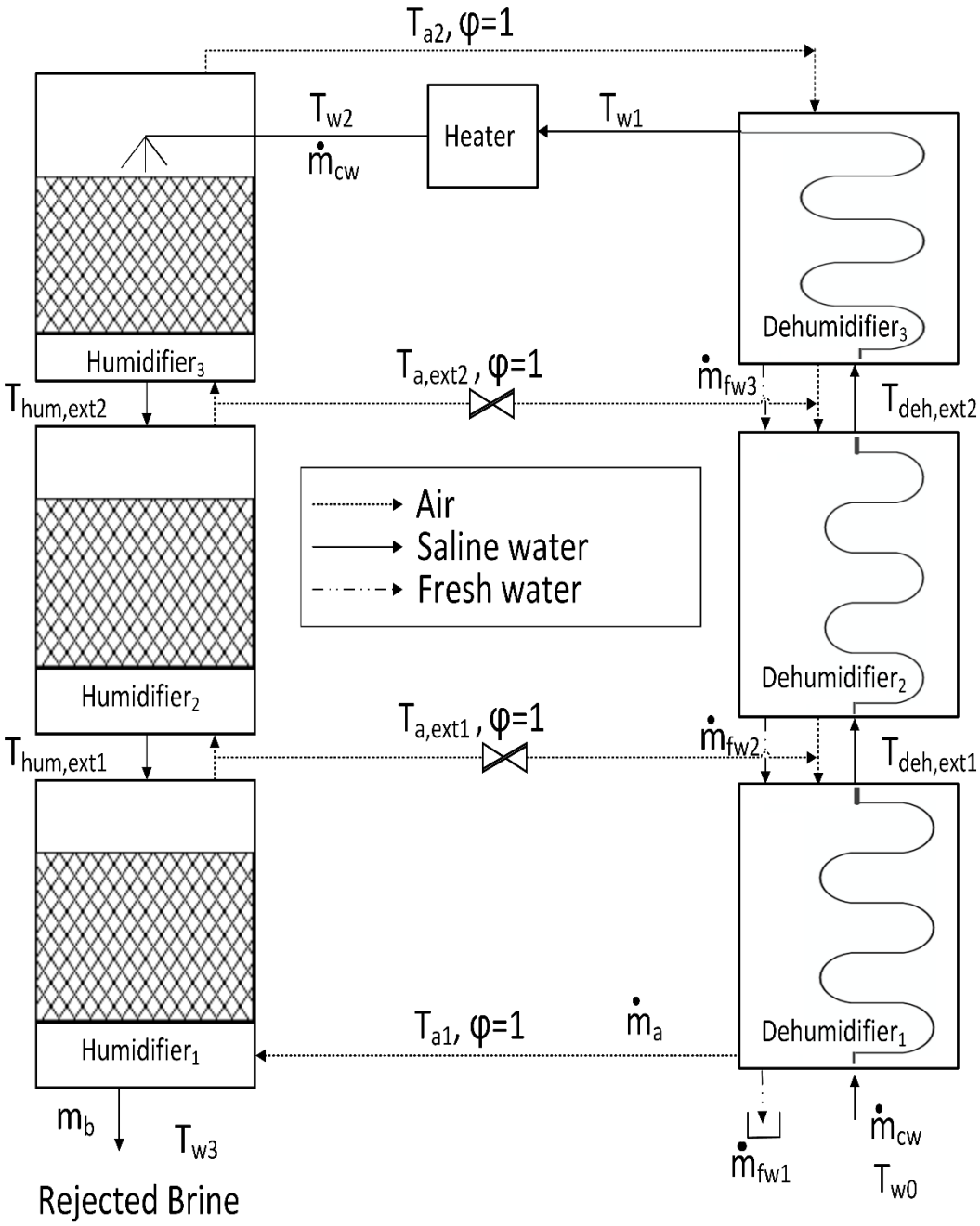

Figure 5.2 Water-heated CAOW HDH cycle with double extractions.

5.2.2 Modified Closed-Air Open-Water with Heat Recovery Options

The modification in this cycle includes adding a heat exchanger, as illustrated in Figures 5.3 and 5.4 wherein the hot brine is piped to a heat exchanger where it is used to heat the saline water coming from the dehumidifier before it enters the heater. The rest of the cycle remains the same as the conventional cycle, which is explained in the previous section.

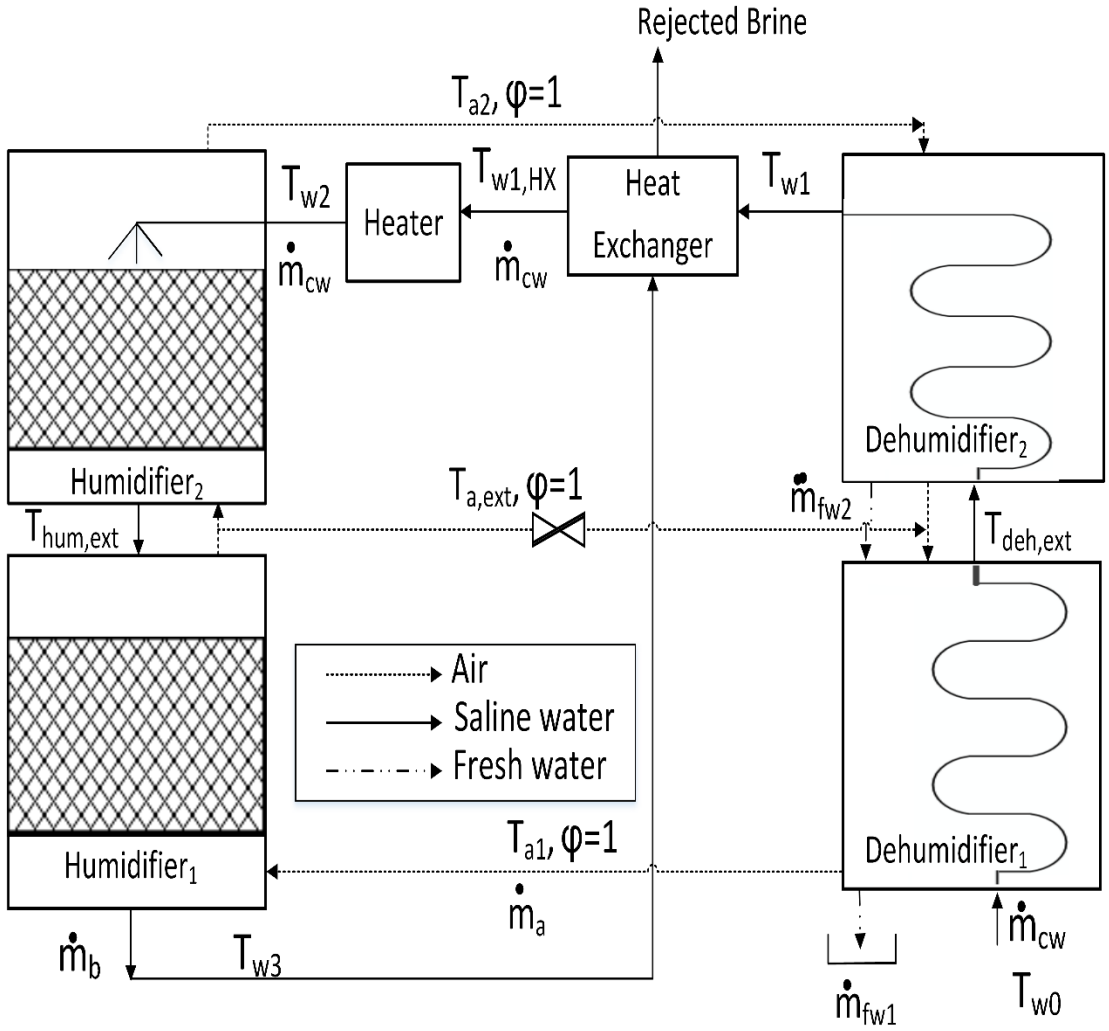

Figure 5.3 Water-heated CAOW HDH cycle after heat exchanger modification with zero and single extraction.

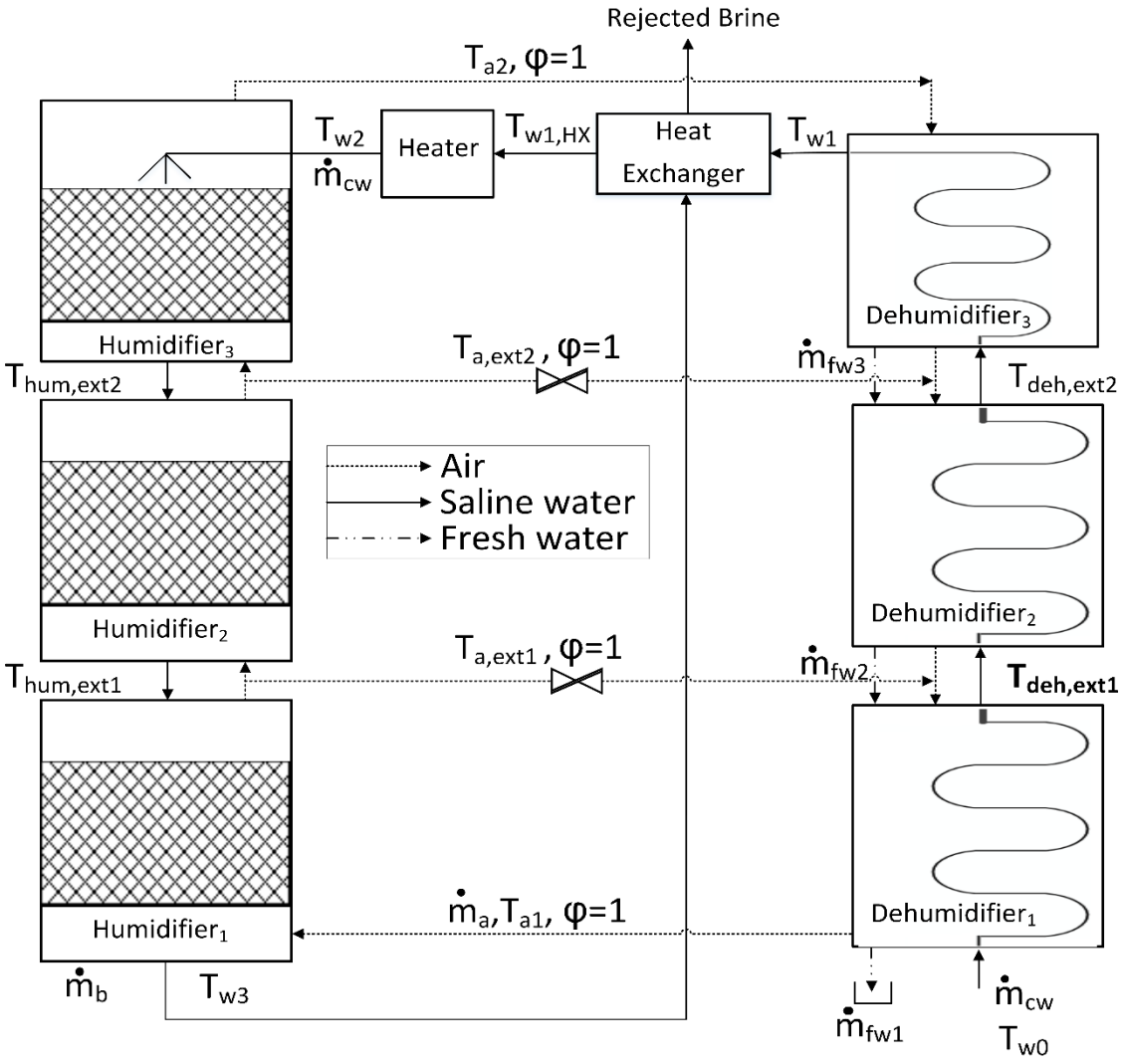

Figure 5.4 Water-heated CAOW HDH cycle after heat exchanger modification with double extractions.

In the other modified cycle, as shown in Figures 5.5 and 5.6, the heat recovery process is carried out by mixing the hot brine with cooling water coming out of the dehumidifier in a mixing chamber. To achieve this and keep the salinity level steady, there is a need to have water from two sources with different salinity levels. A low-salinity cooling water from the dehumidifier; that is, tap water (< 3,000 ppm), and start-up saline-water (40,000 ppm). Saline water is passed through the heater and then sprayed in the humidifier where evaporation process takes place. The remaining hot brine is then collected and part of it is

circulated back to the mixing chamber where it mixes with the make-up low-salinity cooling water to close the water loop. The mixed water is then passed through the heater under steady-state operating conditions. The air loop remains the same as the conventional CAOW; however, for single air extraction, the valve can be opened to allow humid air to flow into the dehumidifier. This cycle is shown schematically in Figure 5.5 for zero and single extraction, while Figure 5.6 presents the double extractions case.

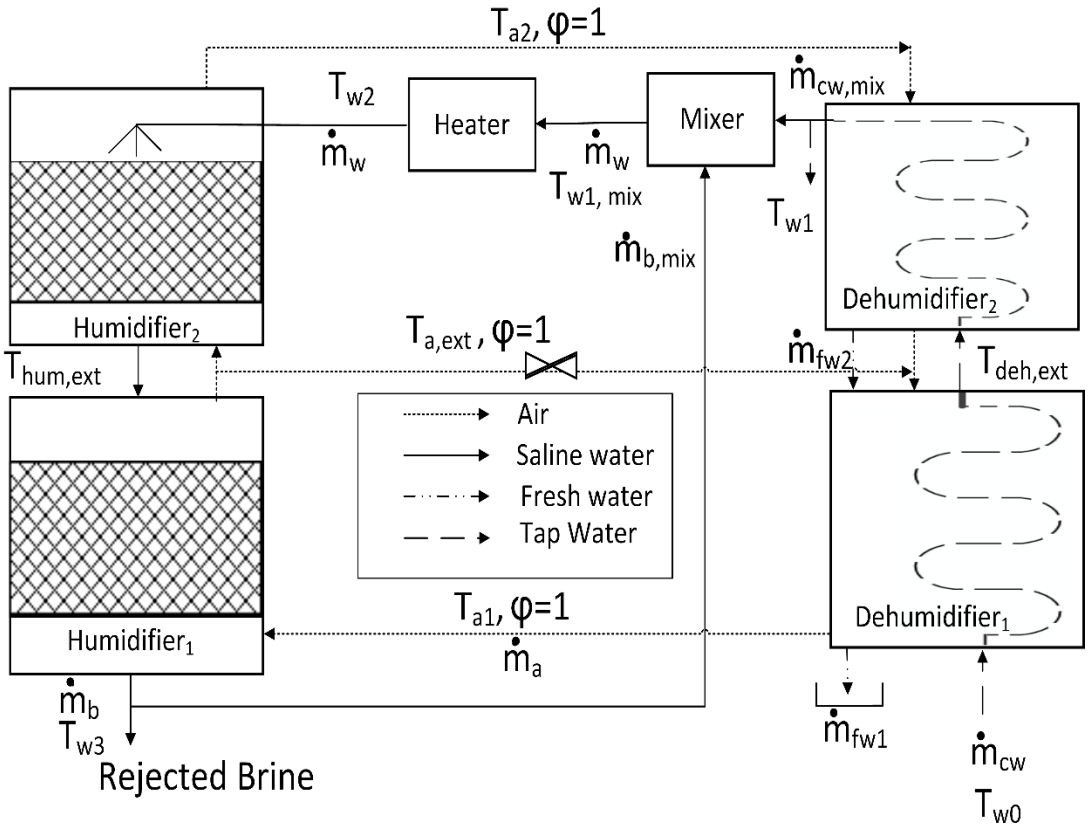

Figure 5.5 Water-heated CAOW HDH cycle after mixing chamber modification with zero and single extraction.

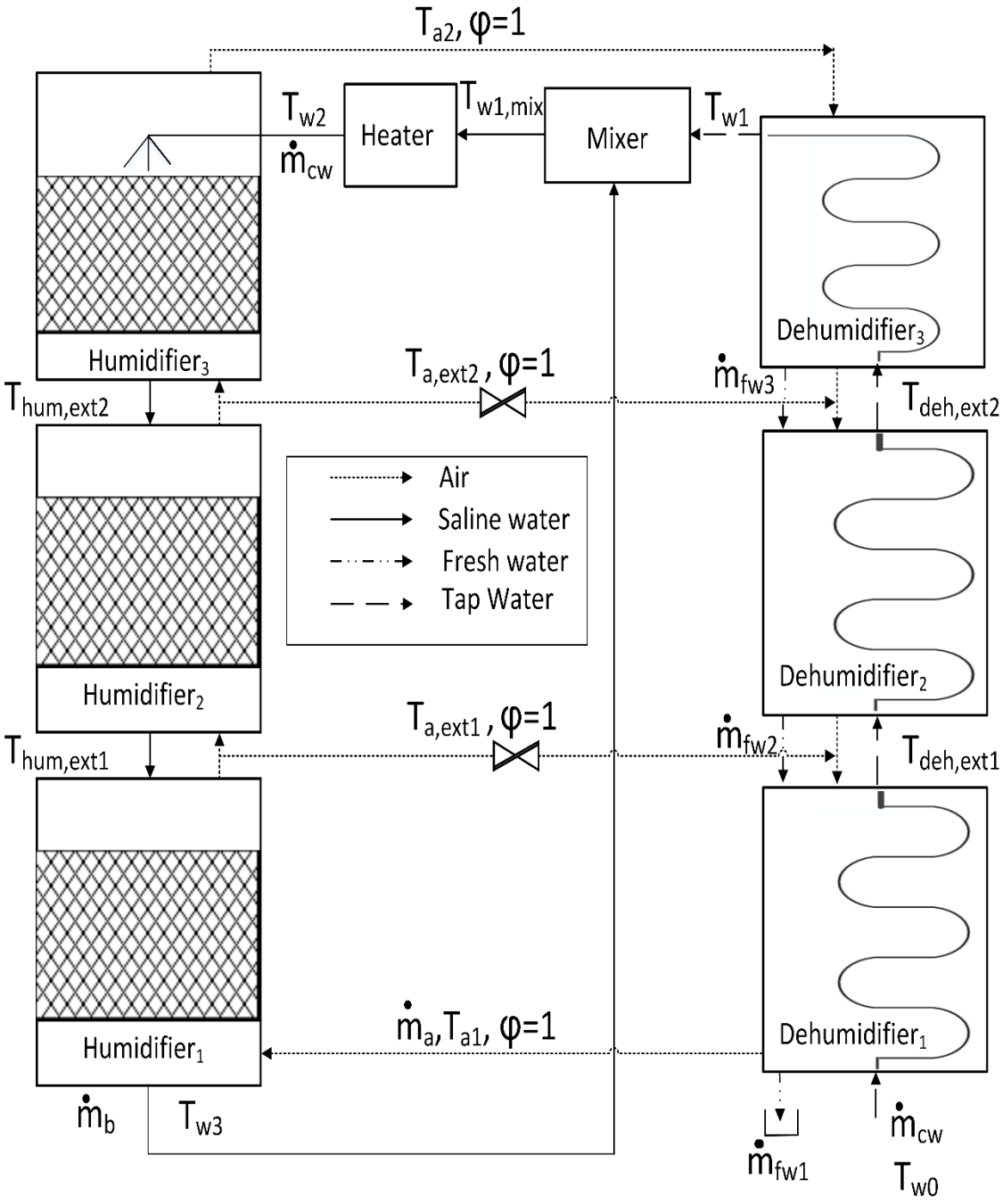

Figure 5.6 Water-heated CAOW HDH cycle after mixing chamber modification with double extractions.

5.3 Modeling

The present study is following the enthalpy pinch model for HME devices as illustrated by Narayan et al. [70]. The enthalpy pinch procedure is a novel procedure introduced to study the effect of mass transfer as well as the heat transfer in humidifiers and dehumidifiers. This method is applied to all the aforementioned systems. For example, a temperature-enthalpy diagram for HDH systems with zero extraction is exhibited in Figure 5.7. The curved line presents the air process through the humidifier and dehumidifier. The solid line presents the water process through the dehumidifier and the dotted line through the humidifier. The enthalpy pinch of the dehumidifier can be expressed as,

$$\Psi_{deh} = h_{a1} - h_a \qquad (5.4)$$

where h_a is calculated at T_{w0}.

While the enthalpy pinch of the humidifier is,

$$\Psi_{hum} = (h\_\tan' - h\_\tan) \qquad (5.5)$$

here $h\_\tan'$ presents the enthalpy calculated at the tangent point at the air saturation curve, and $h\_\tan$ presents the enthalpy obtained at the tangent point at the humidifier line, as illustrated in Figure 5.7.

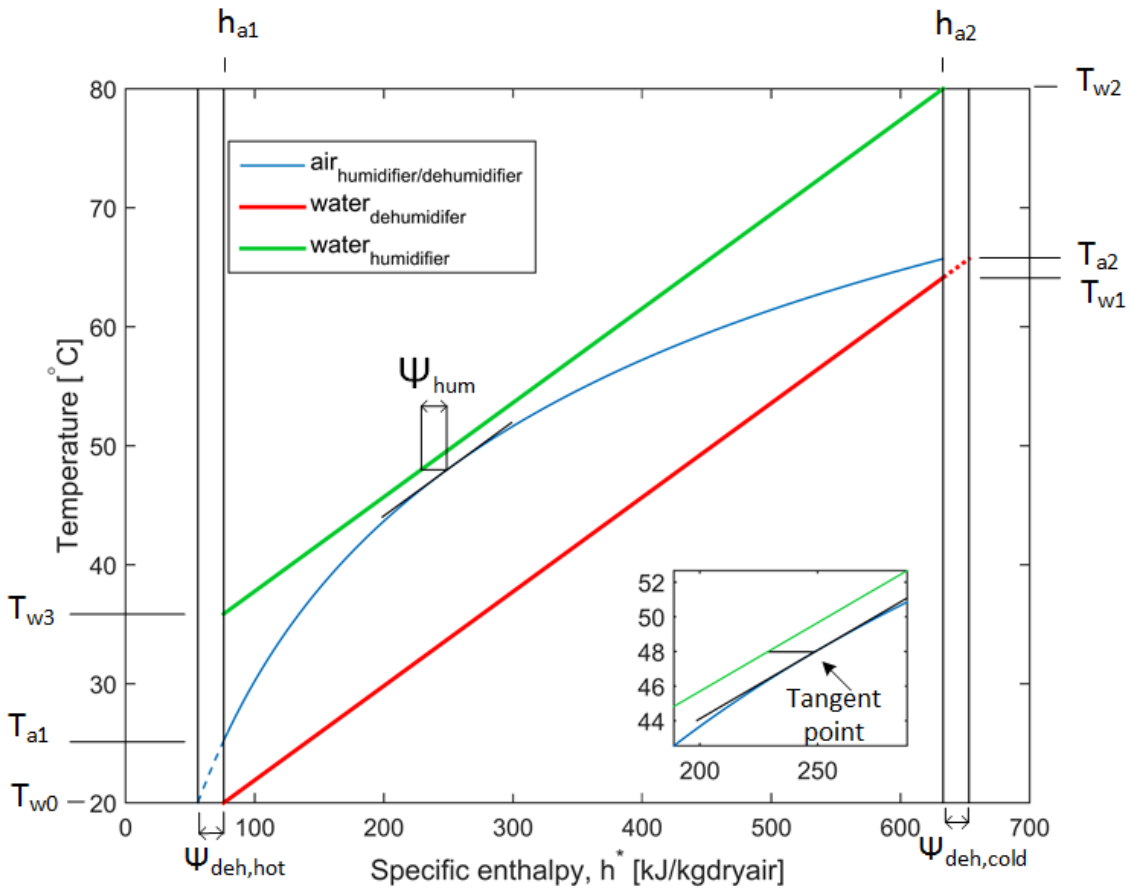

Figure 5.7 Temperature-enthalpy profile of the system without extraction.

5.3.1 Zero Extraction System

Thermal balancing in HME devices is attained through varying mass flow rate ratio (MR). This process can be achieved by extracting air from the humidifier and injecting it into the dehumidifier either at one point or two points (single or double extractions) as illustrated in cycles description in section 5.2. Zero extraction system refers to the case when the extraction valves in all cycles (conventional and modified) are closed i.e. no extraction. Figures 56 through 58 represent the concept for zero, single and double extractions processes, respectively. Visualization and modeling of these systems depend on this figure. The idea is to convert these figures into a mathematical model to evaluate

the performance of zero, single and double extractions system as shown in Figure C.1 of Appendix C. The inputs of the system are as follows: the cooling water temperature, the top brine temperature, the humidifier enthalpy pinch and the dehumidifier enthalpy pinch. The enthalpy pinch method is briefly discussed in the literature [58,60,62,66]. These studies recommended using this method instead of temperature pinch.

As the inputs are the same for the conventional and modified cycles, the only difference is observed in the calculation of heat input, $\dot{Q}_{in}$. The process of calculating $\dot{Q}_{in}$ for CAOW is summarized in the following equations:

$$\dot{Q}_{in} = \dot{m}_{cw} c_p (T_{w2} - T_{w1}) \qquad (5.6)$$

For the CAOW with a heat exchanger,

$$\dot{Q}_{in} = \dot{m}_{cw} c_p (T_{w2} - T_{w1,HX}) \qquad (5.7)$$

and for the CAOW with a mixing chamber,

$$\dot{Q}_{in} = \dot{m}_{cw} c_p (T_{w2} - T_{w1,mix}) \qquad (5.8)$$

In Equation 5.6 the temperature of water at the outlet of the dehumidifier (T_{w1}) is calculated using the mathematical approach as illustrated in Figure C.1 of Appendix C. While $(T_{w1,HX})$ and $(T_{w1,\mathrm{mix}})$ can be found from mass and energy balance for the heat exchanger and mixing chamber, respectively, as shown in the following equations:

$$\varepsilon_{HX} = \frac{\dot{m}_{cw} c_{p,cw} (T_{w1,HX} - T_{w1})}{\dot{m}_{b,HX} c_{p,HX} (T_{w3} - T_{w1})} \quad (5.9)$$

$$\dot{m}_{cw,mix} + \dot{m}_{b,mix} = \dot{m}_w \quad (5.10)$$

$$\dot{m}_{cw,mix} X_{cw} + \dot{m}_{b,mix} X_b = \dot{m}_w X_w \quad (5.11)$$

$$\dot{m}_{cw,mix} h_{w1} + \dot{m}_{b,mix} h_{w3} = \dot{m}_w h_{w1,mix} \quad (5.12)$$

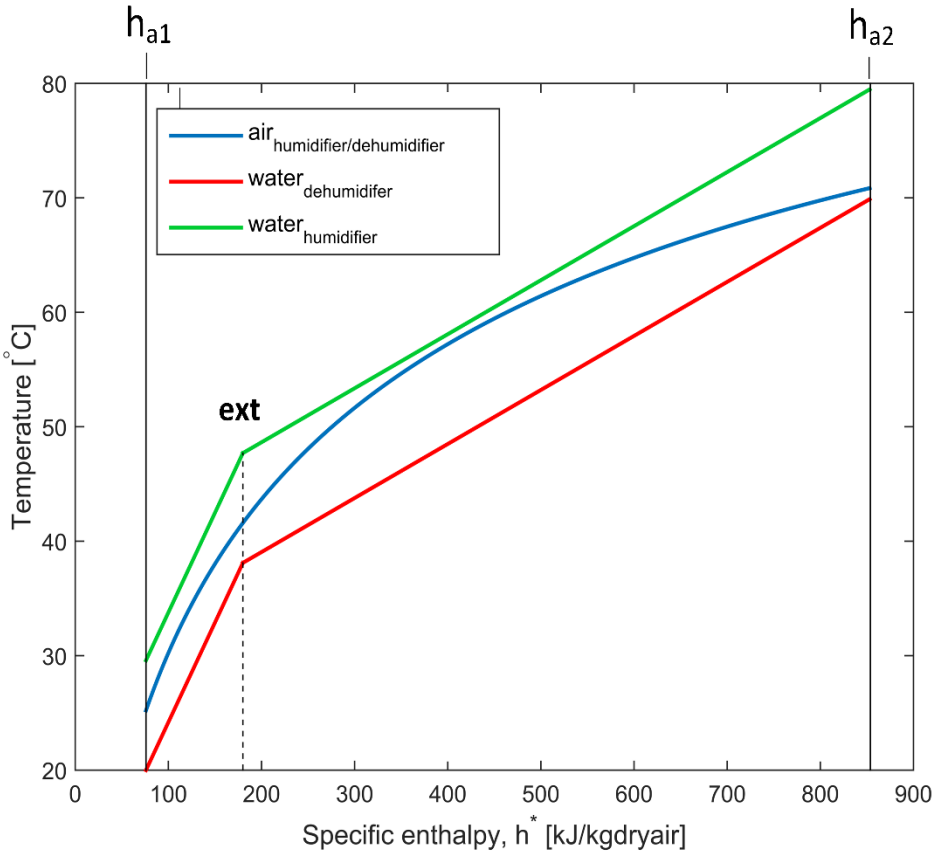

Figure 5.8 Temperature-enthalpy profile of the system with single extraction.

5.3.2 Single Extraction System

The major variation in the single-extraction model is that thermal balancing process is executed in two stages. The algorithm for the single extraction model is illustrated in Figure C.1 of Appendix C. Figure 5.8 presents a temperature-enthalpy profile for all the systems with a single extraction. To avoid entropy generation during the injection process, the air was extracted from state 'ext' at the humidifier and injected at the same state 'ext' at the dehumidifier. This model is applied to the aforementioned systems. In an attempt to validate the results of this work, terminal point temperatures of the current work for the conventional cycle with zero and single extraction has been compared to those reported by Narayan et al. [70] and presented in Table 5.1. The deviation from Narayan work ranged between 0.3 to 2.2 % for zero extraction and between 0.3 to 1.2 % for the single extraction case, which presents a good agreement. It's to be noted, Table 5.1 is a digitized version of Figure 8 from [70]. This figure is generated at enthalpy pinch = 20 kJ/kg dry air (that is, about 97% component effectiveness). This is used merely to validate the authenticity of the code for the basic cycle with extraction. This effectiveness is very high which results in a reverse heat transfer when heat recovery options are applied. However, at low effectiveness regions the water temperature at humidifier outlet (T_{w3}) will be higher than the water temperature at dehumidifier outlet (T_{w1}), hence, the heat recovery process will be feasible as illustrated in Table 5.2. At 77% component effectiveness, the GOR of the proposed modified systems is slightly higher than the conventional system. At 68% and 57% component effectiveness, the GOR is increased by 59.6% and 178.6%, respectively, for heat exchanger option. While for the mixing chamber option the GOR increased by 65.4% and 207.1% at 68% and 57% component

effectiveness respectively. This is will be highlighted in details in the results and discussion section.

Table 5.1 Comparison between Narayan [70] work and the current work for temperatures at the terminal points (refer to Figure 5.1).

	Zero extraction			Single extraction		
Terminal points	Narayan (^{0} C)	Current work (^{0} C)	Error (%)	Narayan (^{0} C)	Current work (^{0} C)	Error (%)
Dehumidifier outlet (T_{w1})	62.6	64	2.2	70.2	69.9	0.4
Humidifier outlet (T_{w3})	36	35.9	0.3	29.8	29.6	0.7
Bottom air temperature (T_{a1})	25.5	25.2	1.2	25.5	25.2	1.2
Top air temperature (T_{a2})	64.3	65.7	2.2	71.1	70.9	0.3
Dehumidifier extraction ($T_{deh,ext}$)	-	-	-	38.5	38.1	1.0
Air extraction ($T_{a,ext}$)	-	-	-	41.9	41.6	1.0
Humidifier extraction ($T_{hum,ext}$)	-	-	-	48.2	47.7	1.0

Table 5.2 Feasibility of heat recovery options at low effectiveness region.

Enthalpy pinch (kJ/kg dry air)	T_{w1} (^{0} C)	T_{w3} (^{0} C)	CAOW	CAOW-HX		CAOW-MX	
			GOR	GOR	Improvement (%)	GOR	Improvement (%)
105 ($\mathcal{E}$ =77%)	49.9	50.1	0.85	0.86	1.2	0.86	1.2
115 ($\mathcal{E}$	47.6	52.3	0.74	0.85	14.9	0.86	16.2

=75%)							
125 ($\mathcal{E}$ =71%)	45.2	54.8	0.63	0.85	34.9	0.86	36.5
135 ($\mathcal{E}$ =68%)	42.6	57.4	0.52	0.83	59.6	0.86	65.4
145 ($\mathcal{E}$ =64%)	39.7	60.3	0.42	0.82	95.2	0.86	104.8
160 ($\mathcal{E}$ =57%)	34.7	65.3	0.28	0.78	178.6	0.86	207.1

5.3.3 Double Extraction System

As discussed in section 5.3.1, the algorithm for the double extractions model is also shown in Figure C.1 of Appendix C. The modeling process of double extraction is performed in three stages rather than two. A temperature-enthalpy profile for all the systems with double extractions is illustrated in Figure 5.9. As explained by the single extraction model, air is also extracted from states 'ext1'and 'ext2' at the humidifier and injected at the same states 'ext1'and 'ext2' to the dehumidifier, this helps to avoid entropy generation. These three models are then used to examine the performance of the conventional and modified cycles. For further validation, the results for GOR for the conventional cycle using double extractions model are compared with Chehayeb et al. [72] and presented in Table 5.3. The results show good agreement with the literature with a maximum deviation of 3.4%.

Table 5.3 Comparison between Chehayeb [72] work and the current work for GOR at different enthalpy pinch for the conventional cycle with double extractions.

Enthalpy pinch (kJ/kg dry air)	Chehayeb	Current work	Error (%)
0	17.4	17.5	0.6

10	8.2	8.2	0
20	4.3	4.2	2.3
30	2.9	2.8	3.4
40	1.9	1.9	0

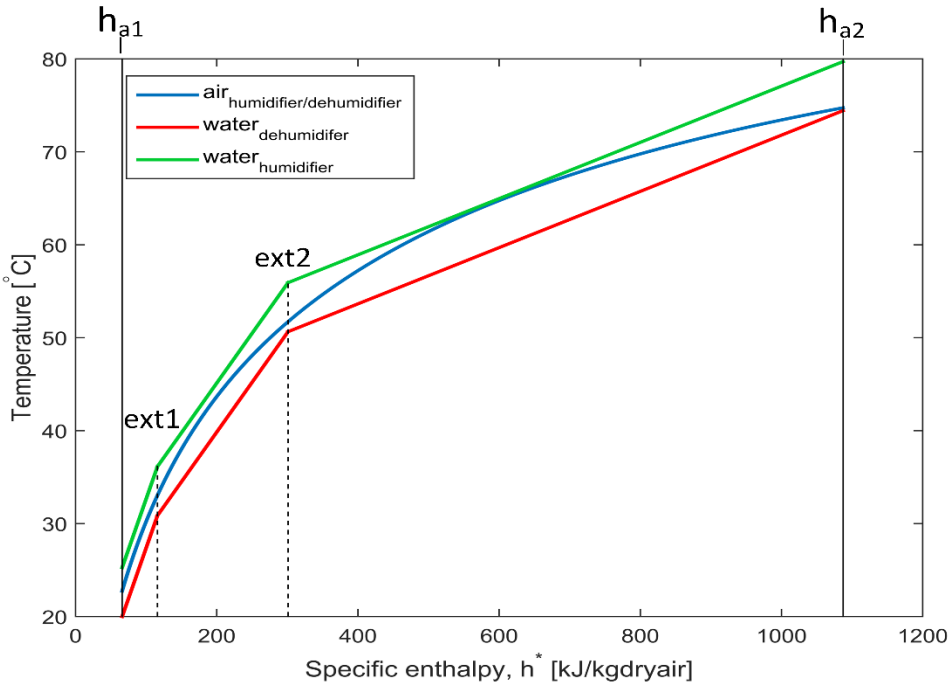

Figure 5.9 Temperature-enthalpy profile of the system with double extractions.

5.4 Results and Discussion

In this section, the performance of the conventional CAOW water heated cycle and the modified cycles (CAOW-HX, CAOW-MX) is evaluated with zero, single and double extractions**.**

5.4.1 Effect of The Difference Between Top and Bottom Temperatures

5.4.1.1 Conventional CAOW Water Heated Cycle

Figure 5.10 illustrates the effect of the temperature difference on water heated CAOW system performance with zero, single and double extractions at zero enthalpy pinch (that is, 100% component effectiveness). It is clear that as the difference increases the GOR decreases for all cases. Since the bottom temperature is fixed for two cases at 20 °C and 30 °C, respectively. It is found that the increase in temperature difference leads to increase in the total heat input. Thus, the GOR drops accordingly. In addition, it is to be noted that at 20 °C the GOR is higher than at 30 °C. This is because of the fact that the ability of cold water to condensate more potable water.

The reduction in entropy generation due to the thermal balance associated with single extraction leads to tremendous increase in GOR, which is almost tripled compared to zero extraction at 40 °C temperature difference for bottom temperatures of 20 °C, and 30 °C. For the double extractions case, we notice the increase in GOR is even higher than five times when compared to zero extraction for the same operating conditions.

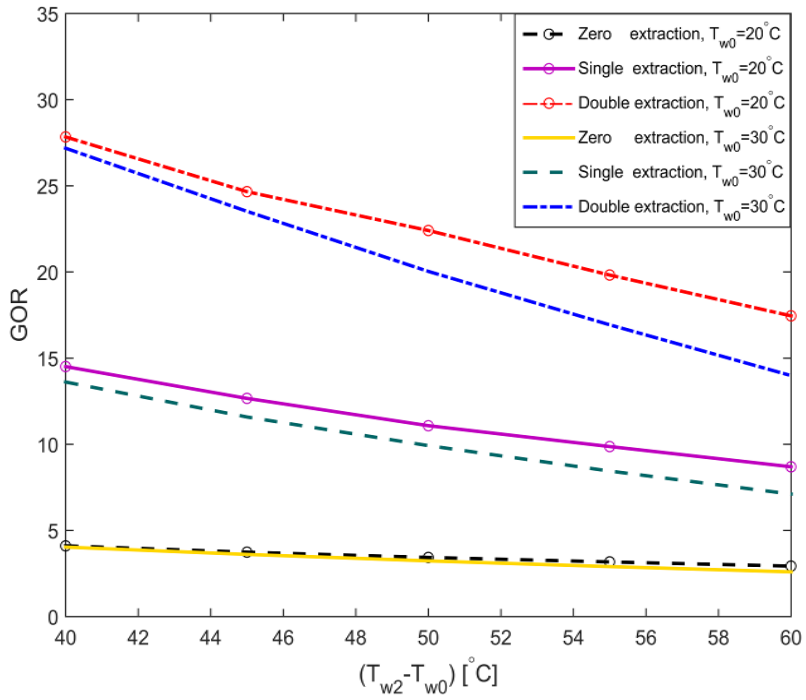

Figure 5.10 Effect of the difference between the top and bottom temperatures on water heated CAOW performance: $\Psi_{deh}= \Psi_{hum}$ =0 kJ/kg dry air.

Figure 5.11 illustrates the behavior of this system under the same operating conditions but at 20 kJ/kg dry air enthalpy pinch (that is, about 97% component effectiveness). The GOR for the 20 °C bottom temperature case increases for all the layouts (with and without extraction) as temperature difference increases. This increase may be associated with the increase in the top cycle temperature which will result in a better evaporation process in the humidifier and consequently more distilled water in the dehumidifier. The single- and double-extraction curves for this case coincide, while the GOR almost doubled compared to zero extraction at 60 °C temperature difference which is mainly due to the thermal balancing.

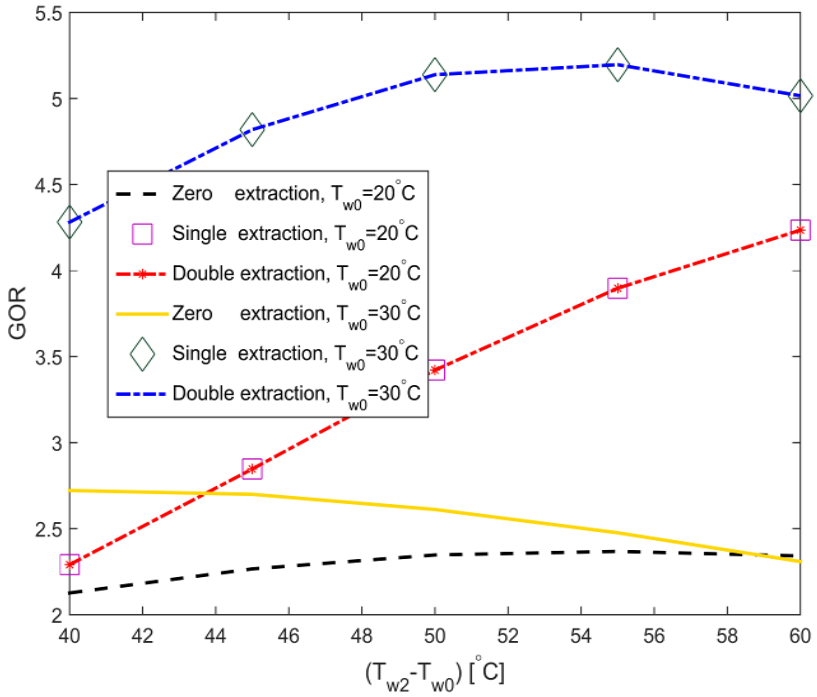

Figure 5.11 Effect of the difference between the top and bottom temperatures on water heated CAOW performance: $\Psi_{deh}= \Psi_{hum}$ =20 kJ/kg dry air.

For the case where the bottom temperature is 30 °C, the GOR for zero extraction decreases as the temperature difference increases due to the increase in the amount of total heat input. Thermal balancing through single and double extractions for this case increases the GOR until temperature difference approaches 55 °C and then starts to drop. This behavior is associated with the increase in the top cycle temperature which means better evaporation until a certain point at which the effect of an increase in total heat input surpasses the effect of vapor generated through increasing the top cycle temperature and thus the GOR drops. By using extraction, GOR increases by more than double for the temperature difference of 55 °C due to the reduction in entropy generation associated with the extraction process. The GOR for 30 °C bottom temperature case is higher when

compared to the 20 °C case for almost zero, single and double extraction. This is mainly because of the less amount of heat input required for 30 °C case.

The GOR for single and double extractions for the case where the bottom temperature = 30 °C is doubled at temperature difference of 40 °C. Then this elevation in GOR decreases until it reaches a difference of almost 0.75 units at temperature difference of 60 °C. This decrease in the difference may be associated with the decrease in the total heat input required compared to the effect of cooler water's ability to condensate more potable water. After reaching a temperature difference of 59 °C, it is noticed that the GOR for the 20 °C case with zero extraction slightly exceeds the 30 °C case. At this point, the effect of the cooler water to condensate the water exceeds that of the total heat input required.

Figures 5.12 and 5.13 show the impact of running the system with the above operating conditions at an enthalpy pinch of 80 and 140 kJ/kg dry air, respectively (that is, 85% and 66% component effectiveness). From both the figures, it is clear that there is no effect of extraction on the GOR with increasing the temperature difference as the thermal balancing effect appears clearly for high effectiveness components. Figure 5.12 illustrates that increase in the temperature difference increases the GOR for all the cases. This increase in GOR is due to the amount of evaporation in the humidifier due to the increase of the top cycle temperature which will result in a higher amount of potable water and thus higher GOR. The GOR for 30 °C bottom temperature case is higher than that of the 20 °C one. This due to the less amount of heat input required for the 30 °C bottom temperature case.

Figure 5.13 shows the increase in temperature difference for the case with Tmin= 20 °C, it decreases the GOR slightly where the GOR, in this case, is very low until the temperature difference reaches 50 °C. After this point, the GOR starts to increase sharply from 0.035 to slightly more than 0.45. This GOR is low mainly due to the low effectiveness of the components. After 50 °C the increase in temperature difference starts to impact the performance as the increase in top cycle temperature results in an adequate amount of evaporation which means more condensation at the dehumidifier and that results in an increase in GOR. For the case of 30 °C bottom temperature, the GOR increases as the temperature difference increases. This increase of condensate flow rate is associated with the increase in top cycle temperature. From this figure, the effect of a smaller amount of total heat input required can be observed since the case with T_{min}= 30 °C has a higher GOR than that of the 20 °C case as the temperature difference increases. The GOR at 60 °C temperature difference for the 30 °C bottom temperature case is more than double when compared to the T_{min} = 20 °C case.

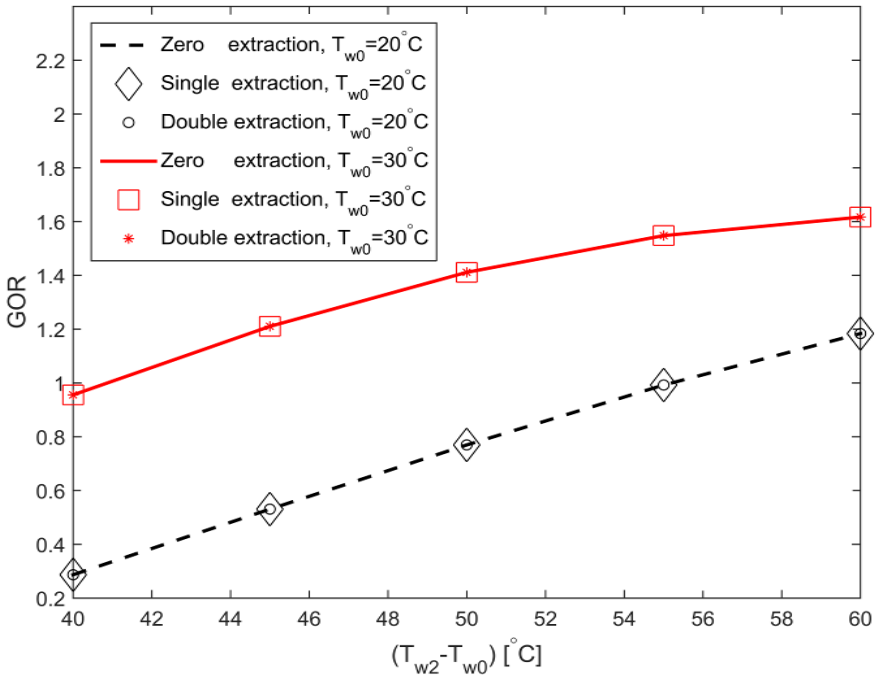

Figure 5.12 Effect of the difference between the top and bottom temperatures on water heated CAOW performance: Ψ_{deh}= Ψ_{hum} =80 kJ/kg dry air.

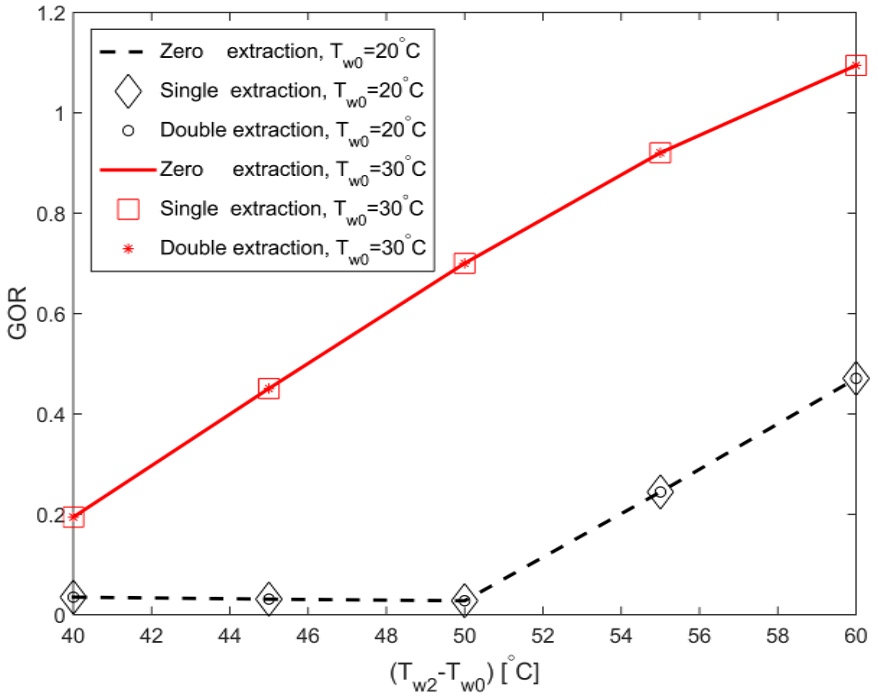

Figure 5.13 Effect of the difference between the top and bottom temperatures on water heated CAOW performance: Ψ_{deh}= Ψ_{hum} =140 kJ/kg dry air.

5.4.1.2 Modified (CAOW)-HX Cycle

Figures 5.14 through 5.17 illustrates the effect of the temperature difference between the top and bottom cycle temperatures on the GOR for the modified cycle with a heat exchanger for a two fixed bottom temperatures cases and at different enthalpy pinch values.

Figure 5.14 shows that at zero enthalpy pinch (that is 100% component effectiveness) for both cases where there is no effect of extraction on the GOR. This is because of the fact that thermal balancing, on one hand, increases the effectiveness of the heat transfer process through the humidifier which will lead to a low temperature of the brine that should be utilized in the heat recovery process. On the other hand, it will increase the temperature of the water coming out of the dehumidifier which then exchanges heat in the heat exchanger with the brine. This means that the effect of increasing temperature of the cooling water will be canceled by the effect of cooling down the brine temperature which will be the case in both CAOW-HX and CAOW-MX modified systems, as illustrated in Figures 5.14 through 5.24.

The GOR of the modified cycles is low when compared to the CAOW conventional cycle. This is mainly due to the use of 100% component effectiveness for the humidifier which will result in a low brine temperature. A high effectiveness humidifier means the hot water that enters will be cooled efficiently which will result in a low temperature of the rejected brine. This brine will exchange heat in the heat exchanger with water coming from the dehumidifier before it is heated in the heater. This process results in high heat input requirements and thus a lower GOR. From this figure and for the 20 °C bottom

temperature case, the increase in temperature difference increases the GOR slightly for this system by almost 3.9% at its peak when there are 58 °C temperature differences.

When the bottom temperature is fixed at 20 °C, increasing the temperature difference means increasing the top cycle temperature which results in relatively higher brine temperature for the heat recovery process; thus, a higher GOR. In contrast to the above case, the 30 °C case increases slightly at the beginning from a temperature difference of 40 to 42°C but then starts to decrease by about 5% as the temperature difference increases. The increase, in the beginning, is due to the increase in brine temperature and evaporation in the humidifier. The decrease after that is associated with the fact that as the top cycle temperature increase, the total heat input required will increase. This will result in a decrease in the GOR. The 30 °C case has a higher GOR than the 20 °C case until 54.5 °C temperature difference after this point the later exceeds the 30 °C case. Before this point, the impact of less heat input required has a higher effect on the GOR than the effect of increasing both the inlet and brine temperatures. After this point, the effect of having better evaporation and heat recovery processes takes over which explains the better GOR for the 20 °C case.

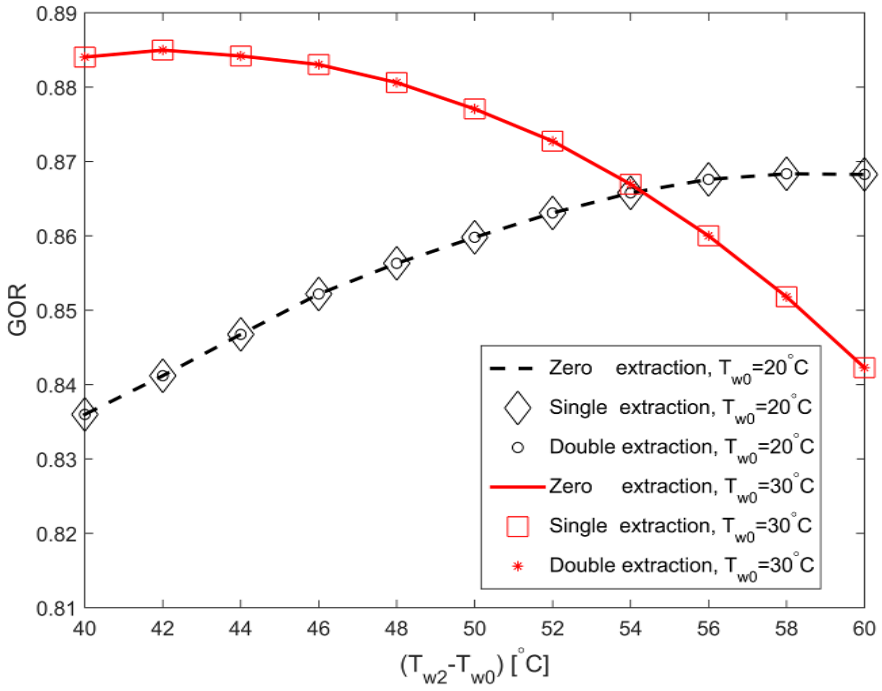

Figure 5.14 Effect of the difference between the top and bottom temperatures on water heated CAOW-HX performance: $\Psi_{deh}= \Psi_{hum}$ =0 kJ/kg dry air.

Figure 5.15 is produced at 20 kJ/kg dry air enthalpy pinch (that is, 97% component effectiveness). It shows similar behavior as explained above for Figure 5.14 The GOR drops slightly for both cases at the start when compared to the previous figure because of using less effective components. However, it increased at 60 °C temperature difference as it suggests that the effect of the higher top cycle and brine temperatures are more influential here. The point after which the 20 °C case exceeds the 30 °C is the temperature difference slightly less than 55 °C.

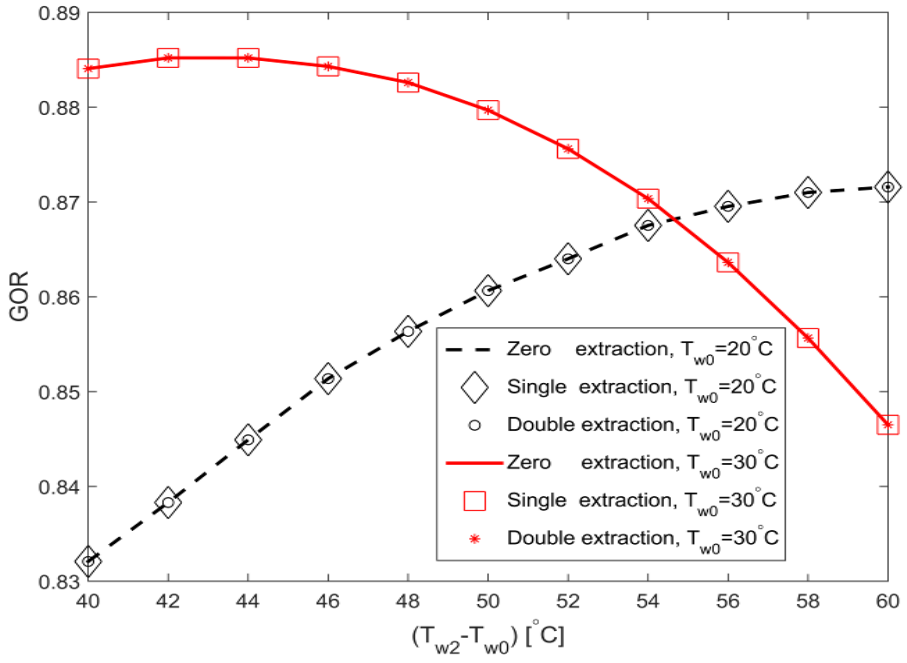

Figure 5.15 Effect of the difference between the top and bottom temperatures on water heated CAOW-HX performance: Ψ_{deh}= Ψ_{hum} =20 kJ/kg dry air.

Figure 5.16 examines this system at an enthalpy pinch of 80 kJ/kg dry air (85% component effectiveness). The GOR for the 30 °C temperature difference reaches a peak of 0.88 at 46 - 50 °C temperature difference. It then starts to decrease as the temperature difference increases which is also similar to what is explained earlier in the case for Figure 5.14. The GOR is slightly less than that of Figure 5.15, because of the lower component effectiveness. The point at which the 20 °C case surpasses the 30 °C one at a temperature difference that is slightly below 58 °C.

This system is examined then at enthalpy pinch of 140 kJ/kg dry air (that is 66% component effectiveness) as shown in Figure 5.17. Similarly, it is found that there is no product until 48 °C for the 20 °C case, which is due to the low effectiveness of the components. After 48 °C, the increase in temperature difference starts to impact the

performance as the increase in top cycle temperature enhances the evaporation process which means more condensate at the dehumidifier and thus higher GOR. The 20 °C case does not exceed the 30 °C case in terms of GOR. The GOR for the 20 °C starts from slightly above 0.73 and then increases as the temperature difference increases to about 0.825 at a temperature difference of 58 °C. The effect of temperature difference increase on the GOR of the 30 °C case is marginal unlike the significant increase in the 20 °C case. This implies that the 20 °C is more sensitive to the component effectiveness and the top cycle temperature. From all the previous figures, we notice that the point at which the 20 °C case exceeds the 30 °C one is shifting from 54.5 to 58 °C until it doesn't surpass the 30 °C case for the last case (refer to Figure 5.17). This indicates that the impact of the top cycle temperature and brine temperature is more dominant at the high effectiveness regions than the impact of total heat input required.

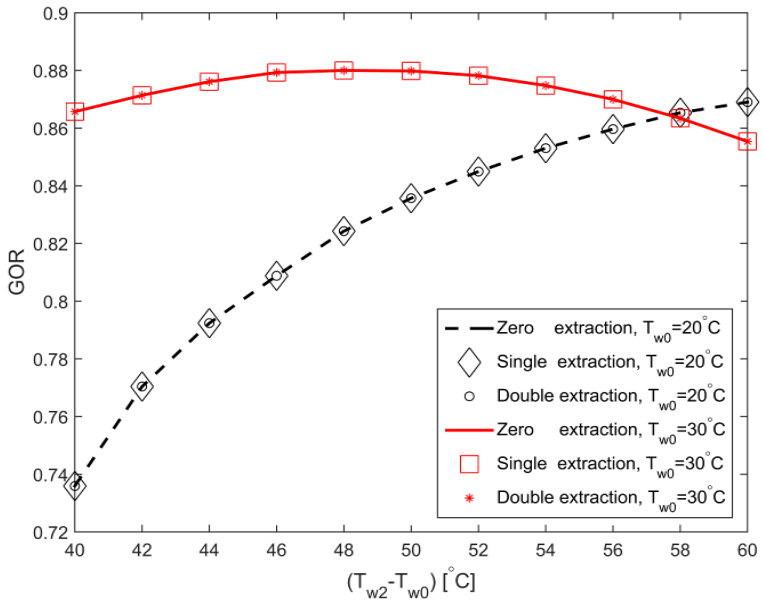

Figure 5.16 Effect of the difference between the top and bottom temperatures on water heated CAOW-HX performance: Ψ_{deh}= Ψ_{hum} =80 kJ/kg dry air.

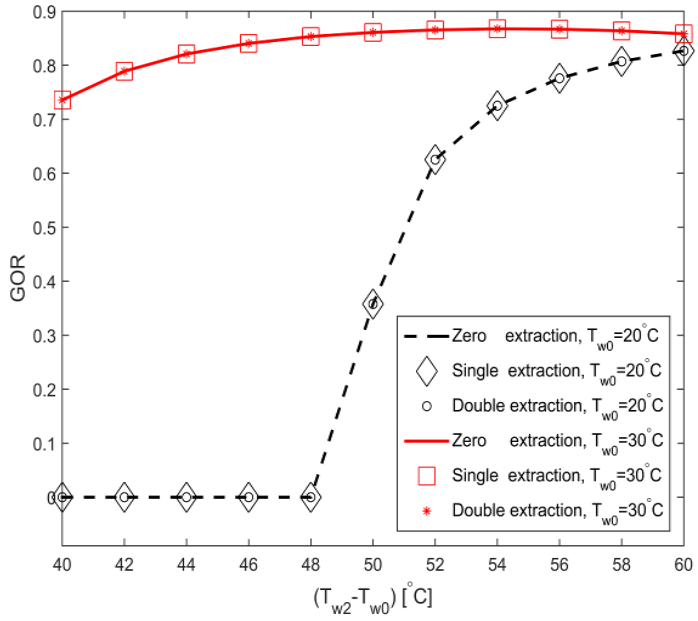

Figure 5.17 Effect of the difference between the top and bottom temperatures on water heated CAOW-HX performance: Ψ_{deh}= Ψ_{hum} =140 kJ/kg dry air.

5.4.1.3 Modified (CAOW)-MX Cycle

Figures 5.18 through 5.21 shows the effect of the temperature difference between the top and bottom cycle temperatures on the GOR for the modified cycle with the mixing chamber for two fixed bottom temperatures cases and at different enthalpy pinch values. All the cases shown in this figure show no effect of extraction which is due to the effect of increasing temperature of the cooling water will be canceled by the effect of cooling down the brine temperature as explained for the previous system.

At zero enthalpy pinch (100% component effectiveness) as shown in Figure 5.18, the GOR increases by slightly more than 4% for the 20 °C bottom temperature case as the temperature difference increases. This increase as explained for the CAOW-HX system is due to the increase of top cycle temperature and the brine temperature which will lead to

both better evaporation and heat recovery. The GOR for the 30 °C temperature difference case reaches a peak of slightly more than 0.85 at 42-43 °C temperature difference and then starts to decrease as the temperature difference increases which is also similar to what is explained previously in the modified system. The 20 °C case surpasses the 30 °C case after almost 54.5 °C which is close to the previous system at this high effectiveness region. The GOR for this system is slightly less than that of the previous one at the same operating conditions.

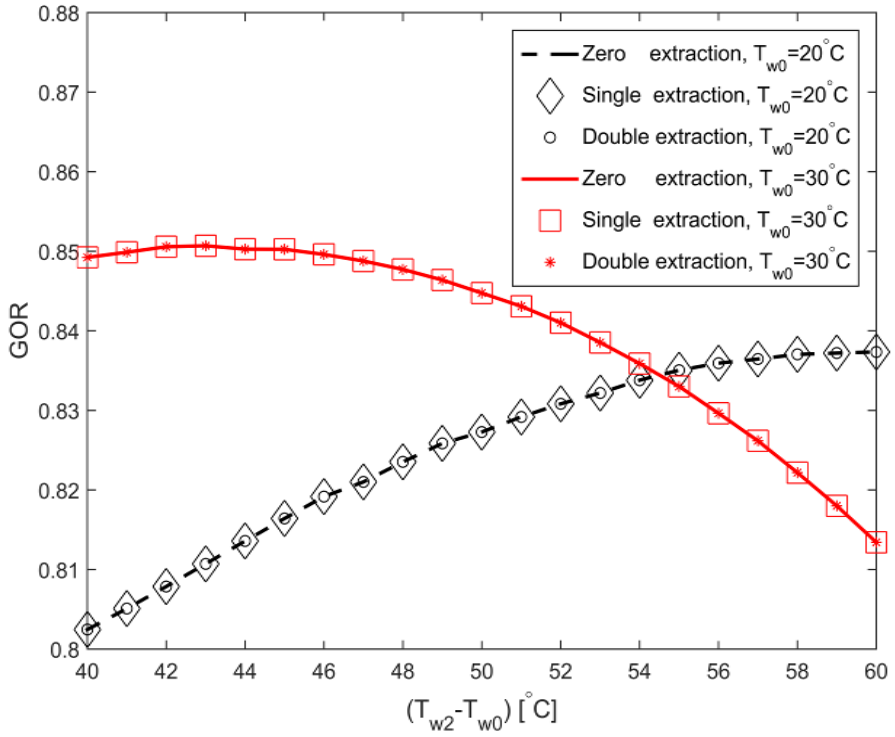

Figure 5.18 Effect of the difference between the top and bottom temperatures on water heated CAOW-MX performance: Ψ_{deh}= Ψ_{hum} =0 kJ/kg dry air.

Figure 5.19 shows the performance of this modified system at an enthalpy pinch of 20 kJ/kg dry air (97% component effectiveness). Also, it can be seen that the behavior for both cases is similar to that of Figure 5.18. The GOR here is slightly higher when

compared to the zero-enthalpy pinch case. This indicates that this system is more sensitive to the brine temperature effect. A less effectiveness humidifier means the hot water that enters will not be cooled adequately which will result in a higher temperature of the brine. The brine here will be mixed with water coming from the dehumidifier before it is heated in the heater. This heat recovery process means less heat input requirements and thus a better GOR. The point after which the 20 ◦C case exceeds the 30 ◦C one remains at 54.5 ◦C.

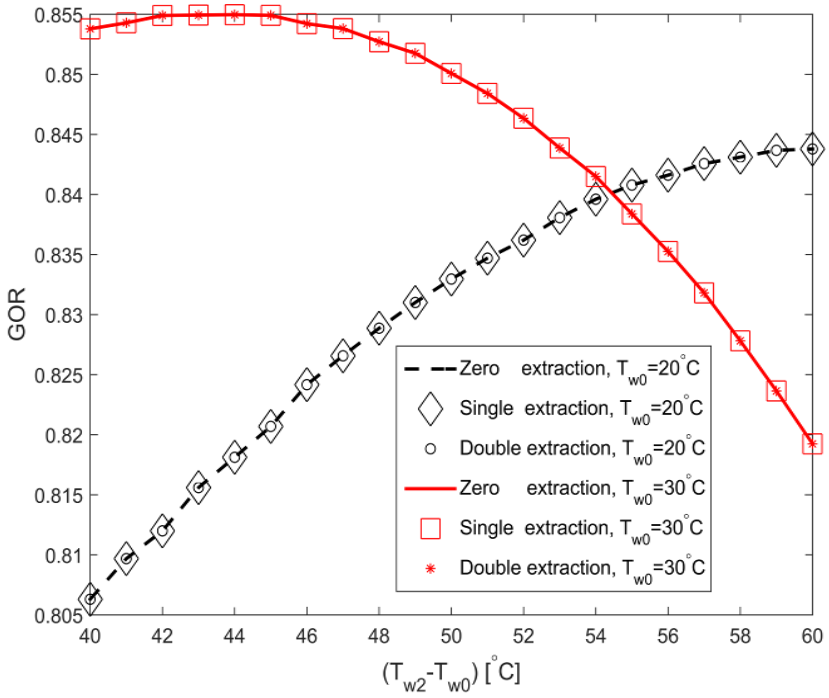

Figure 5.19 Effect of the difference between the top and bottom temperatures on water heated CAOW-MX performance: $\Psi_{deh}= \Psi_{hum}$ =20 kJ/kg dry air.

Figures 5.20 and 5.21 show the impact of running the system with the previous operating conditions at an enthalpy pinch of 80 and 140 kJ/kg dry air, respectively (that corresponds to 85% and 66% component effectiveness). The GOR continued to increase as the component effectiveness decreases for both the figures. Figure 5.20 replicates

Figure 5.19 behavior for both the cases. The point after which the 20 °C case exceeds the 30 °C one is increased to 55.5 °C for Figure 5.20 and to 58 °C for Figure 5.21 when compared to the two previous figures (Figure 5.18 and 5.19). This suggests that the relationship between the impact of both the top cycle temperature and brine temperature as well as the impact of total heat input required is more balanced when the effectiveness of the components decreases.

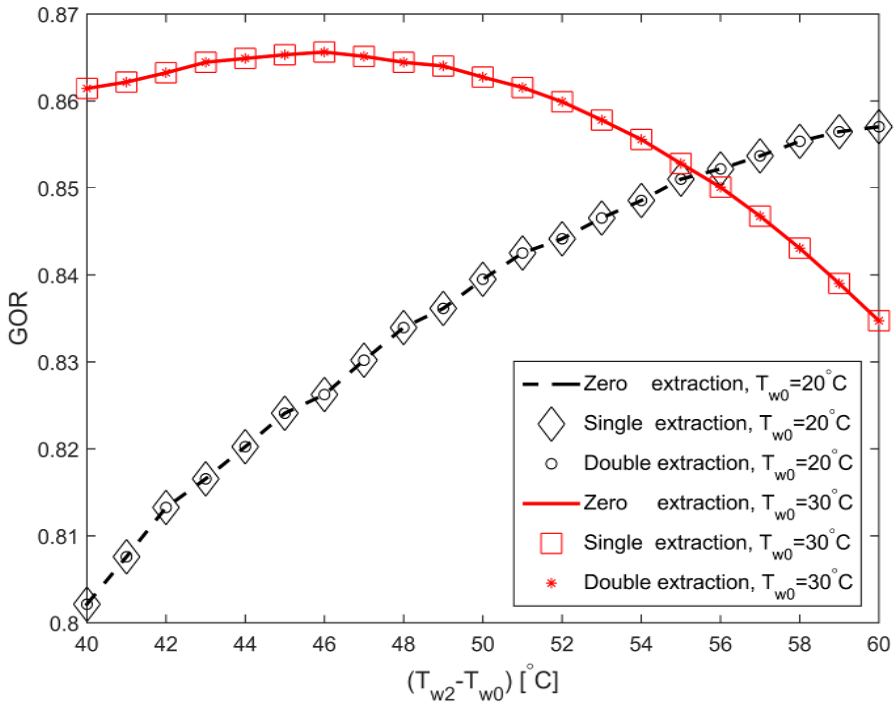

Figure 5.20 Effect of the difference between the top and bottom temperatures on water heated CAOW-MX performance: Ψ_{deh}= Ψ_{hum} =80 kJ/kg dry air.

Figure 5.21 exhibits that no distillate is obtained before 50 °C temperature difference for the 20 °C bottom temperature case, which is similar to the behavior of previous systems at this enthalpy pinch. After this point, as expected, as more heat is consumed the

performance is boosted significantly until it exceeds the 30 °C case after 58 °C temperature difference.

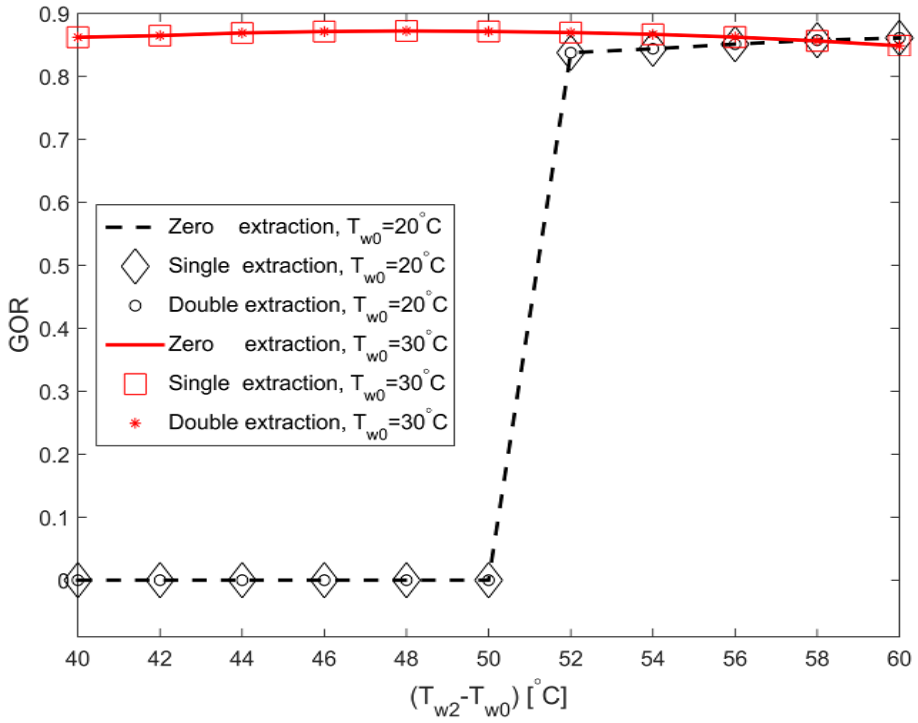

Figure 5.21 Effect of the difference between the top and bottom temperatures on water heated CAOW-MX performance: Ψ_{deh}= Ψ_{hum} =140 kJ/kg dry air.

5.4.2 Effect of The Enthalpy Pinch on Modified Systems Performance

Figures 5.22 and 5.23 exhibit the effect of the enthalpy pinch on the performance of the CAOW-HX and CAOW-MX systems, respectively with zero, single and double extractions. As illustrated in Figure 5.22 the GOR increases as the enthalpy pinch increases up to 40 kJ/kg dry air and then it starts to decrease noticeably to a GOR just below 0.78 at 160 kJ/kg dry air enthalpy pinch. The increase in GOR in the first portion is due to decrease in component effectiveness, which will result in a higher brine temperature for the heat recovery process. In the second portion, the continuous decrease

in GOR is attributed to the decrease in effectiveness of the dehumidifier. Thus, the temperature of the water that enters the heat exchanger will decrease accordingly and more heat will be required at the heater; i.e., less GOR.

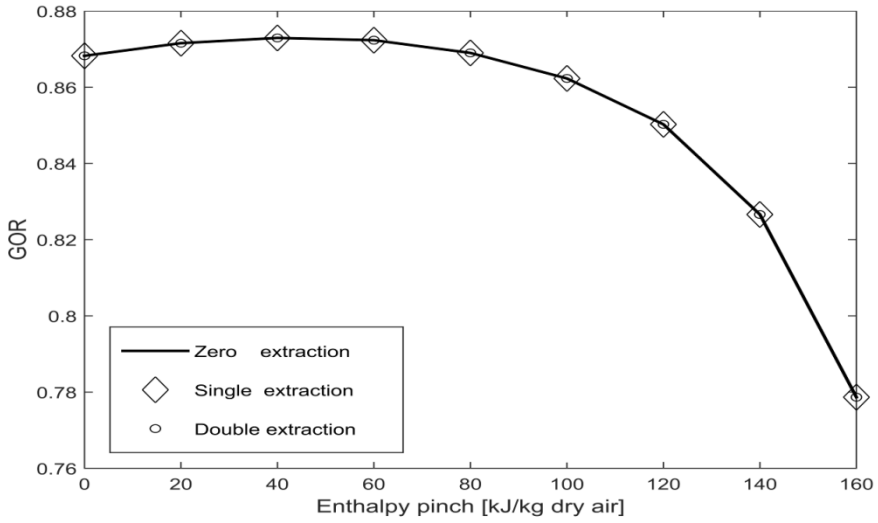

Figure 5.22 Effect of the enthalpy pinch on water heated CAOW-HX performance: T_{w0} =20 °C; T_{w2}=80 °C.

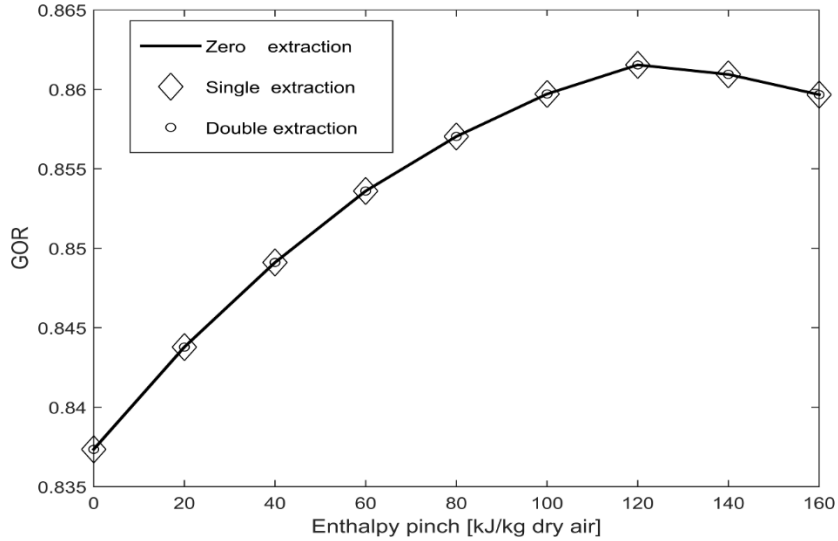

Figure 5.23 Effect of the enthalpy pinch on water heated CAOW-MX performance: T_{w0} =20 °C; T_{w2}=80 °C.

As shown in Figure 5.23 the GOR starts to increase as enthalpy pinch increases until it reaches its peak at GOR slightly above 0.86 at 120 kJ/kg dry air enthalpy pinch and then drops to a GOR of slightly less than 0.86 at 160 kJ/kg dry air. This increase is explained previously as it indicates that this system is more sensitive to the brine temperature effect. The slight drop after 120 enthalpy pinch indicates the impact of low effectiveness in the dehumidifier starts to outplay the benefit of low effectiveness in the humidifier.

The yield of heat recovery process in both the heat exchanger and mixing chamber is dependent on the energy associated with the circulated brine and cooling water at the outlet of the dehumidifier. When single and double extractions are used, the brine is coming out of the humidifier with less energy and the cooling water coming out of the dehumidifier with a higher energy content. This loss in energy across the humidifier is compensated by the increase in energy of the cooling water. In conclusion, the resultant of heat recovery process will remain the same for zero, single and double extractions. This explains the overlapping between zero, single and double extractions lines for modified systems as shown in Figures 5.14 through 5.24.

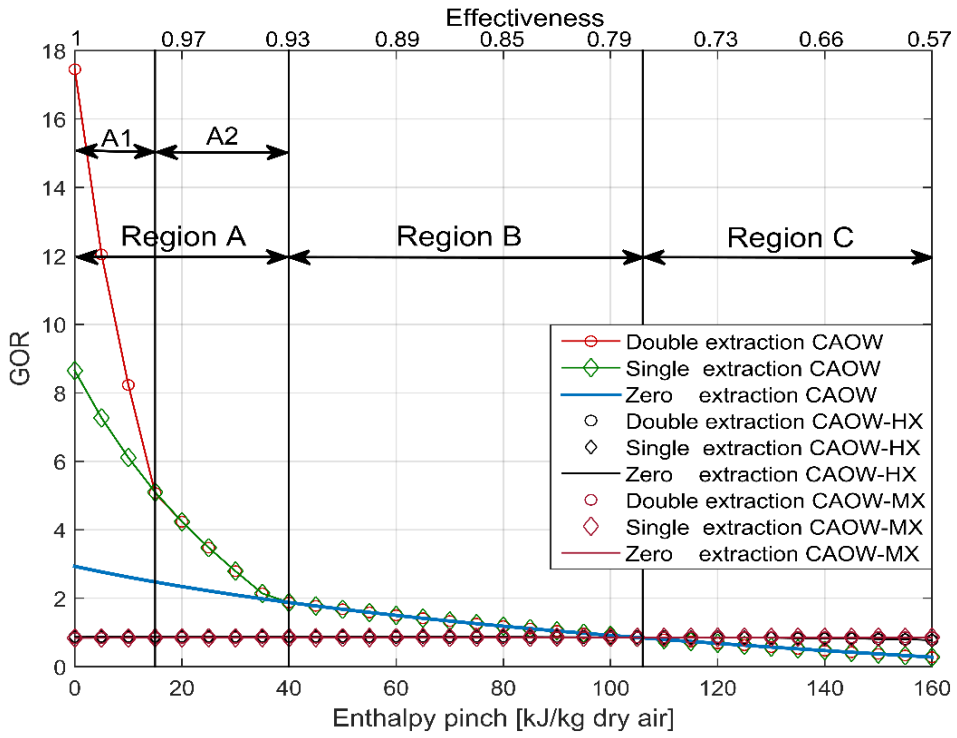

Figure 5.24 Effect of the enthalpy pinch on water heated (CAOW, CAOW-HX, and CAOW-MX) performance: T_{w0}=20 °C; T_{w2}=80 °C.

5.4.3 Effect of Enthalpy Pinch on Water Heated Cycles

Figure 5.24 presents the effect of enthalpy pinch on the performance for all the cycles (investigated in this chapter) with zero, single and double extractions. It can be seen from this figure that the GOR decreases as enthalpy pinch increases for the CAOW system with zero, single and double extractions. The GOR behavior for both CAOW-HX and CAOW-MX is explained earlier in Figures 5.22 and 5.23. Region 'A' is considered the high effectiveness region with enthalpy pinch ranges from 0 to 40 kJ/kg dry air, which is equivalent to effectiveness varying from 100% to 93% for both the humidifier and dehumidifier. This region is further divided into two regions 'A1' and 'A2' with enthalpy pinch ranges from 0 to 18 kJ/kg dry air and 18 to 40 kJ/kg dry air (that is, equivalent to

100% - 98% and 98% - 93% component effectiveness). The double extractions have the highest GOR in region ‘A1’ for the conventional CAOW system. It starts with a GOR of almost 17.5 and then decreases to GOR slightly above 5.

The reduction in entropy generation due to thermal balancing associated with single and double extractions leads to a tremendous increase in GOR for the conventional CAOW while for the modified system there is no effect of extraction as explained previously. In region ‘A2’ the effect of double extractions coincides with the single extraction line for the conventional CAOW system as they start from slightly above 5 to a value of 2, as the component effectiveness drops from 98% to 93%. Both modified cycles with zero, single and double extractions have the lowest GOR in region ‘A’. The conventional CAOW without extraction exhibits a moderate GOR that ranges from almost 3 to 2, which lies between the modified cycles and the conventional one with single and double extractions across region ‘A’.

In region ‘B’ the GOR of the conventional CAOW with zero, single and double extractions coincide, the values are slightly higher at the start than the modified cycles. For this region, the enthalpy pinch starts from 40 to 105 kJ/kg dry air, which is equivalent to effectiveness values from 93% to 77%. While in region ‘C’, the modified cycles have the highest GOR. Region C ranges from 105 to 160 kJ/kg dry air (that is, 77% to 57 % component effectiveness). The right extreme end of region ‘B’ exhibits the point where all systems have the same GOR. As the enthalpy pinch exceeds this point (i.e. 105 kJ/kg dry air) the effectiveness starts to drop noticeably, which justifies the use of heat recovery

option (i.e. the modified systems). The results of this figure are summarized in Table 5.4 to indicate the best configuration for each effectiveness region.

Table 5.4 Recommended configuration for each effectiveness region

Region	Enthalpy Pinch (kJ/kg dry air)	Effectiveness (%)	Recommended Configuration
A1	0-18	100-98	Double Extraction (CAOW)
A2	18-40	98-93	Single Extraction (CAOW)
B	40-105	93-77	Zero Extraction (CAOW)
C	105-160	77-57	Zero Extraction (CAOW-MX), Zero Extraction (CAOW-HX)

Chapter 6

Conclusions and Recommendations

An experimental investigation of the performance of a modified closed-water open-air (CWOA) HDH system is carried out. An experimental set-up is constructed, which is equipped with a data acquisition system to record readings from thermocouples on a real-time basis. The results of different parameters then are analyzed and compared to analytical model results and the deviation was found under ± 5%. The maximum uncertainty is calculated for the experimental GOR and found to be ±2.22%. The maximum GOR was 0.4 with a total heat input of 4.4 kW and under two different water-to-air mass flow rate ratios (MR) of 1.81 and 2.27. The minimum GOR was 0.23 and it was found for a total heat input of 3.2 kW with MR of 1.36.

The analytical model after validated against the experimental results was used to perform a parametric study on both modified CWOA and open-air open-water (OAOW) basic cycle. To study the modified cycle with respect to the basic cycle, the limits of components effectiveness is defined through the basic operating condition; that is, the temperature of water recirculated back to the heater (T_{w4}) to be greater than that of make-up water coming from the dehumidifier (T_{w2}). To satisfy the working range, the operating condition is found to be:

- MR ranged from 1 to 3 the working range of humidifier effectiveness for a dehumidifier having effectiveness $\varepsilon_{deh} = 0.5$ is $\varepsilon_{hum} = 0.4$ to 0.6.

- Also for a dehumidifier of ε_{deh} = 0.6 and 0.7, the effectiveness of the humidifier is ε_{hum} = 0.4 to 0.53.
- And for a dehumidifier of ε_{deh} = 0.8 and 0.85, the effectiveness of the humidifier is ε_{hum} = 0.4 to 0.47.

Based on the operating range of modified cycle in terms of effectiveness of both the humidifier and dehumidifier, the analysis for the performance of the basic cycle OAOW (0% rejected brine recirculation) and modified cycle CWOA (100% rejected brine recirculation) is conducted accordingly. The following observations are noted.

- As the MR increases for the basic OAOW cycle, the GOR increases until it reaches a peak and then starts to drop.
- The GOR increases for the basic OAOW cycle as the effectiveness of the humidifier increases, since higher effectiveness means higher evaporation and consequently higher GOR.
- The GOR increases for the basic OAOW cycle as the dehumidifier effectiveness increases, which is due to the better condensation process.
- Increasing the dehumidifier effectiveness increases the GOR for the modified CWOA cycle, since it reflects a better condensation process that influences the overall performance of the system.

The effect of circulating the rejected brine from the humidifier back to the heater on the performance is also examined. The following results are concluded:

- At 95% and 90% rejected brine recirculation, the behavior mimic that of 100% (the modified cycle); that is, the GOR increases with an increase in MR.
- From 80% to 10% rejected brine recirculation, the system starts to act as the basic cycle by reaching a peak and then drops, since the effect of makeup starts to outplay the effect of recirculated brine.
- The same behavior is replicated when system run at effectiveness range considered in the working range; that is, when the brine temperature is higher than the makeup water temperature.

The system is then explored at effectiveness that falls out of the effectiveness range that fulfills the condition ($T_{w4} > T_{w2}$), the following behavior is observed:

- This shift outside the working effectiveness range has created a point at certain MR at which all curves intersect which means the brine recirculation has no effect on the GOR.
- At this point, a sort of thermal balancing occurs and the system becomes insensitive to the circulation.
- This point then can be used as an indicator of the MR range that allows a better performance for recirculation and when to operate the basic cycle mode (0% recirculation).
- The point of intersection has also moved from higher MR to lower MR as the dehumidifier effectiveness decreases, which is consistent with the explanation that this point marks the region of dominance of the basic cycle, to the left of this point, and is dependent on the dehumidifier effectiveness accordingly.

An extended analysis of the modified CWOA cycle that considers second law analysis of the basic OAOW and modified CWOA cycles is executed. The possibility of coupling RO with the basic cycle as an alternative to the recirculation option is also explored. The system was operated in the range of component effectiveness that meets the condition of brine recirculated temperature to be higher than the makeup temperature. The results can be summarized as:

- The modified cycle (100% brine recirculation) has higher exergetic efficiency than the basic cycle (0% brine recirculation).
- The heater in both the basic as well as modified cycles, dominates in terms of exergy destruction percentage.
- The hybrid HDH-RO system with pressure exchanger has the highest GOR and second-law efficiency, since using a pressure exchanger has reduced the energy consumption considerably. While the hybrid HDH-RO with Pelton turbine was second in terms of both the GOR and second-law efficiency.
- The increase in pump efficiency decreases the actual work supplied and subsequently the specific energy consumption.
- The pump efficiency is more significant for the overall exergetic efficiency than the pressure exchanger or Pelton turbine efficiency.
- Two methods are applied to estimate the production cost of the HDH system and hybrid HDH-RO systems. Both methods provide almost similar results in terms of

product cost; however, the advantageous of cost flow method are highlighted or possible cost-effective improvement of the system.

- The product cost for the basic OAOW cycle that used electrical heater was 6.37 $/m^3 (El-Dessouky method) and 6.56 $/m^3 (cost flow method). The product cost when the system utilized solar heater was 5.81 $/m^3 (El-Dessouky method) and 5.98 $/m^3 (cost flow method).

- The modified system has better second-law efficiency and subsequently a lower production cost as a result of the energy recovery process.

- Coupling HDH systems with renewable energy enhanced its economic performance and tackled one of the main issues of high energy requirement.

- The product cost for combined HDH-RO that used electrical heater was 0.11 $/m^3 (El-Dessouky method) and 0.13 $/m^3 (cost flow method). The product cost when the system utilized solar heater was 0.11 $/m^3 (El-Dessouky method) and 0.12 $/m^3 (cost flow method).

- The utilization of RO module reduced the production cost by almost 57 times for the system with electrical heaters and 52 times for the system with solar heater.

- The product cost for combined HDH-RO with pressure exchanger that used electrical heater were 0.11 $/m^3 (El-Dessouky method) and 0.13 $/m^3 (cost flow method). The product cost when the system utilized solar heater was 0.11 $/m^3 (El-Dessouky method) and 0.12 $/m^3 (cost flow method).

- The production cost of this combined system remained almost the same compared to a simple HDH-RO combined system and HDH-RO with Pelton turbine.
- The combined HDH-RO system with pressure exchanger has the best performance in terms of GOR, second-law efficiency and production cost.
- The addition of RO systems adds a total investment rate of 0.0114 $/hr for the simple RO and 0.0134 $/hr for the RO with PT and RO with PX.
- The hybridization enhanced the performance of the combined system significantly with just 17.5 % increase in the total investment cost rate of the RO section.

Zero, single and double extraction effect on the performance of the conventional water heated closed-air open-water cycle and both modified cycles have been examined. From the aforementioned discussion, we conclude the following:

- There are three regions with different performance behavior, which are classified into high effectiveness region, moderate effectiveness region, and low effectiveness region.
- In the high effectiveness region, which is also divided into two regions, the conventional cycle with extraction has the highest performance. Double extraction is better in the upper portion of this region, while a single extraction is recommended for the lower portion as it coincides with the double extraction one.

- In the moderate effectiveness region, the conventional cycle with zero, single and double extractions are identical and have the highest performance. Since we recommend using the conventional cycle with zero extraction for this region.

- The performance of CAOW with a heat exchanger and CAOW with mixing chamber have been studied.

- These modified cycles have the best performance for the low effectiveness region.

- The extraction lost its significance after the high effectiveness region for the conventional cycle. Furthermore, it has no useful impact for the modified cycles in the three regions.

- The heat exchanger and the mixing chamber modifications show almost identical performance as heat recovery solutions.

- The mixing chamber modification is simpler, cheaper and easy to maintain when compared to the other heat recovery options, thus we recommend to use it in the low effectiveness region.

References

[1] H. M. Ettouney and H. T. El-Dessouky, *Fundamentals of salt water Desalination*. 2002.

[2] A. E. Kabeel, M. H. Hamed, Z. M. Omara, and S. W. Sharshir, "Water Desalination Using a Humidification-Dehumidification Technique—A Detailed Review," *Nat. Resour.*, vol. 4, no. 3, pp. 286–305, 2013.

[3] F. A. Al-Sulaiman, M. I. Zubair, M. Atif, P. Gandhidasan, S. A. Al-Dini, and M. A. Antar, "Humidification dehumidification desalination system using parabolic trough solar air collector," *Appl. Therm. Eng.*, vol. 75, pp. 809–816, 2015.

[4] P. N. Govindan, J. H. Lienhard, R. McGovern, and S. M. Zubair, "Status of Humidification Dehumidification Desalination," *IDA World Congr. Desalin. Water Reuse*, 2011.

[5] T. Mezher, H. Fath, Z. Abbas, and A. Khaled, "Techno-economic assessment and environmental impacts of desalination technologies," *Desalination*, vol. 266, no. 1–3, pp. 263–273, 2011.

[6] A.-N. A. Mabrouk, A. S. Nafey, and H. E. S. Fath, "Steam, electricity and water costs evaluation of power desalination co-generation plants," *Desalin. Water Treat.*, vol. 22, no. 1–3, pp. 56–64, 2010.

[7] A. Abusharkh, A. Giwa, and S. Hasan, "Wind and geothermal energy in desalination: A short review on progress and sustainable commercial processes,"

Ind. Eng. Manag., vol. 4, no. 4, p. 175, 2015.

[8] "Solar Energy and Water: Solar Powering Desalination - Renewable Energy World." [Online]. Available: http://www.renewableenergyworld.com/articles/print/volume-0/issue-0/solar-energy/solar-energy-and-water-solar-powering-desalination.html. [Accessed: 02-Apr-2016].

[9] A. Giwa, H. Fath, and S. W. Hasan, "Humidification-dehumidification desalination process driven by photovoltaic thermal energy recovery (PV-HDH) for small-scale sustainable water and power production," *Desalination*, vol. 377, pp. 163–171, 2016.

[10] M. Zamen, M. Amidpour, and S. M. Soufari, "Cost optimization of a solar humidification-dehumidification desalination unit using mathematical programming," *Desalination*, vol. 238, no. 1–3, pp. 92–99, 2009.

[11] W. Abdelmoez, M. S. Mahmoud, and T. E. Farrag, "Water desalination using humidification/dehumidification (HDH) technique powered by solar energy: a detailed review," *Desalin. Water Treat.*, vol. 52, no. 25–27, pp. 4622–4640, Jun. 2013.

[12] G. Franchini, A. Perdichizzi, and A. Picinardi, "HD desalination by heat rejected from solar cooling systems," in *2010 IEEE International Energy Conference and Exhibition, EnergyCon 2010*, 2010, pp. 63–68.

[13] J. hong Wang, N. yun Gao, Y. Deng, and Y. li Li, "Solar power-driven

humidification-dehumidification (HDH) process for desalination of brackish water," *Desalination*, vol. 305, pp. 17–23, 2012.

[14] G. Yuan and H. Zhang, "Mathematical modeling of a closed circulation solar desalination unit with humidification-dehumidification," *Desalination*, vol. 205, no. 1–3, pp. 156–162, 2007.

[15] G. Yuan, Z. Wang, H. Li, and X. Li, "Experimental study of a solar desalination system based on humidification–dehumidification process," *Desalination*, 2011.

[16] L. Zhang, W. Chen, and H. Zhang, "Study on variation laws of parameters in air bubbling humidification process," *Desalin. Water Treat.*, 2013.

[17] M. T. Ghazal, U. Atikol, and F. Egelioglu, "An experimental study of a solar humidifier for HDD systems," *Energy Convers. Manag.*, vol. 82, pp. 250–258, 2014.

[18] G. P. Narayan, M. H. Sharqawy, E. K. Summers, J. H. Lienhard, S. M. Zubair, and M. A. Antar, "The potential of solar-driven humidification-dehumidification desalination for small-scale decentralized water production," *Renewable and Sustainable Energy Reviews*, vol. 14, no. 4. pp. 1187–1201, 2010.

[19] H. Müller-Holst, M. Engelhardt, M. Herve, and W. Schölkopf, "Solarthermal seawater desalination systems for decentralised use," *Renew. Energy*, vol. 14, no. 1–4, pp. 311–318, 1998.

[20] A. M. I. Mohamed and N. A. El-Minshawy, "Theoretical investigation of solar humidification-dehumidification desalination system using parabolic trough

concentrators," *Energy Convers. Manag.*, vol. 52, no. 10, pp. 3112–3119, 2011.

[21] Y. Marif, H. Benmoussa, H. Bouguettaia, M. M. Belhadj, and M. Zerrouki, "Numerical simulation of solar parabolic trough collector performance in the Algeria Saharan region," *Energy Convers. Manag.*, vol. 85, pp. 521–529, 2014.

[22] N. A. S. Elminshawy, F. R. Siddiqui, and M. F. Addas, "Experimental and analytical study on productivity augmentation of a novel solar humidification-dehumidification (HDH) system," *Desalination*, vol. 365, pp. 36–45, 2015.

[23] Y. Ghalavand, M. S. Hatamipour, and A. Rahimi, "Humidification compression desalination," *Desalination*, vol. 341, no. 1, pp. 120–125, 2014.

[24] A. M. I. Mohamed and N. A. S. El-Minshawy, "Humidification-dehumidification desalination system driven by geothermal energy," *Desalination*, vol. 249, no. 2, pp. 602–608, 2009.

[25] C. Muthusamy and K. Srithar, "Energy and exergy analysis for a humidification–dehumidification desalination system integrated with multiple inserts," *Desalination*, vol. 367, pp. 49–59, 2015.

[26] M. H. Sharqawy, M. A. Antar, S. M. Zubair, and A. M. Elbashir, "Optimum thermal design of humidification dehumidification desalination systems," *Desalination*, vol. 349, pp. 10–21, 2014.

[27] N. Niroomand, M. Zamen, and M. Amidpour, "Theoretical investigation of using a direct contact dehumidifier in humidification–dehumidification desalination unit based on an open air cycle," *Desalin. Water Treat.*, vol. 54, no. 2, pp. 305–315,

Jan. 2014.

[28] E. Paso, “Zero discharge waste brine management for desalination plants,” *Distribution*, no. 89, 2002.

[29] B. Dawoud, Y. H. Zurigat, B. Klitzing, T. Aldoss, and G. Theodoridis, “On the possible techniques to cool the condenser of seawater greenhouses,” *Desalination*, vol. 195, no. 1–3, pp. 119–140, 2006.

[30] M. Al-Sahali and H. M. Ettouney, “Humidification dehumidification desalination process: Design and performance evaluation,” *Chem. Eng. J.*, vol. 143, no. 1–3, pp. 257–264, 2008.

[31] M. K. Abu Arabi and K. V. Reddy, “Performance evaluation of desalination processes based on the humidification/dehumidification cycle with different carrier gases,” *Desalination*, vol. 156, no. 1–3, pp. 281–293, Aug. 2003.

[32] M. Vlachogiannis, V. Bontozoglou, C. Georgalas, and G. Litinas, “Desalination by mechanical compression of humid air,” *Desalination*, vol. 122, no. 1, pp. 35–42, 1999.

[33] H. Ettouney, “Design and analysis of humidification dehumidification desalination process,” *Desalination*, vol. 183, no. 1–3, pp. 341–352, 2005.

[34] H. M. Ettouney, *Chapter 10 Economic Analysis of Desalination Processes*. 2002.

[35] L.-Z. Zhang, Z.-X. Li, T.-S. Zhong, and L.-X. Pei, “Flow maldistribution and performance deteriorations in a cross flow hollow fiber membrane module for air

humidification," *J. Memb. Sci.*, vol. 427, pp. 1–9, Jan. 2013.

[36] P. Gao, L. Zhang, and H. Zhang, "Performance analysis of a new type desalination unit of heat pump with humidification and dehumidification," *Desalination*, vol. 220, no. 1–3, pp. 531–537, Mar. 2008.

[37] G. P. Narayan, R. K. McGovern, G. P. Thiel, J. A. Miller, J. H. Lienhard V, M. H. Sharqawy, S. M. Zubair, and M. A. Antar, "Status of humidification dehumidification desalination technology," in *World Congress/Perth Convention and Exhibition Centre (PCEC)*, 2011, p. 20.

[38] B. M. Hamieh, J. R. Beckman, and M. D. Ybarra, "Brackish and seawater desalination using a 20 ft2 dewvaporation tower," *Desalination*, vol. 140, no. 3, pp. 217–226, 2001.

[39] B. M. Hamieh and J. R. Beckman, "Seawater desalination using Dewvaporation technique: experimental and enhancement work with economic analysis," *Desalination*, vol. 195, no. 1–3, pp. 14–25, 2006.

[40] E. Chafik, "A new type of seawater desalination plants using solar energy," *Desalination*, vol. 156, no. 1–3, pp. 333–348, 2003.

[41] H. Kang, Y. Yang, Z. Chang, H. Zheng, and Z. Duan, "Performance of a two-stage multi-effect desalination system based on humidification–dehumidification process," *Desalination*, vol. 344, pp. 339–349, Jul. 2014.

[42] S. Hou, "Two-stage solar multi-effect humidification dehumidification desalination process plotted from pinch analysis," *Desalination*, vol. 222, pp. 572–

578, 2008.

[43] M. Zamen, S. M. Soufari, S. A. Vahdat, M. Amidpour, M. A. Zeinali, H. Izanloo, and H. Aghababaie, “Experimental investigation of a two-stage solar humidification-dehumidification desalination process,” *Desalination*, vol. 332, pp. 1–6, 2014.

[44] S. A. Nada, H. F. Elattar, and A. Fouda, “Experimental study for hybrid humidification–dehumidification water desalination and air conditioning system,” *Desalination*, vol. 363, pp. 112–125, 2015.

[45] C. Chiranjeevi and T. Srinivas, “Combined two stage desalination and cooling plant,” *Desalination*, vol. 345, pp. 56–63, 2014.

[46] G. P. Narayan, R. K. McGovern, S. M. Zubair, and J. H. Lienhard, “High-temperature-steam-driven, varied-pressure, humidification-dehumidification system coupled with reverse osmosis for energy-efficient seawater desalination,” *Energy*, vol. 37, no. 1, pp. 482–493, 2012.

[47] C. Yildirim, S. K. Soylu, I. Atmaca, and I. Solmuş, “Experimental investigation of a portable desalination unit configured by a thermoelectric cooler,” *Energy Convers. Manag.*, vol. 85, pp. 140–145, 2014.

[48] S. A. Nada, H. F. Elattar, and A. Fouda, “Performance analysis of proposed hybrid air conditioning and humidification–dehumidification systems for energy saving and water production in hot and dry climatic regions,” *Energy Convers. Manag.*, vol. 96, pp. 208–227, May 2015.

[49] A. E. Kabeel, M. H. Hamed, Z. M. Omara, and S. W. Sharshir, “Water Desalination Using a Humidification-Dehumidification Technique—A Detailed Review,” *Nat. Resour.*, vol. 4, no. 3, pp. 286–305, 2013.

[50] A. E. Kabeel and E. M. S. El-Said, “A hybrid solar desalination system of air humidification-dehumidification and water flashing evaporation. Part I. A numerical investigation.,” *Desalination*, vol. 320, pp. 56–72, 2013.

[51] A. E. Kabeel and E. M. S. El-Said, “A hybrid solar desalination system of air humidification, dehumidification and water flashing evaporation: Part II. Experimental investigation,” *Desalination*, vol. 341, no. 1, pp. 50–60, 2014.

[52] A. E. Kabeel, T. A. Elmaaty, and E. M. S. El-Said, “Economic analysis of a small-scale hybrid air HDH-SSF (humidification and dehumidification-water flashing evaporation) desalination plant,” *Energy*, vol. 53, pp. 306–311, 2013.

[53] A. Eslamimanesh and M. S. Hatamipour, “Economical study of a small-scale direct contact humidification-dehumidification desalination plant,” *Desalination*, vol. 250, no. 1, pp. 203–207, 2010.

[54] A. Giwa and S. W. Hasan, “Theoretical investigation of the influence of operating conditions on the treatment performance of an electrically-induced membrane bioreactor,” *J. Water Process Eng.*, vol. 6, pp. 72–82, 2015.

[55] A. Giwa and S. W. Hasan, “Numerical modeling of an electrically enhanced membrane bioreactor (MBER) treating medium-strength wastewater,” *J. Environ. Manage.*, vol. 164, pp. 1–9, 2015.

[56] A. Giwa, I. Ahmed, and S. W. Hasan, “Enhanced sludge properties and distribution study of sludge components in electrically-enhanced membrane bioreactor,” *J. Environ. Manage.*, vol. 159, pp. 78–85, 2015.

[57] S. Jamaly, A. Giwa, and S. W. Hasan, “Recent improvements in oily wastewater treatment: Progress, challenges, and future opportunities,” *J. Environ. Sci.*, vol. 37, pp. 15–30, 2015.

[58] “Müller-Holst H. Solar thermal desalination using the multiple effect humidification meh-method. Solar Desalination for the 21st Century; 2007. p. 215–25.,” .

[59] “H. Müller-Holst, Mehrfacheffekt-Feuchtluftdestillation bei Umgebungsdruck – Verfahrensoptimierung und Anwendungen. PhD thesis, Technische Universität Berlin, 2002.”

[60] “M. Zamen, S.M. Soufari, M. Amidpour, Improvement of solar humidification–dehumidification desalination using multi-stage process, Chem. Eng. Trans. 25 (2011) 1091–1096.”

[61] “T. Schlickum, ‘“Device for separating a liquid from its dissolved matters”’, European Patent, EP 1770068 A2, 2007.”

[62] “T. Brendel, Solare Meewasserental sungsanlagen mit mehrstufiger verdungtung. PhD thesis, Ruhr University Bochum, 2003.”

[63] “T. Brendel, ‘“Process to distil and desalinate water in contra-flow evaporation humidifier unit with progressive removal of evaporated fluid”’, 2003. German

Patent #DE10215079 (A1)."

[64] G. P. Thiel and J. H. Lienhard, "Entropy generation in condensation in the presence of high concentrations of noncondensable gases," *Int. J. Heat Mass Transf.*, vol. 55, pp. 5133–5147, 2012.

[65] "M.A. Younis, M.A. Darwish, F. Juwayhel, Experimental and theoretical study of a humidification–dehumidification desalting system, Desalination 94 (1993) 11–24."

[66] R. K. McGovern, G. P. Thiel, G. Prakash Narayan, S. M. Zubair, and J. H. Lienhard V, "Performance limits of zero and single extraction humidification-dehumidification desalination systems," *Appl. Energy*, vol. 102, pp. 1081–1090, 2013.

[67] G. P. Narayan, J. H. Lienhard V, and S. M. Zubair, "Entropy generation minimization of combined heat and mass transfer devices," *International Journal of Thermal Sciences*, vol. 49, no. 10. pp. 2057–2066, 2010.

[68] K. H. Mistry, J. H. Lienhard, and S. M. Zubair, "Effect of entropy generation on the performance of humidification- dehumidification desalination cycles," *Int. J. Therm. Sci.*, vol. 49, no. 9, pp. 1837–1847, 2010.

[69] J. A. Miller and J. H. Lienhard V, "Impact of extraction on a humidification-dehumidification desalination system," *Desalination*, vol. 313, pp. 87–96, 2013.

[70] G. P. Narayan, K. M. Chehayeb, R. K. McGovern, G. P. Thiel, S. M. Zubair, and J. H. Lienhard V, "Thermodynamic balancing of the humidification dehumidification

desalination system by mass extraction and injection," *Int. J. Heat Mass Transf.*, vol. 57, no. 2, pp. 756–770, Feb. 2013.

[71] G. Prakash Narayan, M. G. St. John, S. M. Zubair, and J. H. Lienhard, "Thermal design of the humidification dehumidification desalination system: An experimental investigation," *Int. J. Heat Mass Transf.*, vol. 58, no. 1–2, pp. 740–748, Mar. 2013.

[72] K. M. Chehayeb, G. Prakash Narayan, S. M. Zubair, and J. H. Lienhard, "Use of multiple extractions and injections to thermodynamically balance the humidification dehumidification desalination system," *Int. J. Heat Mass Transf.*, vol. 68, pp. 422–434, Jan. 2014.

[73] K. M. Chehayeb, G. P. Narayan, S. M. Zubair, and J. H. Lienhard, "Thermodynamic balancing of a fixed-size two-stage humidification dehumidification desalination system," *Desalination*, vol. 369, pp. 125–139, Aug. 2015.

[74] A. Bejan, *Entropy generation minimization the method of thermodynamic optimization of finite-size systems and finite-time processes*. 1996.

[75] G. P. Thiel and J. H. Lienhard, "Entropy generation in condensation in the presence of high concentrations of noncondensable gases," *Int. J. Heat Mass Transf.*, vol. 55, no. 19–20, pp. 5133–5147, 2012.

[76] D. TONDEUR and E. KVAALEN, "Equipartition of Entropy Production - An Optimality Criterion For Transfer and Separation Processes," *Ind. Eng. Chem.*

Res., vol. 26, no. 1, pp. 50–56, 1987.

[77] M. H. Sharqawy, M. a. Antar, S. M. Zubair, and A. M. Elbashir, "Optimum thermal design of humidification dehumidification desalination systems," *Desalination*, vol. 349, pp. 10–21, Sep. 2014.

[78] M. H. Sharqawy, J. H. Lienhard, and S. M. Zubair, "Thermophysical properties of seawater: a review of existing correlations and data," *Desalin. Water Treat.*, vol. 16, no. 1–3, pp. 354–380, Apr. 2010.

[79] G. Prakash Narayan, M. H. Sharqawy, J. H. Lienhard V, and S. M. Zubair, "Thermodynamic analysis of humidifi cation dehumidifi cation desalination cycles," *Desalin. Water Treat.*, vol. 16, pp. 339–353, 2010.

[80] B. A. Qureshi and S. M. Zubair, "Exergetic analysis of a brackish water reverse osmosis desalination unit with various energy recovery systems," *Energy*, vol. 93, pp. 256–265, 2015.

[81] "Energy Recovery Power Model - Energy Recovery." [Online]. Available: http://www.energyrecovery.com/resource/power-model/. [Accessed: 23-Mar-2017].

[82] A. Bejan, G. Tsatsaronis, and M. Moran, *Thermal Design and Optimization*. 1996.

[83] K. H. Mistry, R. K. McGovern, G. P. Thiel, E. K. Summers, S. M. Zubair, and J. H. Lienhard, "Entropy generation analysis of desalination technologies," *Entropy*, vol. 13, no. 10, pp. 1829–1864, 2011.

[84] R. L. Truby, “Seawater Desalination by Ultralow-Energy Reverse Osmosis,” in *Advanced Membrane Technology and Applications*, Hoboken, NJ, USA: John Wiley & Sons, Inc., pp. 87–100.

[85] M. I. Zubair, F. A. Al-Sulaiman, M. A. Antar, S. A. Al-Dini, and N. I. Ibrahim, “Performance and cost assessment of solar driven humidification dehumidification desalination system,” *Energy Convers. Manag.*, vol. 132, pp. 28–39, 2017.

[86] Y. M. El-Sayed, “Designing desalination systems for higher productivity,” *Desalination*, vol. 134, no. 1–3, pp. 129–158, 2001.

[87] R. S. El-Emam and I. Dincer, “Thermodynamic and thermoeconomic analyses of seawater reverse osmosis desalination plant with energy recovery,” *Energy*, vol. 64, pp. 154–163, 2014.

[88] E. Deniz and S. Çınar, “Energy, exergy, economic and environmental (4E) analysis of a solar desalination system with humidification-dehumidification,” *Energy Convers. Manag.*, vol. 126, pp. 12–19, 2016.

[89] F. A. Al-Sulaiman, G. Prakash Narayan, and J. H. Lienhard, “Exergy analysis of a high-temperature-steam-driven, varied-pressure, humidification-dehumidification system coupled with reverse osmosis,” *Appl. Energy*, vol. 103, pp. 552–561, 2013.

[90] A. Eslamimanesh and M. S. Hatamipour, “Economical study of a small-scale direct contact humidification-dehumidification desalination plant,” *Desalination*, vol. 250, no. 1, pp. 203–207, 2010.

[91] A. E. Kabeel, T. A. Elmaaty, and E. M. S. El-Said, “Economic analysis of a small-

scale hybrid air HDH-SSF (humidification and dehumidification-water flashing evaporation) desalination plant," *Energy*, vol. 53, pp. 306–311, 2013.

[92] M. K. Wittholz, B. K. O'Neill, C. B. Colby, and D. Lewis, "Estimating the cost of desalination plants using a cost database," *Desalination*, vol. 229, no. 1–3, pp. 10–20, 2008.

Appendix A

The results obtained from the experiments are presented in this section in a tabulated form. The discussion of these results is covered in Chapter 3 wherein the experimental values are compared with the analytical results.

Tables from A.1 to A.4 presents the experimental data including the total heat input (Q), minimum and maximum water temperatures (T_{min}, T_{max}), mass flow rate of air ($\dot{m}_a$), mass flow rate of the cooling water ($\dot{m}_{cw}$), mass flow rate of the feedwater ($\dot{m}_w$), mass flow rate ratio (MR), effectiveness of both the humidifier and dehumidifier (ε_{hum}, ε_{deh}), GOR obtained both from experimental and analytical results and the deviation between them.

Table A.1 Effect of changing heat input at a fixed MR=2.27 on GOR

Q (kW)	T_{min} (°C)	T_{max} (°C)	$\dot{m}_a$ (kg/s)	$\dot{m}_{cw}$ (kg/s)	$\dot{m}_w$ (kg/s)	MR	ε_{hum}	ε_{deh}	GOR (Experimental)	GOR (analytical)	Error (%)
5.6	27.4	53	0.055	0.1	0.125	2.27	0.41	0.81	0.37	0.38	1.5
4.4	29.5	50.7	0.055	0.1	0.125	2.27	0.44	0.81	0.40	0.41	2.3
3.2	29.7	45.2	0.055	0.1	0.125	2.27	0.56	0.85	0.28	0.29	2.7

Table A.2 Effect of changing heat input at a fixed MR=1.81 on GOR

Q (kW)	T_{min} (°C)	T_{max} (°C)	$\dot{m}_a$ (kg/s)	$\dot{m}_{cw}$ (kg/s)	$\dot{m}_w$ (kg/s)	MR	ε_{hum}	ε_{deh}	GOR (Experimental)	GOR (analytical)	Error (%)
5.6	29.6	52	0.055	6	6	1.81	0.48	0.80	0.36	0.37	2.2
4.4	27.7	48	0.055	6	6	1.81	0.52	0.83	0.40	0.42	4.9
3.2	26.6	42.3	0.055	6	6	1.81	0.52	0.79	0.32	0.34	4.2

Table A.3 Effect of changing heat input at a fixed MR=1.36 on GOR

Q (kW)	T_{min} (°C)	T_{max} (°C)	$\dot{m}_a$ (kg/s)	$\dot{m}_{cw}$ (kg/s)	$\dot{m}_w$ (kg/s)	MR	ε_{hum}	ε_{deh}	GOR (Experimental)	GOR (analytical)	Error (%)
5.6	29.6	51.6	0.055	6	4.5	1.36	0.54	0.78	0.33	0.35	4.9
4.4	28.9	47.2	0.055	6	4.5	1.36	0.55	0.83	0.32	0.33	2.5
3.2	28.3	41.5	0.055	6	4.5	1.36	0.57	0.78	0.23	0.23	0.6

Table A.4 Effect of varying air mass flowrate on GOR

Q (kW)	T_{min} (°C)	T_{max} (°C)	$\dot{m}_a$ (kg/s)	$\dot{m}_{cw}$ (kg/s)	$\dot{m}_w$ (kg/s)	MR	ε_{hum}	ε_{deh}	GOR (Experimental)	GOR (analytical)	Error (%)
5.6	29.1	53.3	0.055	6	7.5	2.27	0.38	0.77	0.35	0.36	3.7
5.6	30.7	52.3	0.066	6	7.5	1.89	0.41	0.79	0.28	0.29	3.4
5.6	31	51.2	0.08	6	7.5	1.56	0.53	0.85	0.24	0.24	1.1

Uncertainty Analysis

Since we are measuring temperatures and volumetric flow rates, it is necessary to evaluate the effect of these measured values on the system performance, GOR. EES provides this tool to perform the analysis. K-type thermocouples have an uncertainty of ±0.1 °C. Flowmeters are of type FL50000, which have an uncertainty of ±5%. Air flowmeter is used to measure the speed of air and then from that, the mass flow rate of air is calculated, which has an uncertainty of ±0.5%. The GOR calculated from the experiments is dependent only on the temperature and flow rate of the distillate water. The flow rate of is calculated from the produced fresh water over a period of 1 hour which is collected in a graduated cylinder with an accuracy of ±12 ml.

Table A.5 Effect of changing heat input at a fixed MR=2.27 on GOR

Q (kW)	MR	ε_{hum}	ε_{deh}	GOR (experimental)
5.6	2.27±0.11	0.41±0.003	0.81±0.013	0.37±0.003
4.4	2.27±0.11	0.44±0.003	0.81±0.015	0.40±0.004
3.2	2.27±0.11	0.56±0.004	0.85±0.018	0.28±0.005

Table A.6 Effect of changing heat input at a fixed MR=1.81 on GOR.

Q (kW)	MR	ε_{hum}	ε_{deh}	GOR (experimental)
5.6	1.81±0.09	0.48±0.003	0.80±0.013	0.36±0.003

4.4	1.81±0.09	0.52±0.003	0.83±0.013	0.40±0.004
3.2	1.81±0.09	0.52±0.004	0.79±0.025	0.32±0.005

Table A.7 Effect of changing heat input at a fixed MR=1.36 on GOR.

Q (kW)	MR	ε_{hum}	ε_{deh}	GOR (experimental)
5.6	1.36±0.07	0.54±0.004	0.78±0.015	0.33±0.003
4.4	1.36±0.07	0.55±0.004	0.83±0.015	0.32±0.004
3.2	1.36±0.07	0.57±0.004	0.78±0.025	0.23±0.005

Table A.8 Effect of varying air mass flow rate on GOR.

Q (kW)	MR	ε_{hum}	ε_{deh}	GOR (experimental)
5.6	2.27±0.11	0.38±0.002	0.77±.016	0.35±0.003
5.6	1.89±0.10	0.41±0.003	0.79±0.018	0.28±0.003
5.6	1.56±0.08	0.53±0.003	0.85±0.013	0.24±0.003

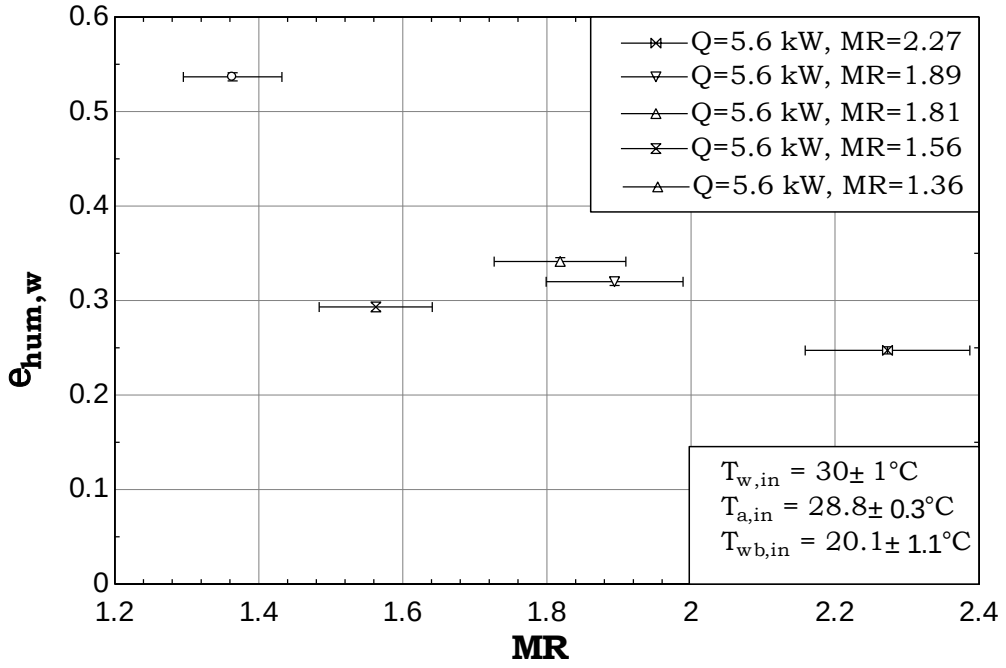

Figure A.1 Variation of humidifier water effectiveness versus MR at a heat input of 5.6 kW.

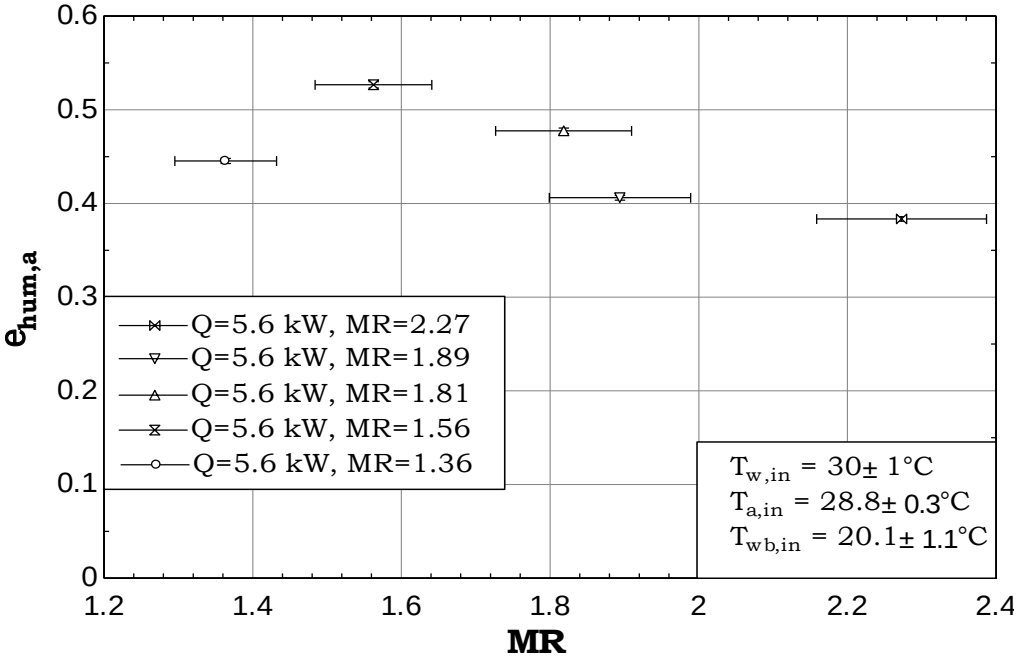

Figure A.2 Variation of humidifier air effectiveness versus MR at a heat input of 5.6 kW.

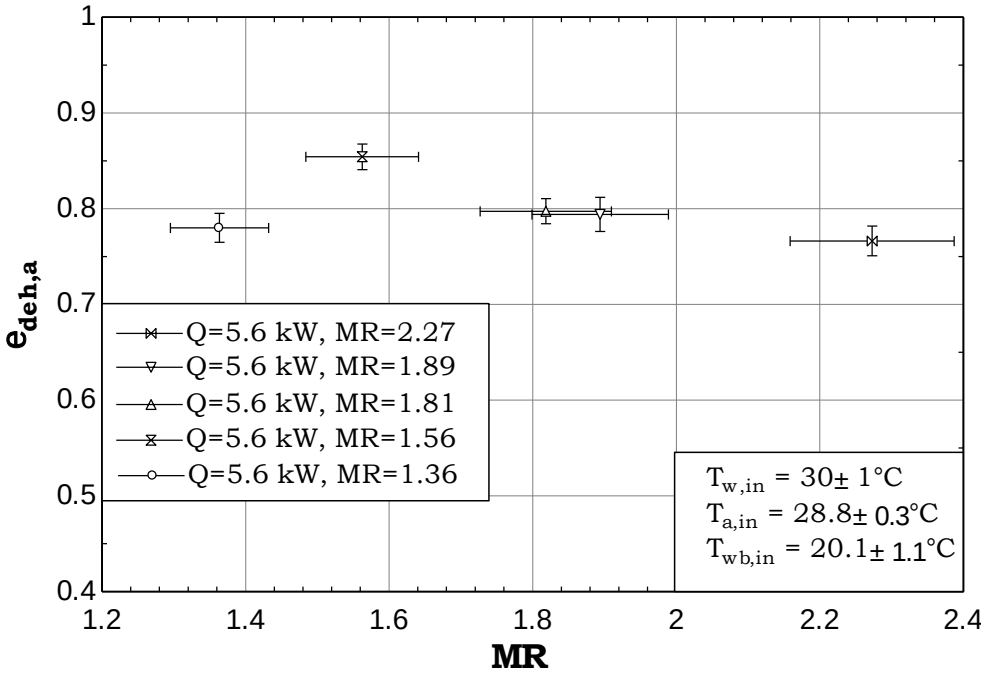

Figure A.3 Variation of dehumidifier air effectiveness versus MR at a heat input of 5.6 kW.

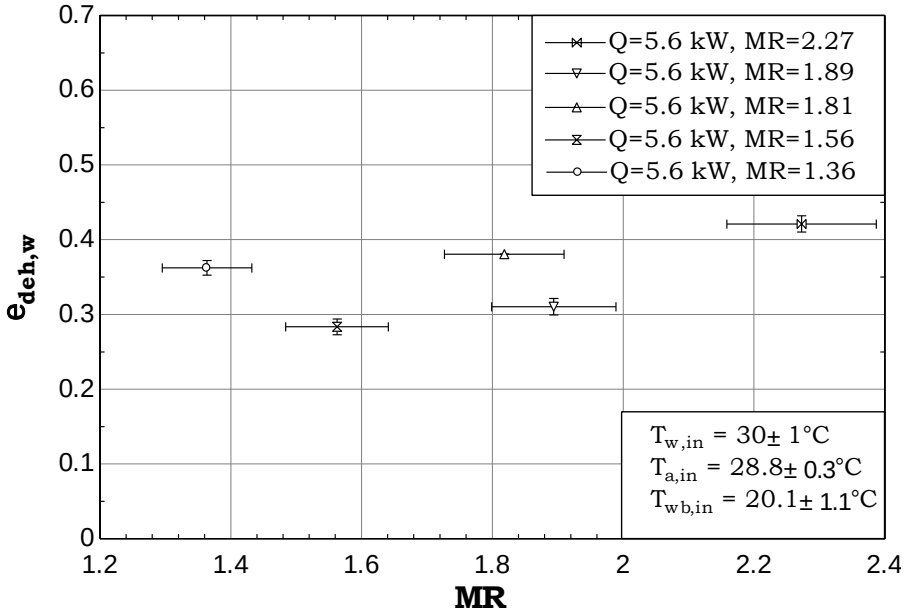

Figure A.4 Variation of dehumidifier water effectiveness versus MR at a heat input of 5.6 kW.

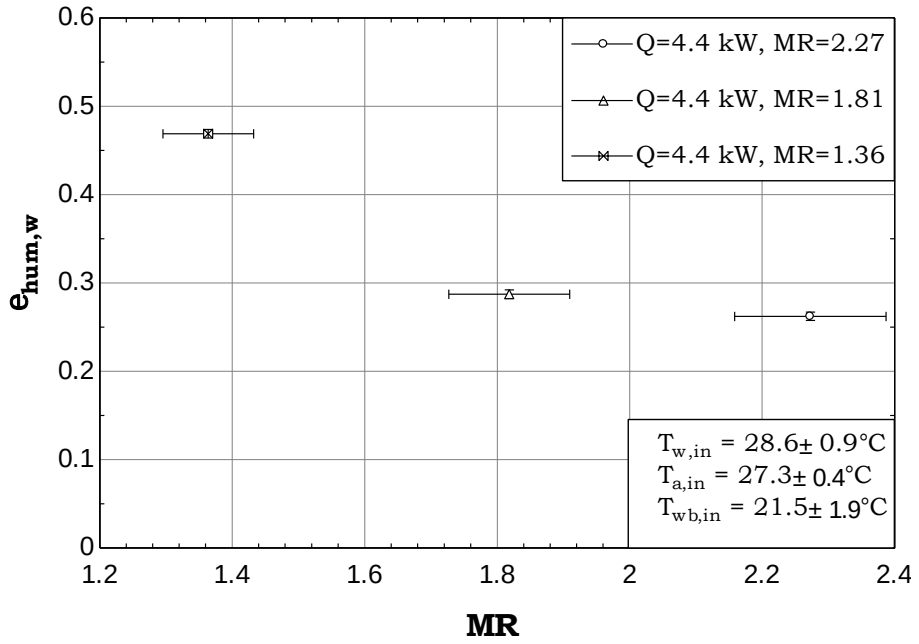

Figure A.5 Variation of humidifier water effectiveness versus MR at a heat input of 4.4 kW.

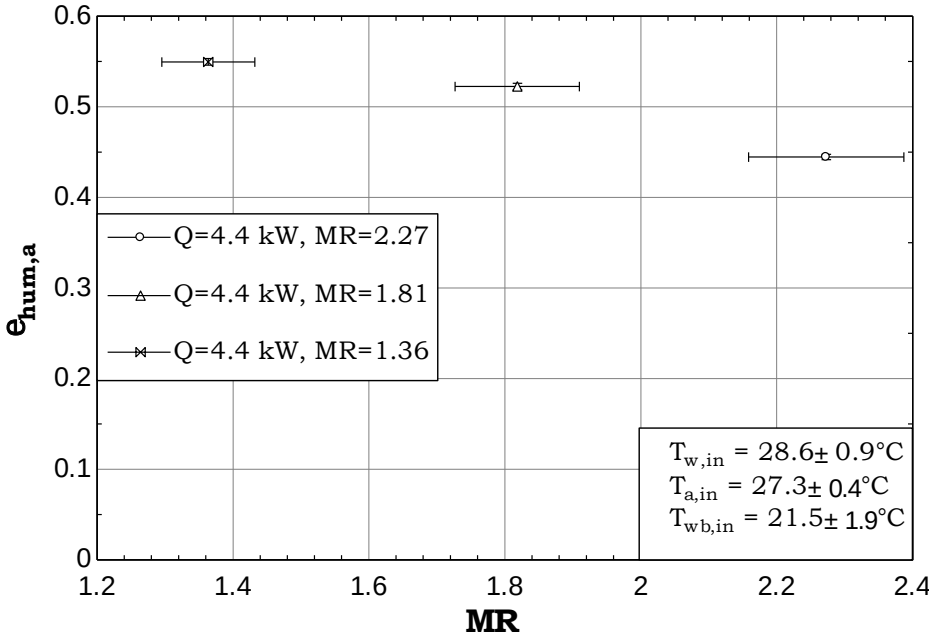

Figure A.6 Variation of humidifier air effectiveness versus MR at a heat input of 4.4 kW.

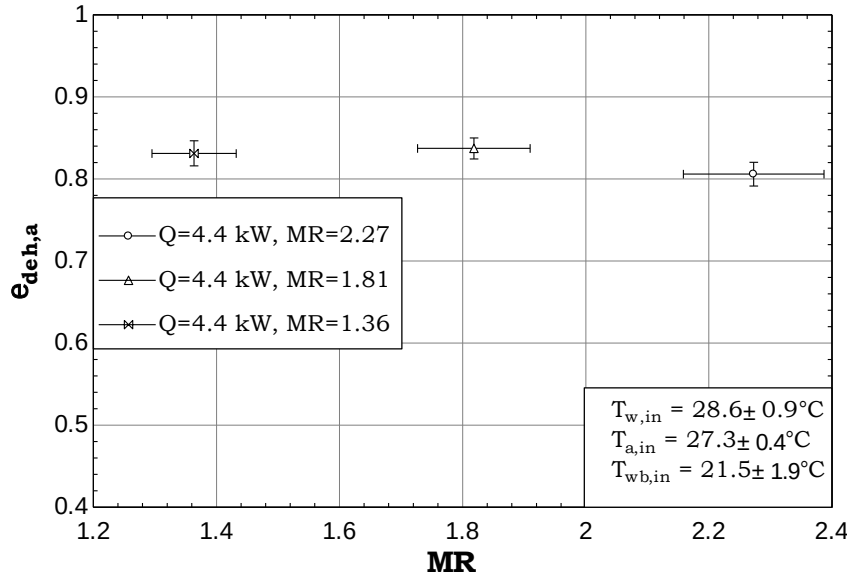

Figure A.7 Variation of dehumidifier air effectiveness versus MR at a heat input of 4.4 kW.

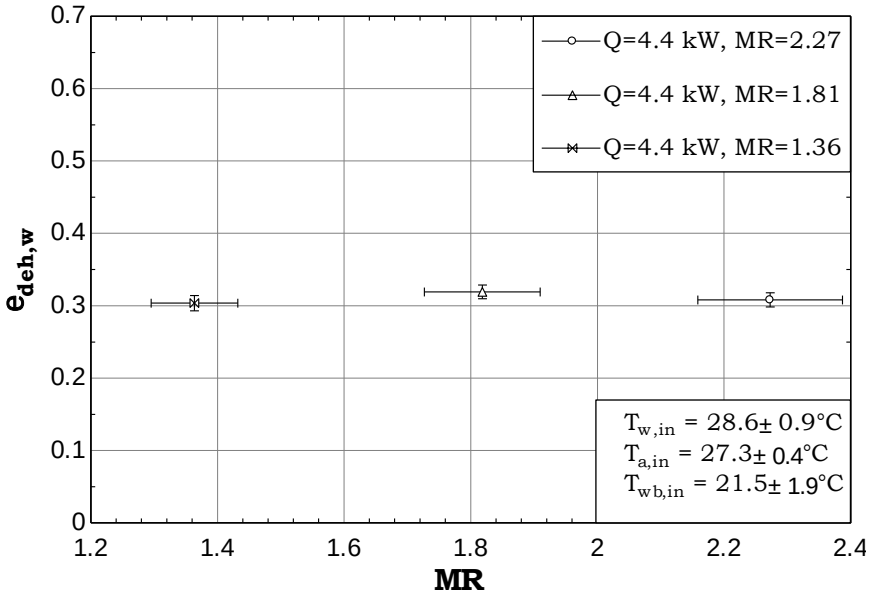

Figure A.8 Variation of dehumidifier water effectiveness versus MR at a heat input of 4.4 kW.

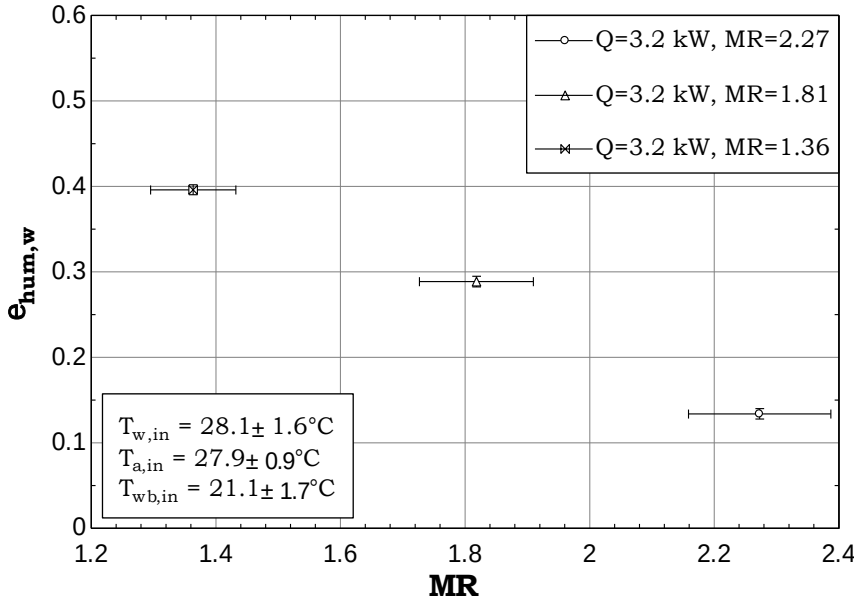

Figure A.9 Variation of humidifier water effectiveness versus MR at a heat input of 3.2 kW.

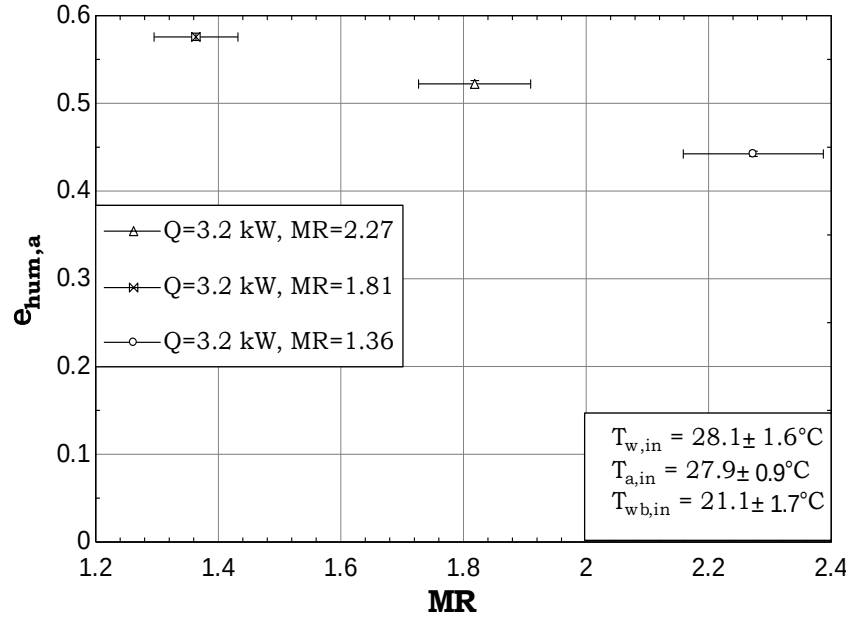

Figure A.10 Variation of humidifier air effectiveness versus MR at a heat input of 3.2 kW.

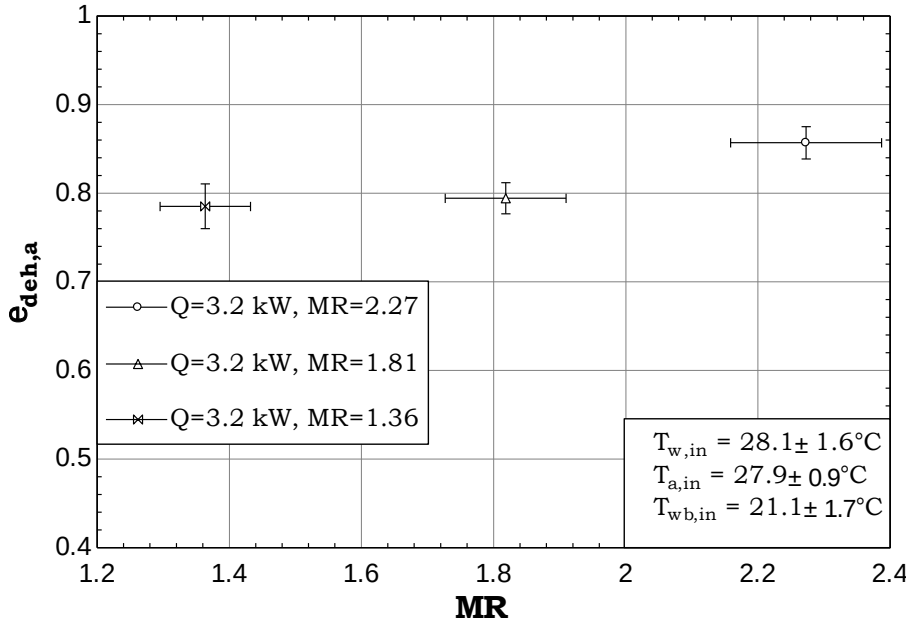

Figure A.11 Variation of dehumidifier air effectiveness versus MR at a heat input of 3.2 kW.

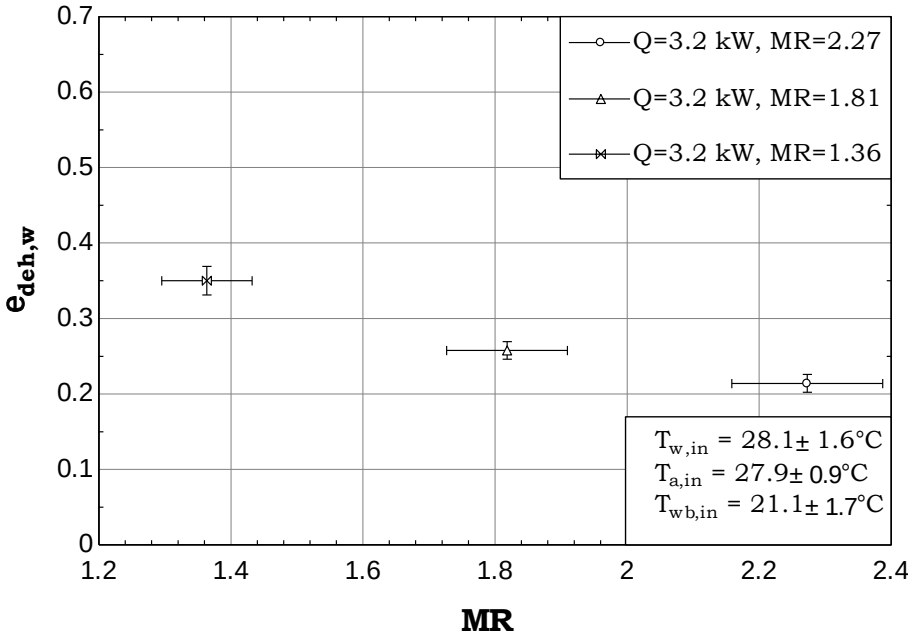

Figure A.12 Variation of dehumidifier water effectiveness versus MR at a heat input of 3.2 kW.

Appendix B

Thermodynamic Balancing Concept (Entropy Generation Minimization)

Effect of Heat Capacity Rate Ratio (HCR)

A major portion of the entropy produced in the HDH system is due to the heat and mass transfer mechanisms occurring in the humidifier and dehumidifier. In order to reduce entropy production of the system, we have to address the entropy produced in the humidifier and dehumidifier.

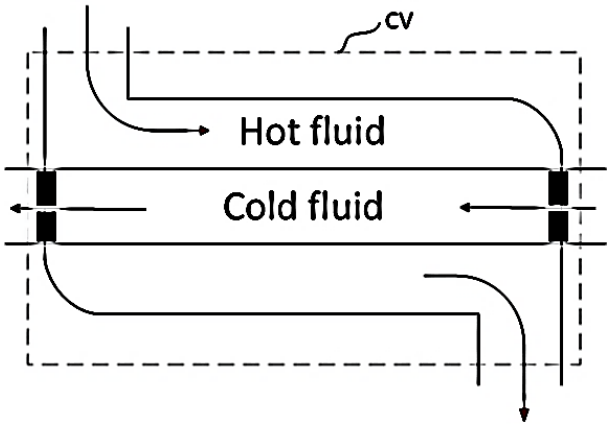

Figure B.1 Counter flow heat exchanger control volume.

To explain the concept of thermodynamic balancing in heat and mass exchanger devices, a simple case of a heat exchanger as shown in Figure B.1 is considered. In a heat transfer with infinite area; i.e., $\varepsilon = 1$, the entropy generation rate in such a device will be totally due to thermal imbalance or irreversibility residual. This is directly associated with operating conditions at which the heat capacity rate of the streams exchanging heat is not equal. The heat capacity rate ratio is defined as in Equation B.1:

Heat capacity rate:

$$HCR = \frac{\left(\dot{m}c_p\right)_{cold}}{\left(\dot{m}c_p\right)_{hot}} \tag{B.1}$$

Using this definition and applying the second law on the control volume, entropy generation can be calculated as in B.2 and B.3 [67]:

Case 1: $\left(\dot{m}c_p\right)_{cold} < \left(\dot{m}c_p\right)_{hot}$:

$$\frac{\dot{S}_{generation}}{\left(\dot{m}c_p\right)_{cold}} = \frac{1}{HCR} * ln\left(1 - HCR * \varepsilon * \left(1 - \frac{T_{in,cold}}{T_{in,hot}}\right)\right) + ln\left(1 + \varepsilon * \left(\frac{T_{in,hot}}{T_{in,cold}} - 1\right)\right) \tag{B.2}$$

Case 2: $\left(\dot{m}c_p\right)_{hot} < \left(\dot{m}c_p\right)_{cold}$:

$$\frac{\dot{S}_{gen}}{\left(\dot{m}c_p\right)_{hot}} = HCR * ln\left(1 + \frac{1}{HCR} * \varepsilon * \left(\frac{T_{in,hot}}{T_{in,cold}} - 1\right)\right) + ln\left(1 + \varepsilon * \left(1 - \frac{T_{in,cold}}{T_{in,hot}}\right)\right) \tag{B.3}$$

From equations B.2 and B.3, a heat exchanger with the operating condition at which the fluid streams have constant heat capacity rate; that is, HCR = 1, is thermally balanced i.e., reversible (or zero remnant irreversibility). This concept of thermodynamic balancing is well known for heat exchangers and was recently extended to heat and mass exchanger devices in the desalination literature [67].

The driving force for energy transfer in a combined heat and mass exchanger is a combination of both the temperature and concentration differences. An example for a humidifier is taken to explain how the entropy generation can be minimized by balancing this driving force. It is important to note that the heat exchanger terminology that is used in the previous section is not directly applicable to combined heat and mass exchangers. Taking this into consideration, the humidifier effectiveness should be carefully defined before considering the balancing of these devices.

The effectiveness is defined as the actual enthalpy variation to the maximum possible enthalpy variation for a simultaneous heat and mass exchanger. From Figure B.2, the key model equation for the humidifier effectiveness can be expressed as:

$$\varepsilon_{hum} = max\left\langle \frac{h_{a,out} - h_{a,in}}{h_{a,out,ideal} - h_{a,in}}, \frac{h_{w,in} - h_{w,out}}{h_{w,in} - h_{w,out,ideal}} \right\rangle \tag{B.4}$$

where the ideal outlet air enthalpy is calculated when outlet air is saturated at the water inlet temperature, while the ideal outlet brine enthalpy is when its temperature is equal to the inlet air dry-bulb temperature.

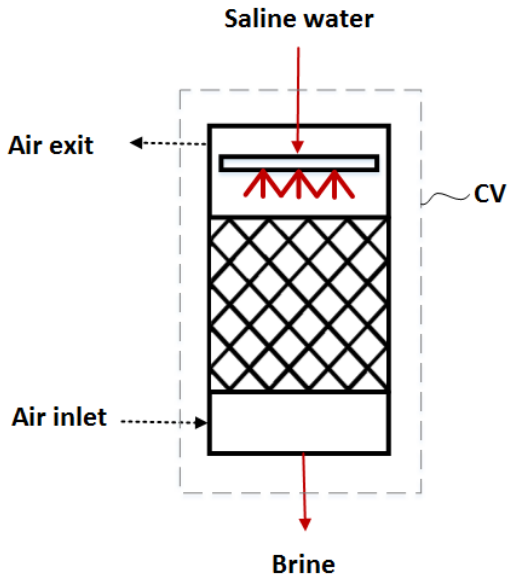

Figure B.2 Humidifier control volume.

Applying first and second laws of thermodynamics to the control volume in Figure B.2, entropy production in a heat and mass exchanger can be expressed as,

$$(\dot{m}\, h)_{w,out} - (\dot{m}\, h)_{w,in} = \dot{m}_a(h_{a,in} - h_{a,out}) \tag{B.5}$$

$$\dot{S}_{gen} = (\dot{m}\, s)_{w,out} - (\dot{m}\, s)_{w,in} + \dot{m}_a(s_{a,out} - s_{a,in}) \tag{B.6}$$

and mass balance of the control volume of Figure B.2 gives:

$$\dot{m}_{w,in} - \dot{m}_a\left(\omega_{a,out} - \omega_{a,in}\right) = \dot{m}_{w,out} \tag{B.7}$$

These equations cannot be solved as there is one extra unknown. Another equation should be introduced to close the set of equations. As mentioned earlier, due to the difference between the "heat exchanger" and "heat and mass exchanger" devices; a modified HCR should be defined. Based on heat exchanger analysis, HCR can be expressed as in Equation B.1:

$$HCR_{hx} = \frac{\left(\dot{m}c_p\right)_{cold}}{\left(\dot{m}c_p\right)_{hot}} \tag{B.8}$$

or,

$$HCR_{hx} = \frac{\Delta\dot{H}_{max,cold}}{\Delta\dot{H}_{max,hot}} \tag{B.9}$$

Since maximum temperature difference is the same for cold and hot streams in the heat exchanger i.e. $\Delta\dot{H}_{max,state} = \left(\dot{m}c_p\right)_{state}(T_{in,hot} - T_{in,cold})$, where state = cold or hot. In like manner, Equation B.8 can be used for heat and mass exchanger device taking in to consideration a new definition for $\Delta\dot{H}_{max}$. Hence, HCR for heat and mass exchanger devices can be defined, as the ratio of the maximum change in total enthalpy rate of the cold stream to that of the hot stream, as shown in Equation B.10:

$$HCR = \frac{\dot{m}_{cold,out}h_{cold,out,ideal} - \dot{m}_{cold,in}h_{cold,in}}{\dot{m}_{hot,in}h_{hot,in} - \dot{m}_{hot,out}h_{hot,out,ideal}} \tag{B.10}$$

The effect of HCR on entropy regeneration can be determined by solving Equations B.4 through B.9 simultaneously, as shown in Figure B.3.

Figure B.3 shows the effect of water inlet temperature, air inlet temperature, humidifier effectiveness, air inlet and outlet relative humidity on the entropy generation vs. heat capacity rate ratio. The factor of interest in these figures to be studied is HCR; it is important to note that, entropy generation is minimum at HCR=1 regardless of the operating conditions. This is an important result and based on that, it could be said, HCR equals unity defines the balanced state for heat and mass exchanger devices regardless of

the operating conditions. Operationally, HCR can be varied by only changing the water-to-air mass flow rate ratio (MR). However, this is a ‘control volume’ balanced state wherein the design does not include mass extractions and injections; i.e., zero extraction. This could be extended to formulate a concept of complete thermodynamic balancing in heat and mass exchanger devices by variation of mass flow rate ratio along the humidifier or dehumidifier processes path (infinity extraction) or to discrete balancing (single extraction).

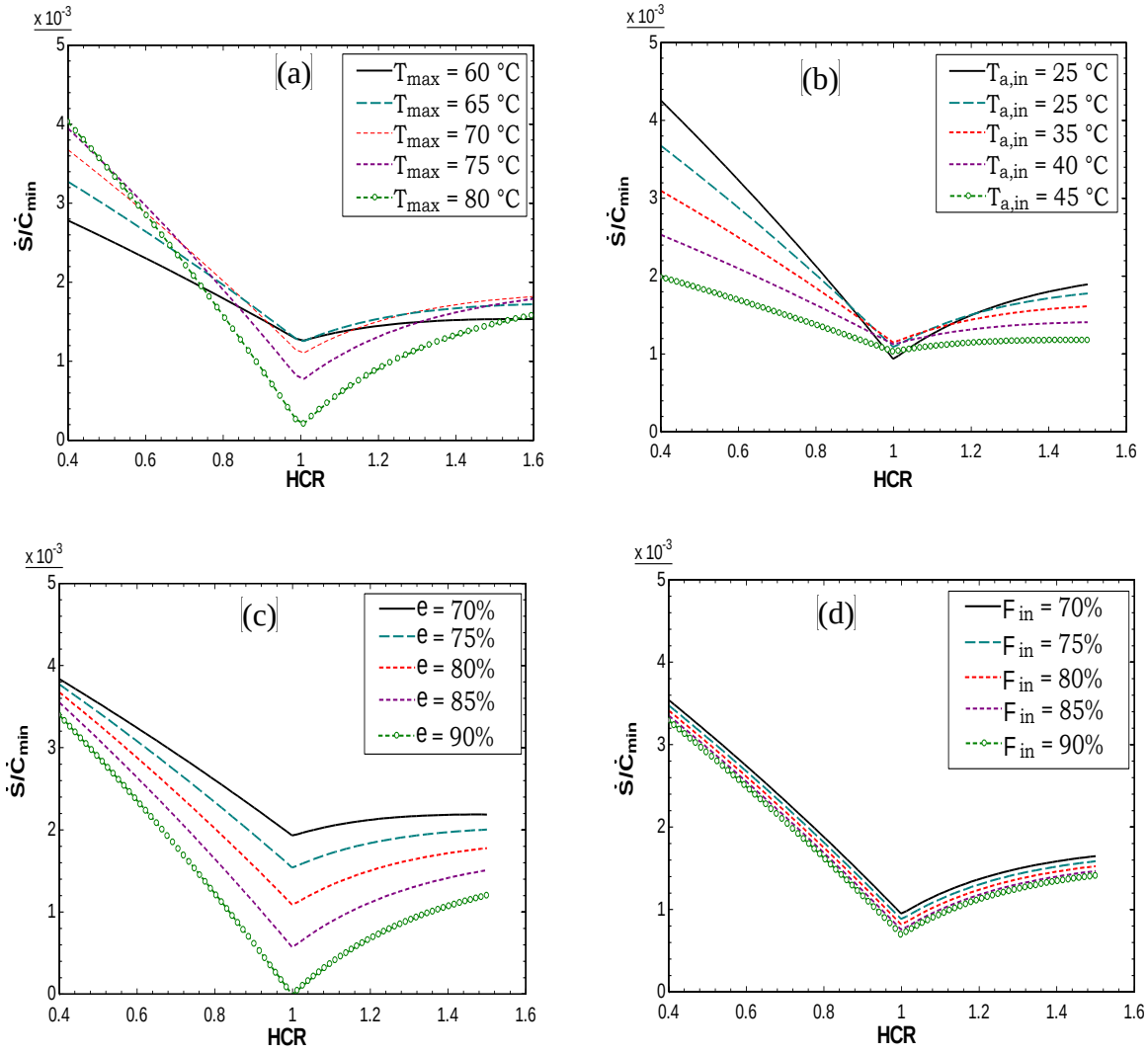

Figure B.3 Entropy generation vs. heat capacity ratio. T_{maz}=70 °C; $T_{a,in}$=30 °C; ε_{hum}=80%; Φ_{in}=60%; Φ_{out}=90%; ε_{hum}=80%; Φ_{in}=60%; Φ_{out}=90%; (a) effect of water inlet temperature; (b) effect of air inlet temperature; (c) effect of humidifier effectiveness; (d) effect of air inlet relative humidity.

Enthalpy Pinch: Appropriate Alternative to the Effectiveness and Temperature Pinch:

To clearly visualize simultaneous heat and mass transfer processes in the humidifier and dehumidifier, a temperature versus enthalpy diagram is plotted, as shown in Figure B.4.

The curved line d-e presents the air process through the humidifier and dehumidifier. The line 4-5 and the line 6-7 represent the water process through the dehumidifier and humidifier, respectively.

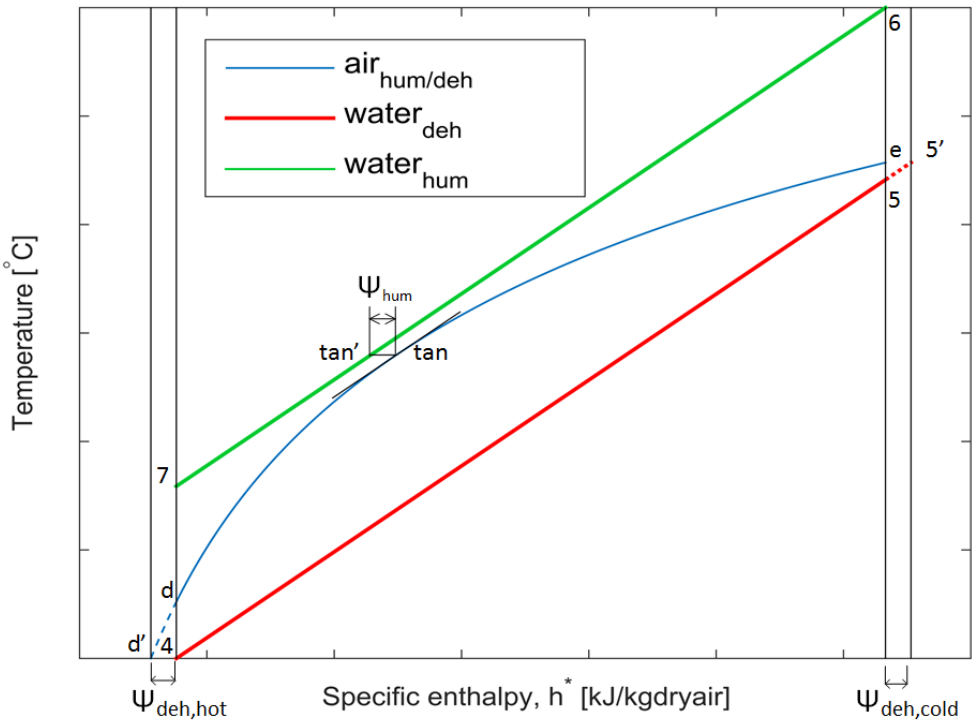

Figure B.4 Temperature enthalpy diagram for HDH system without extraction.

b' and 5' represent the hypothetical ideal states the moist air and water streams would have, respectively, reached if the dehumidifier had been of infinite size. Hence, $h^*_d - h^*_{d'}$ is represented as $\Psi_{deh,\,hot}$ and $h^*_{5'} - h^*_5$ is represented as $\Psi_{deh,\,cold}$ and they can be defined as the loss in enthalpy rates (per unit amount of dry air circulated in the system) because of having a finite-sized heat and mass exchanger device and it cannot be reduced by thermal balancing without increasing the area associated with the heat and mass transfer in such a device. In the case of a heat exchanger, Ψ will be analogous to the temperature

pinch and like temperature pinch, Ψ can be defined as the minimum loss in enthalpy rate due to a finite device size at any point in the exchanger and not just at terminal locations. Based on that, it could be said Ψ for heat and mass exchanger device is analogous to temperature pinch for a heat exchanger device. The energy effectiveness is commonly used as a performance metric for "heat exchangers" and "heat and mass exchangers". However, this parameter accounts only for terminal differences. In order to design for balancing by altering water-to-air mass flow rate ratio along the process path, local differences are needed to be considered. From Figure B.4, the humidifier pinch point does not occur at the terminal locations but rather at an intermediate point. This behavior cannot be captured using energy effectiveness definition. Another design issue, that high value of effectiveness for the humidifier in extreme case could lead to an internal cross of temperature or concentration lines. Enthalpy pinch [67] does not have this problem; hence it is a local parameter. Therefore, it is used in this work as a defining parameter of performance for heat and mass exchanger devices (humidifier and dehumidifier).

Balanced System Definition

Control Volume Balancing (Zero Extraction)

As stated earlier, a balanced system could be defined as a system in which entropy generation is minimized at fixed energy effectiveness when the modified heat capacity rate ratio (HCR) in the dehumidifier is equal to one. This could be extended to enthalpy pinch by dividing both numerator and denominator in Equation B.8 by the mass flow rate of dry air, the resulting equation can be expressed as [67]:

$$HCR = \frac{\Delta h^*_{max,cold}}{\Delta h^*_{max,hot}} = \frac{\Delta h^* + \Psi_{deh,cold}}{\Delta h^* + \Psi_{deh,hot}} \quad \text{(B.11)}$$

For HCR to be equal to unity in the dehumidifier, $\Psi_{deh,cold} = \Psi_{deh,hot}$ is needed. It should be noted, in this case also, that the enthalpy pinch point is located at the inlet and outlet of the dehumidifier, and at a single intermediate location in the humidifier. The same definition could be extended for a system with single extraction and injection, where each stage satisfies these conditions.

Balancing Based on Mass Extractions and Injections (Single Extraction)

In zero extraction system, the closed air loop is impounded between state *d*-*e*. The single extraction process can be divided into two zero extraction processes (or stages). The first stage is impounded between state *d*-*ext* and the second is impounded between state *ext*-e. Hence, the zero-extraction model can be used for the first and second stages simultaneously as shown in Figure B.5.

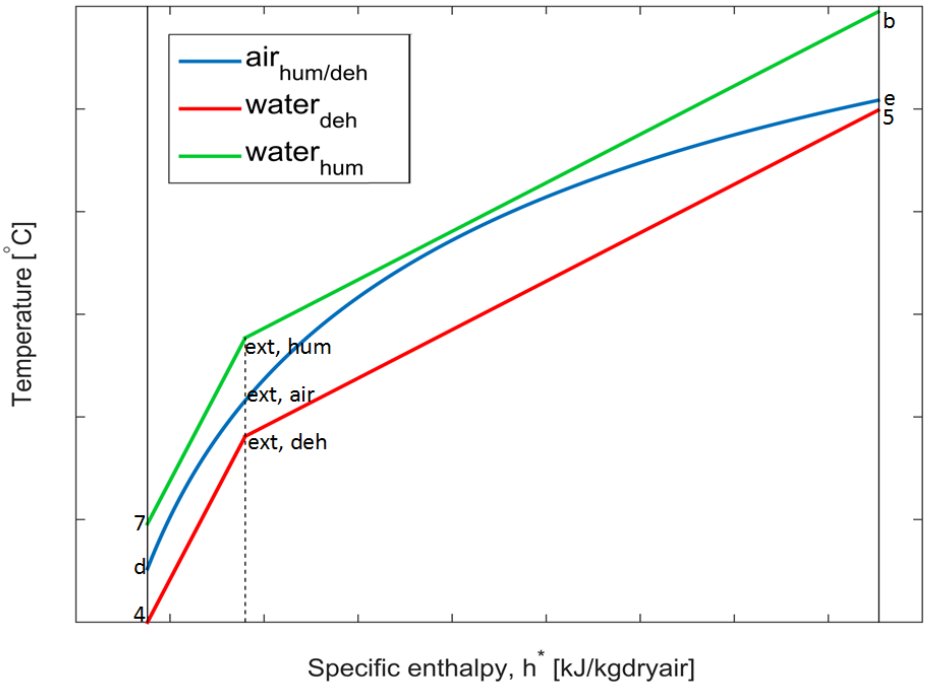

Figure B.5 Temperature enthalpy diagram for HDH system with single extraction.

From Figure B.5, it is clear that in a control volume balanced dehumidifier; i.e., zero extraction system, the local enthalpy pinch is minimum at the terminal locations, and is higher at all intermediate points. Single extraction brings local enthalpy pinch to a minimum value at one intermediate location; in other words, it brings HCR to unity at that location and the two terminal ones which lead to a tremendous decrease in entropy generation.

Appendix remarks:

- A modified HCR is defined for heat and mass exchanger devices. Bringing HCR to unity reduces entropy generation and improves the system performance noticeably.

- Enthalpy pinch is introduced as an appropriate alternative to the effectiveness and temperature pinch [67].
- Varying water-to-air mass flow rate ratio using single extraction and injection brings HCR at extraction point to unity. Hence, local enthalpy pinch through the dehumidifier is tremendously decreased i.e. leads to better system performance.
- The concept established in this Appendix results mainly in generating of Figures B.4 and B.5 for zero and single extraction processes, respectively. Visualization and modeling of these systems depend on these figures. The idea is to convert these figures into a mathematical model to evaluate the performance of zero and single extraction system, as shown in Figure C.1 of Appendix C.

Appendix C

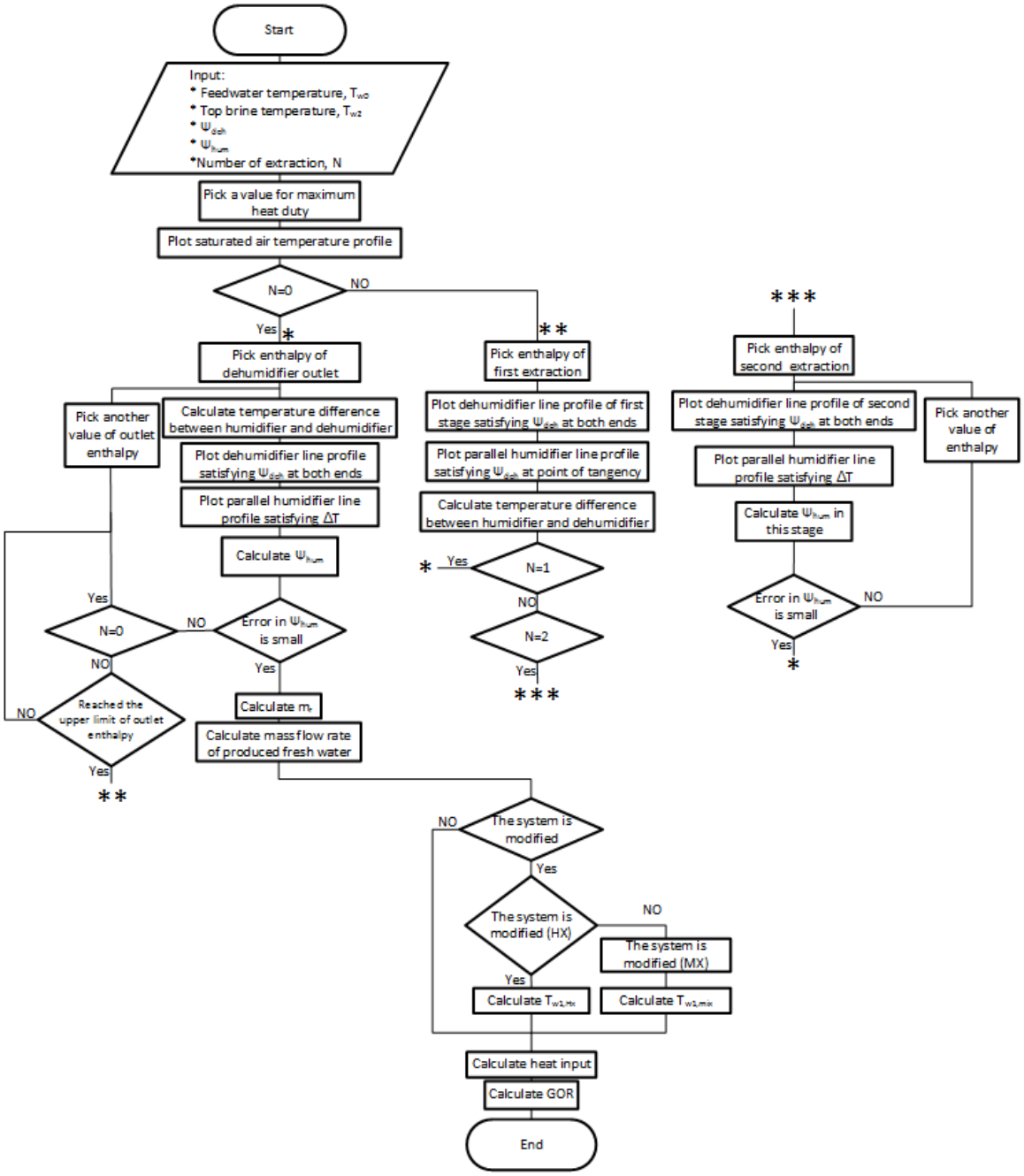

Figure C.1 Zero, single and double extractions algorithm for all cycles flowchart.

Vitae

Name	:Samih Mubarak Elmutasim Elshiekh
Nationality	:Sudanese
Date of Birth	:5/3/1990
Email	:sam_mutasim@hotmail.com
Address	:Almamoura Block 85 house No.54, Khartoum, Sudan
Academic Background	:B.Sc (honor) in Mechanical Engineering from University of Khartoum, October 2012. M.Sc in Mechanical Engineering from King Fahd University of Petroleum and Minerals, April 2017.
Projects:	"Design and Operational Impact of Addition of Sub-main to the Main Pipeline of Khartoum Refinery –Medani at Suba" A Thesis submitted and presented as partial fulfillment of B. Sc. (Hon) in Mechanical Engineering. "Theoretical and Experimental Studies of Modified Humidification Dehumidification Cycles" A Thesis submitted and accepted as partial fulfillment of M.Sc. in Mechanical Engineering.